

# **Layer by Layer Fabricated Gold Nanoparticles for Nucleic Acid Delivery**

Dissertation to obtain the Degree of Doctor of Natural Sciences

(Dr. rer. nat.)

from the Faculty of Chemistry and Pharmacy

University of Regensburg



Presented by

**Asmaa Mohamed Elbakry**

from Cairo, Egypt

August 2010

This work was carried out from October 2006 until July 2010 at the Department of Pharmaceutical Technology of the University of Regensburg.

The thesis was prepared under the supervision of Prof. Dr. Achim Göpferich.

Submission of the PhD application:

05.08.2010

Date of examination:

17.09.2010

Examination board:

Chairman:

Prof. Dr. S. Elz

1. Expert:

Prof. Dr. A. Göpferich

2. Expert:

Prof. Dr. T. Blunk

3. Examiner:

Prof. Dr. J. Wegener



To my family

---

Im Namen Allahs,  
des Erbarmers, des Barmherzigen !

Und über jedem, der Wissen besitzt, steht einer, der (noch mehr) weiß.

- *Koran, Sure Yusuf*

## **Table of contents**

<b>Chapter 1</b>	Introduction and Goals of the Thesis .....	7
<b>Chapter 2</b>	Preparation, Characterization, and Stabilization of Gold Nanoparticles .....	39
<b>Chapter 3</b>	Polyelectrolyte Coated Gold Nanoparticles via Layer-by-Layer Technology .....	65
<b>Chapter 4</b>	Layer-by-Layer Assembled Gold Nanoparticles for siRNA Delivery .....	99
<b>Chapter 5</b>	Size Dependent Uptake of Layer-by-Layer Coated Gold Nanoparticles into Mammalian Cells .....	121
<b>Chapter 6</b>	Summary and Conclusion .....	147
<b>Appendix</b>	Abbreviations .....	157
	Curriculum Vitae .....	159
	List of Publications .....	160
	Acknowledgements .....	161



# **Chapter 1**

## **Introduction and Goals of the Thesis**

Asmaa Elbakry, Miriam Breunig, Achim Goepperich

Department of Pharmaceutical Technology, University of Regensburg,  
Universitätsstraße 31, 93040 Regensburg, Germany

**Nucleic acid delivery**

Over the past two decades, nucleic acid delivery has shown tremendous promise and gained significant attention as a potential method for treating both genetic and acquired diseases, including severe combined immunodeficiency [1], cystic fibrosis [2], Parkinson's disease [3], cancer [4], and acquired immune deficiency syndrome (AIDS) [5]. The importance of nucleic acid delivery for disease treatment is reflected in the plethora of clinical trials in the scientific literature, which in 2009 exceeded 1500 [6]. A common approach to nucleic acid delivery has been to transfect cells with plasmid DNA designed to replace a defective gene in the target cell genome. Alternatively, RNA interference has emerged as a novel therapeutic pathway by which harmful genes can be "silenced" by complementary short interfering RNA (siRNA). The advantages of siRNA are the potent, specific inhibition of selected proteins. Moreover, siRNA acts primarily in the cytoplasm, which is easier to access than the nucleus, thus avoiding the nuclear barrier, a major obstacle of plasmid DNA delivery [7].

Today, there are many siRNA formulations in animal studies or preclinical phases at many major pharmaceutical companies, who are developing these novel siRNA therapeutics. In addition, some siRNA therapeutics are showing progress in the clinic (please see Table 1 [adapted from 8]). Many of the most advanced trials rely on forms of localized delivery. Such a methodology offers several benefits, including the potential for both higher bioavailability due to the proximity of the target tissue and reduced unfavourable distribution typically associated with systemic administration [8]. The most advanced clinical trials currently underway are specifically focusing on the treatment of age-related macular degeneration (AMD). Here, naked siRNA targeting to genes against the vascular endothelial growth factor (VEGF) or its receptor (VEGFR) has shown therapeutic potential in its inhibition of the excessive vascularization of the eye that leads to AMD [9] and has already reached phase III clinical trials in humans [6].

**Table 1:** Current clinical trials for siRNA therapeutics [adapted from 8]

Company	Disease	Mode of administration	Status	Preclinical reference
Allergan	Age-related macular degeneration	Topical	Phase II	[10]
Alnylam	Respiratory syncytial virus	Local/direct	Phase II	[11]
	Cancer	Systemic	Phase I	[12, 13]
Nucleonics	Hepatitis B virus	Systemic	Phase I	
Quark /Pfizer	Acute renal failure	Systemic	Phase I	
Tekmira	Hypercholesterolemia	Systemic	Phase I	[14, 15]
Opko Health	Age-related macular degeneration	Topical	Phase III	[16]
Silence/Quark /Pfizer	Diabetic macular oedema	Topical	Phase II	
Transderm	Pachyonychia congenita	Topical	Phase Ia/b	[17, 18]
Calando	Cancer (solid tumor)	Systemic	Phase I	[19]

### RNAi discovery and mechanism

The effects of RNA interference (RNAi) were first reported by Napoli et al. [20] in 1990, as a result of their attempt to overexpress chalcone synthetase (CHS), an enzyme largely responsible for plant coloration in petunias. The authors were surprised that the introduction of this gene blocked pigment synthesis, which caused the growth of white or partly white flowers instead of the normal purple phenotype [21, 22]. Although not fully understood at the time, an explanation for this result and other similar phenomena was revealed by Fire and Mello in 1998 when they discovered that the gene expression in the nematode *Caenorhabditis elegans* (*C. elegans*) can be silenced by delivering long, double-stranded RNAs (dsRNAs) [23].

This method of RNAi uses the long, double-stranded RNAs that are delivered to cells or expressed intracellularly from plasmids. These RNAs are processed into short 21–23 base pair (bp) fragments called small interfering RNAs (siRNAs) by an endogenous RNase III-type enzyme known as Dicer [24,25] (Figure 1). Thereafter, each siRNA molecule is loaded into an RNA-induced silencing complex (RISC). Argonaute 2 (Ago2) which is an enzymatic component of RISC, cleaves and discards one strand (passenger or sense strand) of the siRNA and retains the other (guide or antisense strand) to activate the mature RISC complex [26, 27]. Then the siRNA

guide strand directs the RISC to mRNA molecules containing a complementary nucleic acid sequence. Through Watson–Crick base pairing, the siRNA guide strand binds to the complementary portion of the mRNA molecule and the endonuclease region of RISC cleaves the mRNA in this region of homology. The cleaved mRNA, which is subsequently degraded by intracellular nucleases, is no longer available for translation of the corresponding protein. By this mechanism, long dsRNAs are able to induce gene silencing with very high specificity.

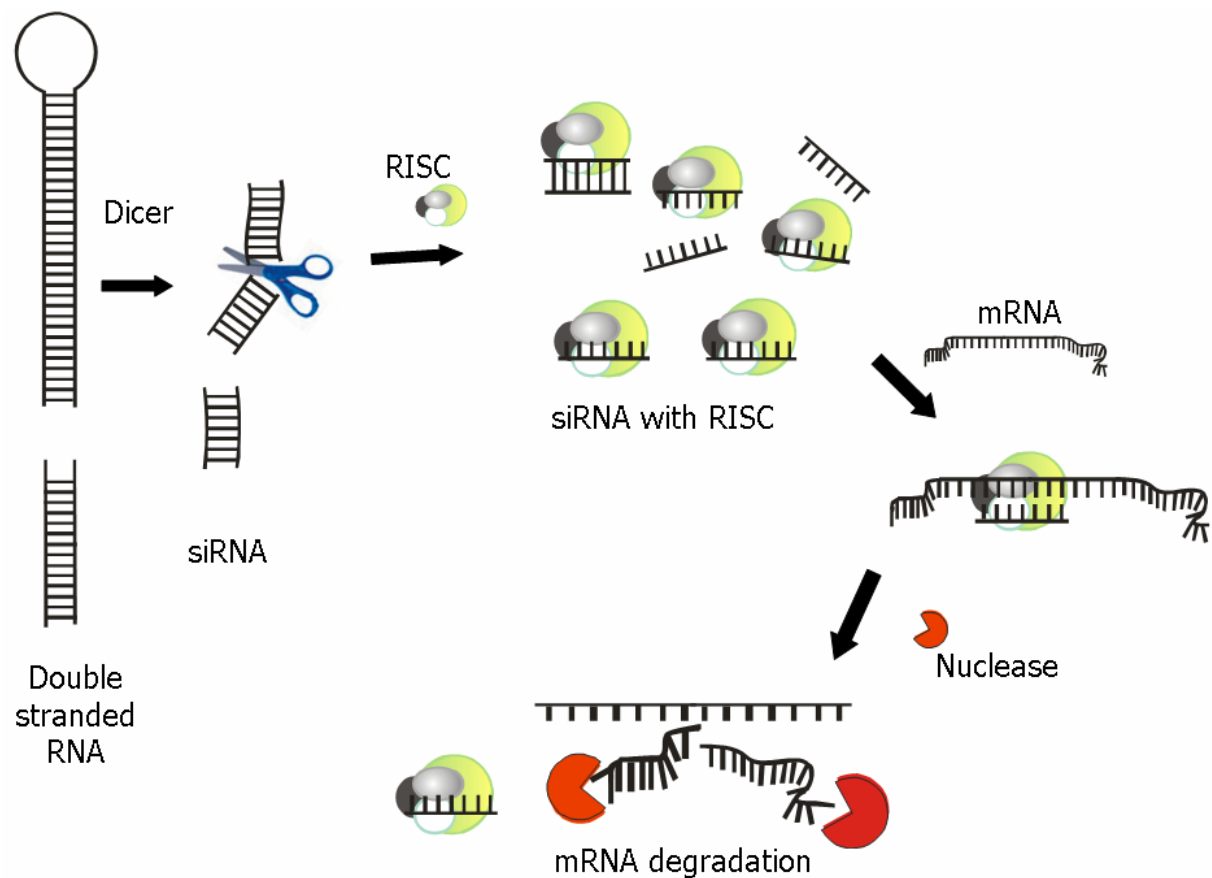


**Figure 1:** Mechanism of RNAi: The doubled-stranded RNA is cleaved into shorter fragments of 21-23 base pair siRNA by the enzyme Dicer. A multiprotein complex called RISC (RNA-induced silencing complex) combines with the siRNA, retaining the guide strand and discarding the passenger strand. The siRNA then guides RISC to the homologous mRNA. RISC-associated endonuclease cleaves the target mRNA resulting in the silencing of the target gene.

For therapeutic purposes, siRNA can be synthetically produced and then directly introduced into the cells, thereby circumventing the Dicer mechanism (Figure 1). This shortcut reduces the potential for an innate immune interferon response and the shutdown of cellular protein expression that can occur following the interaction of long pieces (>30 nucleotides) of double stranded RNA with intracellular RNA



receptors [28-30]. Since the RNAi machinery is available in every cell and any gene can be targeted [31-33], this process cannot only be exploited to investigate gene function in eukaryotic cells, but it also holds great potential for suppressing the expression of disease-related genes [34-37].

### **siRNA delivery**

One of the primary challenges of siRNA-based therapeutics is their delivery to cells [38]. The major limitations for the use of siRNA, both *in vitro* and *in vivo*, are the inability of naked siRNA to passively diffuse through cellular membranes due to its high molecular weight (~13 KDa) and the strong anionic charge of its phosphate backbone, which causes electrostatic repulsion from the anionic cell membrane surface [39]. Furthermore, fast degradation by endogenous enzymes and the lack of targeting ability limits the delivery of siRNA [36, 40]. Therefore, the success of siRNA applications depends upon the use of suitable carriers for delivery. The therapeutic application of siRNA requires the development of carriers that will protect siRNA from degradation during circulation [41], deliver the siRNA to the target cells while avoiding non-target cell types, facilitate cellular uptake, and release the siRNA intracellularly so that it will be accessible to the cellular RNAi machinery [42]. Numerous delivery strategies, both viral and nonviral, have been developed to circumvent the aforementioned problems, and some of them have been successfully used for the introduction of siRNA into cells both *in vitro* and *in vivo* [43, 44].

Viral vectors are highly efficient delivery systems due to the inherent ability of viruses to transport genetic material into cells; they are currently the most powerful tool for gene transfection. Unfortunately, fundamental problems exist with viral vector transfection, including high production cost, difficulties in large scale production, and, most importantly, severe safety risks arising from their oncogenic potential and inflammatory and immunogenic effects, which prevent repeated administration to patients [45-48]. In the light of these concerns and limitations, non-viral carriers have emerged as a promising alternative for siRNA delivery both *in vitro* and *in vivo* [37, 49-53]. They have a number of advantages, including increased stability and safety, relatively low production cost, and the possibility of modification via the incorporation of ligands, aiding cell type specific targeting. However, the regulatory effect over gene expression levels by these carries is lower when compared with viral vectors. Non-viral carries still suffer from their own limitations, including high toxicity and the

inability to overcome the numerous biological barriers of the extracellular environment after local and systemic application [54, 55].

In non-viral delivery approaches, the double-stranded siRNA is either naked, chemically modified [56, 57], or covalently attached to other molecules to enhance its stability. This siRNA is then complexed with a carrier material that binds to the siRNA via electrostatic interactions to form particles. These particles usually range in size from nano- to micrometers, depending on the physical characteristics of the material and the formulation conditions [40]. The resulting particle should protect the siRNA from degradation in the circulatory system, bring the siRNA into the target tissue, enter the cell through endocytosis, and release the siRNA in the cytoplasm. The formulation of nanoparticles used for *in vitro* and *in vivo* delivery of siRNA via either systemic and/or local administration has exploited various kinds of materials, including cationic lipids (liposomes), polymers, covalently conjugated polymers to siRNA, peptides, proteins (including antibodies), and inorganic nanoparticles such as quantum dots [29,58-63]. Table 2 represents some examples of non-viral carries used for siRNA delivery both *in vitro* and *in vivo*. This table reveals that different materials, either synthetic or naturally occurring, can be complexed with siRNA and deliver the siRNA to various cell lines. However, the table also demonstrates that the size of the siRNA complexes and the different carrier materials have a high variation in the particle size distribution.

Among various delivery systems, cationic polymers have gained a prominent position over other system for siRNA delivery, due to their ease of preparation, purification and chemical modification to meet the particular needs of siRNA delivery [91-96]. Of the many cationic polymers, poly(ethylene imine) (PEI) has been extensively investigated for its ability to transport siRNA into cells both *in vitro* and *in vivo* [97-100].

**Table 2:** Some examples of non-viral vectors for siRNA delivery

siRNA Delivery system	Diameter (nm)	Type	Targeted mRNA/tissue/diseases	Refs.
<b>Liposomes and Lipids</b>				
DOTAP (1,2 Dioleoyl-3 trimethylammonium-propane)	Not shown	Cationic liposomes	Various cell types (mouse in vivo)	[64]
DOTAP/DOPE (1,2-dioleoyl-sn-glycero-3 phosphatidylethanolamine)	Not shown	Cationic liposomes	Targeting the luciferase mRNA in mouse L- cells	[65]
DOPE/CDAN (N-cholesteryloxycarbonyl-3,7-diazanonane-1,9-diamine)	300-500	Liposomes	HeLa and IGROV-1 cells	[66]
SNALP(stable nucleic acid lipid particles)		Cationic lipid nanoparticles	Targeting apoB gene in mice	[67]
DOPC (1,2-dioleoyl-sn-glycero- 3 phosphatidylcholine)	65	Neutral nanoliposome	EphA2 in mice	[68]
<b>Polymers</b>				
P(MDS-co-CES) poly {(Nmethyldietheneaminesesecate) co [(cholesteryloxocarbonylamidoethyl) methylbis(ethylene)ammoniumbromide] seacate}	175	Cationic core-shell nanoparticles	MDA-MD-231 human breast cancer cells	[69]
Poly(ethylene glycol)-block-poly(aspartic acid) (PEG-PAA) with calcium phosphate	100-300	Poymer nanoparticles	HeLa cells	[70]
MPEG/PCL(Methoxy(polyethyleneglycol) /poly(ε-caprolactone)	150	Di-block co-polymeric nanoparticles	Not shown	[71]
Chitosan	200-500	Cationic polysaccharide nanoparticles	H1299 human lung carcinoma cells CHO K1 and HEK 293 cell lines	[72,73]
Polyisobutylcyanoacrylate	325	Noncationic aqueous-core nanocapsules	Ewing sarcoma (metastatic bone cancer)	[74]
Hyaluronic acid	200-500	Nanogel	HCT116 human colon carcinoma cell lines	[75]
Polyethylenglycol–polypropylenesulfidepeptide (PEG–PPS-peptide)	171-601	ABC tri-block co-polymer	HeLa cells	[76]

Continued on next page

siRNA Delivery system	Diameter (nm)	Type	Targeted mRNA/tissue/diseases	Refs.
Atelocollagen	100-300	Nanoparticles	Human nonseminomatous germ cell tumor	[77-79]
<b>Peptide/Protein-based</b>				
Acetyl – GALFLGFLGAAGSTMGAWSQPKKKRKV cysteamide	200	Noncovalent nanoparticles	Various cell types	[80]
Ternary proticles (HSA-Protamine-ODN)	202	Self-assembled nanoparticles	Murine fibroblast	[81]
<b>Cell-Penetrating Peptides</b>				
TAT	Not shown	Peptide	EGFP, CDK98, MAP kinase	[82, 83]
Penetratin	Not shown	Peptide	GFP, luciferase, SOD, caspase, MAP kinase	[83-85]
<b>siRNA conjugate</b>				
Aptamer-siRNA	Not shown	Conjugate	Lamini A/C siRNA	[86]
Antibody-siRNA	Not shown	Conjugate	Luciferase	[87]
<b>Metal and Semiconductor Nanoparticles</b>				
Quantum dot	Not shown	Semiconductor nanoparticles	GFP, HeLa cell	[88]
Iron oxide	Not shown	Metal nanoparticles	GFP	[89]
Carbon nanotube	Not shown	Nanoparticles	Luciferase	[90]

The effectiveness of PEI as a siRNA carrier is a result of the electrostatic interaction between the positively charged amino groups of PEI and the negatively charged phosphate groups in the backbone of siRNA. This interaction leads to the formation of small complexes (polyplexes) that are stable enough to transport genetic material into cells. PEI-siRNA polyplexes are taken up by cells via endocytosis. Once inside the cell, the polyplexes escape from the endocytotic compartment to the cytoplasm via the proton sponge mechanism. This release is aided by the augmented influx of protons and water due to the presence of PEI, which causes endosomal swelling and

the osmotic release of the polyplexes [97,101-104]. Thereafter, the siRNA can be incorporated into the RNAi machinery (Figure 2).

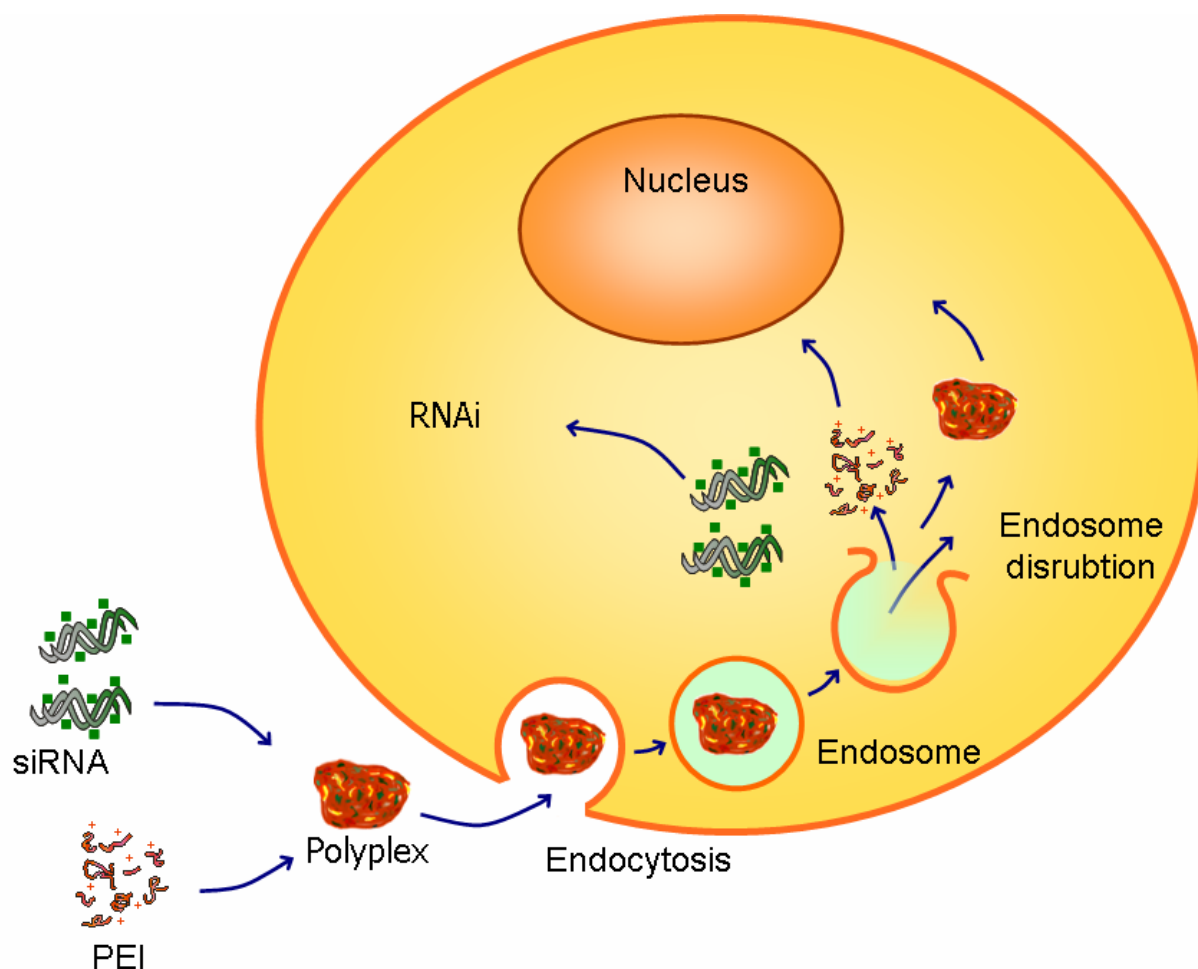


**Figure 2:** Proposed mechanism of PEI-mediated siRNA transfer: Due to electrostatic interactions, PEI is able to complex with negatively charged siRNAs, leading to a compaction and the formation of small complexes which are endocytosed. The "proton sponge effect" exhibited by PEI complexes leads to osmotic swelling and ultimately to the disruption of the endosomes. Upon their release from the PEI-based complex, intact siRNAs are incorporated into the RISC complex and induce RNAi.

PEI offers significantly more protection against nuclease degradation in comparison to other polycations, such as poly (L-lysine), possibly due to its higher charge density and more efficient complexation ability [105]. The mean size of PEI/siRNA polyplexes depends on the N/P ratio, which is defined as the ratio of the number of nitrogens in the polycation divided by the number of phosphate groups in the nucleic acid. For instance, polyplexes prepared with the commercially available product jetPEI® (linear PEI 22 KDa) using a N/P ratio of 10 have a diameter of about 40 nm [106], whereas an N/P ratio of 2 leads to a larger polyplexes size (between 120 and 170 nm) [107]. It

is noteworthy that the molecular weight of the PEI influences the transfection capability of polyplexes. High molecular weight PEI like branched PEI 25 KDa polyplexes are highly efficient for transfection [108]. However, branched PEI 25 KDa is also characterized by significant cytotoxicity [109-113]. The toxicity can be reduced by masking the charges but, at the expense of decreased transfection efficiency [110,111,114]. Therefore, much effort has been spent on the modification of PEI in order to improve its stability and allow for a high transfection efficacy accompanied by a low toxicity [101,115,116]. For example, the amino group modifications of branched PEI with several functional moieties were introduced into cells, which revealed that succinylation of branched PEI resulted in up to tenfold reduction of polymer toxicity in comparison to unmodified branched PEI 25 KDa [115]. Moreover, succinylated PEI/siRNA complexes were able to induce remarkable knockdown of the targeted luciferase gene at siRNA concentrations as low as 50 nM. Ketalization of PEI also leads to a dramatic reduction of the polymer's toxicity [116]. The modified PEI becomes labile at a pH values close to 5.0 and degrades when it reaches the endosome (pH 6.5) of the cells, where it can release the nucleic acid. Additionally, biodegradable PEI-based nanoparticles containing disulfide bonds offer several advantages, including high transfection efficiency and endosomal escape with reduced cytotoxicity [101].

Polyplexes, however, do not come without limitations. The most egregious problem currently facing this technology is the huge size variation in individual polyplexes. For instance, a closer look at the particle size distribution shows that nearly all of the produced polyplexes have a particle distribution ranging from 100 nm to more than 500 nm with a relatively high polydispersity index, which is a numerical representation of particle size distribution. Considering that the size and surface properties of polyplexes have a great impact on the cellular uptake, internalization, and biodistribution of siRNA, such a heterogeneous particle collective is highly unfavorable for the transfection process.

### **Limitation of existing carriers**

In general, the delivery vehicles can affect the resulting biodistribution through passive and/or active targeting. Passive targeting occurs as a result of the intrinsic physicochemical properties of the carrier. Important aspects that control the biodistribution and transfection are the charge and size of the delivery vehicle [117].

While the size and surface properties of the delivery carriers have an influence on the circulation and biodistribution of siRNA, they also have an impact at the stage of the cellular entry. There are a number of different endocytic pathways to internalize macromolecules by cells. These pathways include phagocytosis, macropinocytosis, clathrin-mediated endocytosis, caveolin-mediated endocytosis, and clathrin- and caveolin-independent endocytosis (Figure 3, bottom) [118,119]. The endocytic pathways differ with regard to the size of the endocytic vesicle, the nature of the cargo, and the mechanism of vesicle formation. Each of those pathways is able to deliver siRNA into cells. For an efficient RNAi activity, the nucleic acid has to reach its cellular target (the cytoplasm) after gaining entry into the cell. This ability strongly depends on the internalization pathway and it is highly dependent on the delivery system used. It is known that the physicochemical characteristics of particle, as well as the actual cell type being targeted, affects cellular uptake [120-123]. In addition, the particle's surface properties determine which biomolecules of the extracellular environment interact with the particles, which also affects access into cells [124-126].

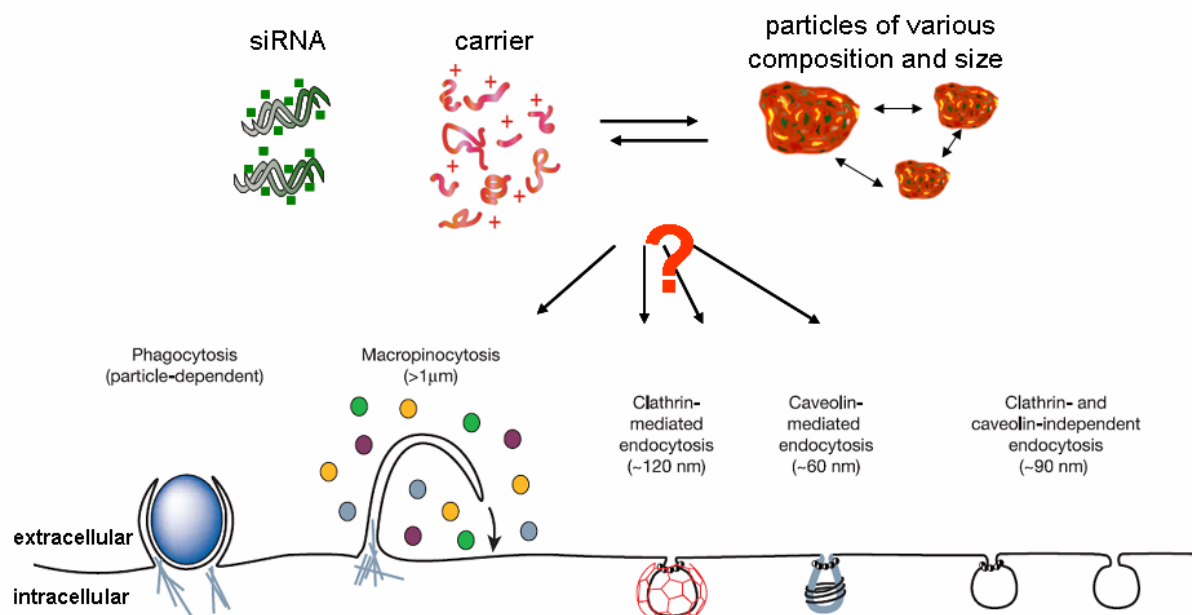


**Figure 3:** Top: The various sub-species existing in random siRNA formulation: nanoparticles of various composition and size, free siRNA and free carrier. Bottom [taken from 118]: The endocytotic pathways into cells can be classified by the mechanism of vesicle formation as well as the nature and size of the cargo.

Most of the aforementioned nano-carriers have been used to form nanosized complexes with siRNA, which produce random self-assembled aggregates with siRNA that are often larger than 100 nm. These systems are generally

heterogeneous and poorly defined particle collectives [127-129]. Thus the resulting collectives contain particles of various composition and size that are in equilibrium with the free polymer and free siRNA (Figure 3 top).

These polyplexes can be taken up by the cells via different pathways at the same time. For example, smaller particles can be taken up via caveolin-mediated endocytosis (mean size ~ 60 nm). Larger particles are taken up via clathrin- and caveolin-independent endocytosis or clathrin-mediated endocytosis (mean size ~ 90 and 120 nm respectively) or even via macropinocytosis. The onset of internalization will be different according to each particle's size in this random aggregate. Therefore, this heterogeneous collective is taken up by the cell by the various mechanisms as illustrated above. Consequently, the polyplexes are unloaded at different places inside the cell. This means that the use of random aggregates leads to a decrease in the efficacy of siRNA formulations tremendously, since not every sub-species in these random preparations is able to elicit the same biological effect. In addition, the interpretation of the experimental results is complicated due to the presence of different subspecies, since it is not evident which particular subspecies is responsible for the overall biological effect. The biological effect of such a collective will be an average of e.g. highly efficient and inactive components coexisting in the siRNA formulation. Furthermore, toxic effects may be exhibited by only a fraction of the preparation, e.g. the free carrier may appear to be intrinsic properties of the whole collective. As well as, it is also difficult to identify the exact pathway of entry and intracellular fate of these heterogeneous nanocomplexes. Consequently, it is impossible to establish strategies for the design of new and advanced materials for siRNA delivery.

Therefore, new strategies for the fabrication of small and uniform nanoparticles with a defined zeta potential and surface chemistry are necessary to deliver siRNA to specific intracellular destinations and elicit a distinctive biological effect.

### **Gold nanoparticles**

Recently, various metal and semiconductor nanoparticles such as quantum dots, carbon nanotubes, iron oxide, and gold nanoparticles have been utilized for the development of multifunctional nanoparticles for biomedical applications. In particular, gold nanoparticles (AuNPs) have attracted great attention in a variety of biomedical fields including DNA mismatch detection [130], biomolecular sensing



[131], rapid and sensitive diagnostic assays [132], radiotherapy and imaging [133,134] and hyperthermal cancer therapy [135]. This biomedical versatility is mainly due to the fact that colloidal gold has well defined chemical, physical, electronic, and optical properties with respect to shape and size [136]. Recently, many attempts have been made to utilize AuNPs as gene carriers to deliver oligonucleotides or plasmid DNA [137-139] and even siRNA into cells [140,141]. For instance, AuNPs provide attractive candidates for siRNA delivery because of several advantages, including straightforward synthesis, easy surface modification, availability in different size range with narrow size distribution, and high biocompatibility with cells or tissues [142,143]. Park and co-workers [140] used amine-functionalized AuNPs for intracellular delivery of siRNA. The positively charged amine AuNPs formed stable polyelectrolyte complexes via electrostatic interactions with negatively charged siRNA–polyethylene glycol (PEG) conjugates. This siRNA-(PEG) conjugates had a cleavable di-sulfide linkage under the reductive conditions found in the cytosol. The presence of PEG chains improved the dispersion stability of the polyelectrolyte complexes by protecting them from uncontrollable aggregation. The polyelectrolyte complexes of the AuNPs with PEG-conjugated siRNA were internalized to a higher extent by human prostate carcinoma cells than the polyelectrolyte complexes prepared with siRNA and PEI alone. Furthermore, the green fluorescence protein (GFP) expression was suppressed within the cells without eliciting the severe cytotoxicity demonstrated in branched PEI. Nagasaki and co-workers conjugated thiolated siRNA (SH-siRNA) to AuNPs for cellular delivery [144]. RNA-modified particles were coated with poly(ethyleneglycol)-block-poly (2-(N, N -dimethylamino) ethyl methacrylate) copolymer to enhance cellular internalization. These delivery systems were effective for gene silencing in HuH-7 cells. Recently, Mirkin and co-workers attached siRNA molecules to the surface of AuNPs via thiol groups [141]. The polyvalent siRNA-nanoparticle conjugates showed a six-fold increase in half-life in 10% serum and prolonged gene knock down compared to free RNA duplexes. Anderson and co-workers conjugated siRNA to poly (ethylene glycol) modified AuNPs via a biodegradable disulfide linkage [145]. Further coating of these AuNPs with poly ( $\beta$ -amino ester)s facilitated the siRNA delivery *in vitro*. Without a coating of poly ( $\beta$ -amino ester)s, however, siRNA-conjugated AuNPs did not exhibit any silencing effect. These approaches demonstrate the general applicability of AuNPs as delivery vehicle, but in some of the described cases AuNPs seemed to aggregate

after assembly with nucleic acid [137,140], the delivered nucleic acid showed low activity inside cells [139], or the efficacy of the nucleic acid relied on an additional transfection reagent [138].

It is for these reasons that an alternative technique is needed for siRNA delivery using AuNPs as a carrier. This technique should be simple, versatile and ease to prepare. The technique should not covalently attach the siRNA, thereby avoiding any chemical alteration in its structure. An advantage to this requirement is reduced cost; unmodified siRNA is much less expensive than modified siRNA. An additional and extremely important stipulation is that the particles still be monodisperse after loading with siRNA to avoid formation of random aggregates. Such a technique could use a Layer-by-Layer (LbL) strategy. We thought that LbL technique would fulfill these requirements. This LbL technique would allow us to use monodisperse AuNPs as a template for the manufacture of a carrier that remains monodisperse during assembly and deliver active siRNA into cells via the deposition of negatively charged siRNA and positively charged transfecting agent in alternative order on AuNPs, thereby circumventing the limitations of previous systems.

### **Layer-by-Layer technique**

In the early 1990s, Decher developed a simple, elegant, and extremely powerful approach to the formation of controlled architecture multilayer polymer films based upon the LbL assembly of oppositely charged polyelectrolytes on a charged solid surface [146,147]. These multilayered polyelectrolyte films provide unique and attractive thin-film platforms for the controlled release of both small-molecule drugs [148-152] and macromolecular therapeutics such as DNA [153-156], and even siRNA [157,158]. Caruso and colleagues have pushed the use of LbL assembly technique from solid substrate to colloidal particles [159-162]. Colloidal cores of various composition (lattices, metal nanoparticles, enzymes, low molecular weight species, and cells) and size (nanometer–micrometer–millimeter range) have been coated with multilayers of diverse composition and controllable thickness [160-162]. In this strategy, depicted in Figure 4, the first added species usually has an opposite charge to that of the colloids, thereby adsorbing through electrostatic interactions. An overcompensation of charge often results with adsorption of each layer, and at this stage the charge on the surface of the particles is reversed. This facilitates the alternate deposition of subsequent layers of a wide range of charged components.

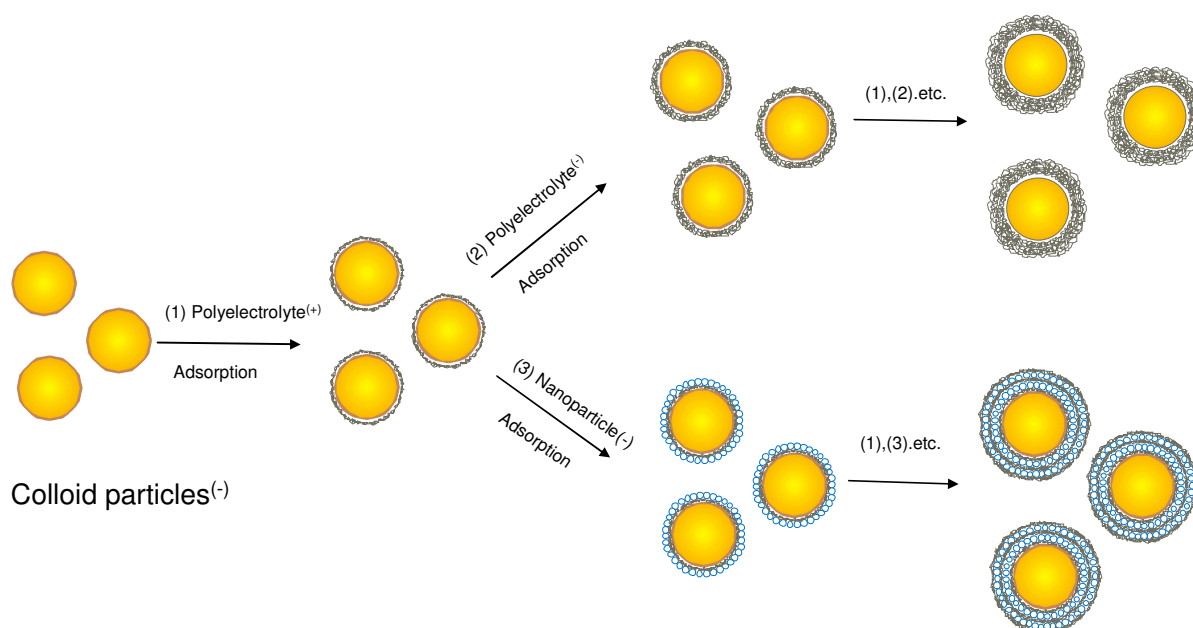


**Figure 4:** Schematic illustration of the LbL technique for the surface modification of colloid particles. The coatings can be polyelectrolytes (steps 1 and 2), or nanocolloids such as inorganic nanoparticles or proteins (steps 1 and 3). The templates can be of different composition, size, and shape (latex particles, metal nanorods and nanoparticles, proteins, and cells) [adapted from 163].

Generally, a polyelectrolyte is used to separate layers of the same or different materials. These polyelectrolyte interlayers not only act as molecular glue, but they can also impart enhanced colloidal stability to the coated particles via electrostatic as well as steric contributions. Following deposition of each polymer layer, excess polyelectrolyte is removed by centrifugation or filtration, with intermediate water washings [163].

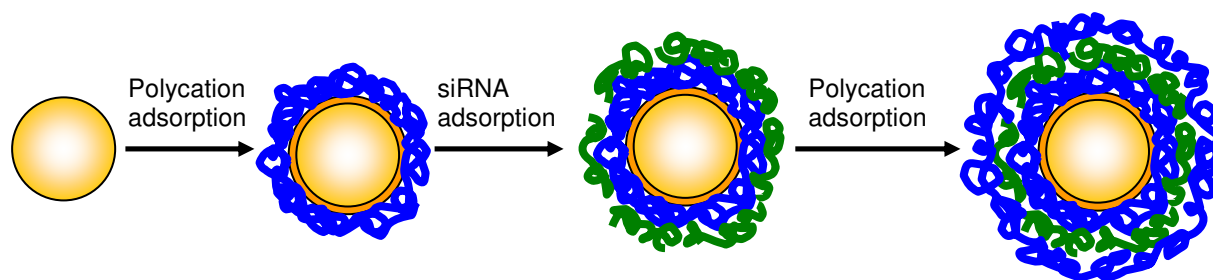
Although there are various experimental parameters that have an impact on LbL coating of colloidal particles, the chief issue in transferring the LbL technology from planar supports to colloid particles is the effective separation of the remaining free (unadsorbed) charged polyelectrolyte species from the colloidal dispersion prior to the next deposition cycle. This avoids the formation of polyelectrolyte complexes in bulk solution [163]. Coating nanoparticles via the LbL methodology has presented tremendous challenges, such as identifying the appropriate parameters for controlling particle aggregation and enhancing dispersion stability. These parameters include the nature of the polymer, polymer length, concentration, and stiffness. The nanoparticles' curvature, concentration, size, and ionic strength of the adsorption solution have a great influence on colloidal stability as well (for review see [164-166]).

Amongst the colloidal cores utilized for LbL techniques, AuNPs are especially attractive for this recombination due to their optical properties. These optical properties can be used to investigate the deposition of the coating on their surface. In addition, the intensity and aggregation sensitive color of the AuNPs facilitates the monitoring of the dispersion stability during all functionalization steps. Lastly, AuNPs are biocompatible and gold cores are also easily dissolved by mild methods to form a hollow capsule template [163-165].

## Goals of the thesis

Most of the carriers used for siRNA delivery form random self-assembled aggregates with siRNA. These aggregates are generally heterogeneous and create poorly defined particle collectives. In addition, these particles of different sizes and compositions are in equilibrium with free carrier molecules (e.g polymer) and free siRNA. Consequently, it is not clear which species is responsible for the overall biological effect and the optimization of existing formulations is difficult to achieve. Therefore, new and optimized strategies are urgently needed for the highly efficient delivery of siRNA to cells.

In order to get homogeneously distributed nano-carriers with well defined size and surface properties for the delivery of siRNA to specific intracellular destinations and elicit a distinctive biological effect, we hypothesized that the Layer-by-Layer (LbL) strategy using colloidal gold nanoparticles (AuNPs) as a template could allow us to manufacture a carrier for siRNA delivery that remains monodisperse during the assembly process and delivers active siRNA into cells. In order to fabricate such uniform nanoparticles, our approach was to deposit the siRNA as a negatively charged polyelectrolyte and a positively charged polyelectrolyte (transfecting agent) in alternative order on AuNPs, via the LbL technique as illustrated in (Scheme 1).



**Scheme 1:** LbL coating of AuNPs

LbL-coated AuNPs are expected to be excellent agents to surmount the described limitations due to their high uniformity. In addition, the straightforward tailoring of their physicochemical properties makes them a favorable tool to identify parameters for highly efficient delivery of siRNA into cells.

Therefore, the first goal presented in this thesis aimed to the preparation, stabilization, and optimization of AuNPs suitable for the coating with siRNA and a cationic polyelectrolyte by the LbL technique. First, small AuNPs with a narrow size distribution had to be prepared via the citrate reduction method. These nanoparticles

then had to be stabilized with a strong ligand to be suitable for the subsequent coating steps. Thereafter, it was necessary to identify the optimal pH and ionic strength of these nanoparticles for the subsequent coating steps that still garners sufficient nanoparticle stability while maintaining optimal wrapping of the polyelectrolytes ([chapter 2](#)).

The next goal was to identify the appropriate parameters to successfully coat the stabilized AuNPs via the LbL technique, such that the selection of the appropriate polyelectrolytes (polycation), concentration of polyelectrolytes, and ionic strength of the adsorption solution was achieved. In addition, a very important point was the purification of the AuNPs after each coating step before the subsequent deposition cycle with the opposite charged polyelectrolyte, which avoids the formation of inter-polyelectrolyte complexes and aggregation of nanoparticles. Moreover, the toxicity and stability of LbL-coated AuNPs in cell culture medium had to be investigated as prerequisite for a successful cellular uptake ([chapter 3](#)).

According to the optimized parameters chosen from chapter 3, the intention of ([chapter 4](#)) was to fabricate LbL-coated AuNPs for siRNA delivery using PEI as a polycation. Important parameters to investigate concerning the quality of the coating were the physicochemical characteristics and surface properties of the produced nanoparticles. Afterwards, the potential of these nanoparticles for use in cellular uptake studies had to be evaluated. Therefore, their stability under cell culture conditions was investigated as a prerequisite to maintain monodispersity and avoid the formation of aggregates. In addition, the functionality of the successfully coated AuNPs had to be determined by measuring the gene knockdown and cellular viability of nanoparticles in CHO-K1 cells.

Last but not least, endocytosis is governed by highly sophisticated and well regulated principles, and it is known that physicochemical characteristics of the particles strongly influence their cellular uptake. Therefore, in order to determine how the size and surface properties influence the cellular uptake into the cells, LbL-coated AuNPs of different sizes (20, 30, 50, and 80 nm) were produced. Thereafter, the physicochemical properties of these LbL-coated AuNPs had to be investigated. In addition, the cellular uptake kinetics of different sizes of LbL-coated AuNPs had to be determined in different cell lines, since it is known that physicochemical characteristics of particles as well as the actual cell type affect cellular uptake. Finally, the cell viability of CHO-K1 cells had to be investigated after incubation with

different sized LbL-coated AuNPs in order to investigate the suitability of these nanoparticles for therapeutic applications (chapter 5).

## References

- [1] Cavazzana-Calvo, M.; Hacein-Bey, S.; De.Saint Basile, G.; Gross, F.; Yvon, E.; Nusbaum, P.; Selz, F.; Hue, C.; Certain, S.; Casanova, J. L.; Bousso, P.; Le Deist, F.; Fischer, A. Gene therapy of human severe combined immunodeficiency(SCID)-X1 disease. *Science* 2000; **288**: 669– 672.
- [2] Boyd, A. C. Gene and stem cell therapy; Karger: Basel; New York, 2006.
- [3] Kaplitt, M. G.; Feigin, A.; Tang, C.; Fitzsimons, H. L.; Mattis, P.; Lawlor, P. A.; Bland, R. J.; Young, D.; Strybing, K.; Eidelberg, D.; During, M. J. Safety and tolerability of gene therapy with an adeno-associated virus (AAV) borne GAD gene for parkinson's disease: an open label, phase 1 trial. *Lancet* 2007; **369**: 2097–2105.
- [4] Yang, Z. R.; Wang, H. F.; Zhao, J.; Peng, Y. Y.; Wang, J.; Guinn, B.-A.; Huang, L. Q. Recent developments in the use of adenoviruses and immunotoxins in cancer gene therapy. *Cancer Gene Ther.* 2007; **14**: 599–615.
- [5] Rossi, J.J. RNAi as a treatment for HIV-1 infection. *BioTechniques.* 2006; **40**: s25-s29.
- [6] Clinical trials. Available at: <http://www.wiley.co.uk/genetherapy/clinical/>; accessed: December 2009.
- [7] Durcan, N.; Murphy, C.; Cryan, S-A. Inhalable siRNA: potential as a therapeutic agent in the lungs. *Molecular Pharmaceutics* 2008; **5**: 559-566.
- [8] Whitehead KA, Langer R, Anderson DG. Knocking down barriers: advances in siRNA delivery. *Nat. Rev. Drug Discov.* 2009; **8**: 129–138.
- [9] Fattal, E.; Bochot, A. Ocular delivery of nucleic acids: antisense oligonucleotides, aptamers and siRNA. *Adv.Drug Deliv.Rev.* 2006; **58**: 1203-1223.
- [10] Shen, J.; Samul, R.; Silva, RL. et al. Suppression of ocular neovascularization with siRNA targeting VEGF receptor 1. *Gene Ther.* 2006; **13**: 225–234.
- [11] Alvarez, R.; Elbashir, S.; Borland, T. et al. RNA interference-mediated silencing of the respiratory syncytial virus nucleocapsid defines a potent antiviral strategy. *Antimicrob Agents Chemother* 2009; **53**: 3952–3962.
- [12] Akinc, A.; Zumbuehl, A.; Goldberg, M. et al. A combinatorial library of lipid-like materials for delivery of RNAi therapeutics. *Nat. Biotechnol.* 2008; **26**: 561–569.
- [13] Akinc, A.; Goldberg, M.; Qin, J. et al. Development of lipidoid siRNA formulations for systemic delivery to the liver. *Mol Ther.* 2009; **17**: 872–879.



- [14] Judge, AD.; Robbins, M.; Tavakoli, I. et al. Confirming the RNAi mediated mechanism of action of siRNA-based cancer therapeutics in mice. *J Clin Invest* 2009; **119**: 661–673.
- [15] Chikh, G.; de Jong, SD.; Sekirov, L. et al. Synthetic methylated CpG ODNs are potent in vivo adjuvants when delivered in liposomal nanoparticles. *Int. Immunol.* 2009; **21**: 757–767.
- [16] Singerman, L. Combination therapy using the small interfering RNA bevasiranib. *Retina* 2009; **29**: S49–S50.
- [17] Leachman, SA; Hickerson, RP; Hull, PR. et al. Therapeutic siRNAs for dominant genetic skin disorders including pachyonychia congenita. *J. Dermatol. Sci.* 2008; **51**: 151–157.
- [18] Hickerson, RP; Smith, FJ; Reeves, RE. et al. Single-nucleotide specific siRNA targeting in a dominant-negative skin model. *J. Invest. Dermatol.* 2008; **128**: 594–605.
- [19] Davis, ME. The first targeted delivery of siRNA in humans via a self-assembling, cyclodextrin polymer-based nanoparticle: from concept to clinic. *Mol. Pharm.* 2009; **6**: 659–668.
- [20] Napoli, C; Lemieux, C; Jorgensen, R. Introduction of a chimeric chalcone synthase gene into petunia results in reversible co-suppression of homologous genes in trans. *Plant Cell* 1990; **2**: 279–289.
- [21] Van der Krol, A. R.; Mur, L. A.; Beld, M.; Mol, J. N.; Stuitje, A. R. Flavonoid genes in petunia: addition of a limited number of gene copies may lead to a suppression of gene expression. *Plant Cell* 1990; **2**: 291–299.
- [22] Navina, C. D.; Sharp, P. A. The RNAi revolution. *Nature* 2004; **430**: 161–164.
- [23] Fire, A.; Xu, S.; Montgomery, M. K.; Kostas, S. A.; Driver, S. E.; Mello, C.C. Potent and specific genetic interference by double-stranded RNA in *Caenorhabditis elegans*. *Nature* 1998; **391**: 806–811.
- [24] Bernstein, E.; Caudy, A. A.; Hammond, S. M.; Hannon, G. J. Role for a bidentate ribonuclease in the initiation step of RNA interference. *Nature* 2001; **409**: 363–366.
- [25] Zhang, H.; Kolb, F. A.; Jaskiewicz, L.; Westhof, E.; Filipowicz, W. Single processing center models for human Dicer and bacterial RNase III. *Cell* 2004; **118**: 57–68.
- [26] Rand, T. A.; Ginalski, K.; Grishin, N. V.; Wang, X. Biomedical identification of Argonaute 2 as the sole protein required for RNA-induced silencing complex activity. *Proc. Natl. Acad. Sci. USA* 2004; **101**: 14385–14389.
- [27] Matranga, C. et al., Passenger-strand cleavage facilitates assembly of siRNA into Ago2-containing RNAi enzyme complexes, *Cell* 2005; **123**: 607–620.

- [28] Girmm, D. et al. Fatality in mice due to oversaturation of cellular microRNA/short hairpin RNA pathway. *Nature* 2006; **441**: 537-541.
- [29] Gary, D. J.; Puri, N.; Won, Y. Y. Polymer-based siRNA delivery: perspectives on the fundamental and phenomenological distinctions from polymer-based DNA delivery. *Journal of Controlled Release* 2007; **121**:64-73.
- [30] Sioud, M. RNA interference and innate immunity. *Adv. Drug Delivery Rev.* 2007; **121**: 64-73.
- [31] Caplen, N.J. Gene therapy progress and prospects. Downregulating gene expression: the impact of RNA interference. *Gene Ther* 2004; **11**: 1241–1248.
- [32] Hannon, G.J.; Rossi, J.J. Unlocking the potential of the human genome with RNA interference. *Nature* 2004; **431**: 371–378.
- [33] Minhyung, L. Gene regulation for effective gene therapy. *Advanced Drug Delivery Reviews* 2009; **61**: 487-488.
- [34] Dykxhoorn, D.M.; Lieberman, J. The silent revolution: RNA interference as basic biology, research tool, and therapeutic, *Annu. Rev. Med.* 2005; **56**: 401–423.
- [35] Vilgelm, A. E.; Chumakov, S. P.; Prassolov, V.S. RNA interference: biology and prospects of application in biomedicine and biotechnology. *Mol. Biol.* 2006; **40**:339– 354.
- [36] Bumcrot, D.; Manoharan, M.; Koteliansky, V.; Sah, D.W. Y. RNAi therapeutics: a potential new class of pharmaceutical drugs, *Nat. Chem. Biol.* 2006; **2**:711–719.
- [37] de Fougerolles, A.; Vornlocher, H.P.; Maraganore, J.; Lieberman, J. Interfering with disease: a progress report on siRNA-based therapeutics. *Nat. Rev. Drug Discov.* 2007; **6**: 443– 453.
- [38] Ryther, RC; Flynt, AS.; Phillips, JA; Patton, JG. siRNA therapeutics: big potential from small RNAs. *Gene Ther.* 2004; **12**: 5–11.
- [39] Aagaard, L.; Rossi, J.J.; RNAi therapeutics: principles, prospects and challenges, *Adv. Drug Deliv. Rev.* 2007; **59**: 75 –86.
- [40] Reischl, D.; Zimmer, A. Drug delivery of siRNA therapeutics: potentials and limits of nanosystems, *Nanomedicine: Nanotechnology, Biology and Medicine* 2009; **5**: 8-20.
- [41] Larson, SD.; Jackson, LN.; Chen, LA.; Rychahou, PG.; Evers, BM. Effectiveness of siRNA uptake in target tissues by various delivery methods. *Surgery* 2007; **142**: 262–9.
- [42] Schroeder, A.; Levins, C. G.; Cortez, C.; Langer, R. Anderson, D. G. Lipid-based nanotherapeutics for siRNA. *J. Intern. Med.* 2010; **267**: 9-21.

- [43] Li, S. D.; Huang, L. Non-viral is superior to viral gene delivery. *J. Controlled Release* 2007; **123**:181-183.
- [44] Mintzer, M. A. Simanek, E. E. Non viral vectors for gene Delivery. *Chemical Review* 2009; **109**:259-302.
- [45] Lehrman, S. Virus treatment questioned after gene therapy death. *Nature* 1999; **401**:517–518.
- [46] Liu Q, Muruve DA. Molecular basis of the inflammatory response to adenovirus vectors. *Gene Therapy*. 2003; **10**: 935–940.
- [47] Sun, J Y.; Anand-Jawa, V.; Chatterjee, S.; Wong KK, Jr. Immune responses to a deno-associated virus and its recombinant vectors. *Gene Therapy*. 2003; **10**:964–976.
- [48] Donahue, R. E.; Kessler, SW.; Bodine, D. et al. Helper virus induced T cell lymphoma in nonhuman primates after retroviral mediated gene transfer. *Journal of Experimental Medicine* 1992; **176**:1125–1135.
- [49] Xie, F. Y.; Woodle, M. C.; Lu, P. Y. Harnessing in vivo siRNA delivery for drug discovery and therapeutic development. *Drug discovery Today* 2006; **11**: 67–73.
- [50] Martin, S. E.; Caplen, N. J. Applications of RNA interference in mammalian systems. *Annu. Rev. Genomics Hum. Genet.* 2007; **8**: 81–108.
- [51] Liu, G.; Wong-Staal, F.; Li, Q. X. Development of new RNAi therapeutics. *Histol. Histopathol.* 2007; **22**: 211–217.
- [52] Leung, R. K.; Whittaker, P. A. RNA interference: from gene silencing to gene-specific therapeutics. *Pharmacol. Ther.* 2005; **107**: 222–239.
- [53] Aigner, A. Delivery Systems for the Direct Application of siRNAs to Induce RNA Interference (RNAi) In Vivo. *J. Biomed. Biotechnol.* 2006; **2006**: 71659.
- [54] Akhtar, S. Benter, I. F. Non viral delivery of synthetic siRNAs in vivo, *J. Clin. Invest.* 2007; **117**: 3623 – 3632.
- [55] Park, T.G.; Jeong, J.H.; Kim, S.W. Current status of polymeric gene delivery systems, *Adv. Drug Deliv. Rev.* 2006; **58**: 467 –486.
- [56] Chiu, Y.L.; Rana, T.M. RNAi in human cells: basic structural and functional features of small interfering RNA. *Mol. Cell* 2002; **10**: 549-561.
- [57] Chiu, Y.L.; Rana, T.M. siRNA function in RNAi: a chemical modification analysis. *RNA* 2003; **9**: 1034-1048.
- [58] Aigner, A. Non viral in vivo delivery of therapeutic small interfering RNAs. *Curr. Opin. Mol. Ther.* 2007; **9**: 345-352.

- [59] Juliano, R; Alam, M.R; Dixit, V; Kang, H. Mechanisms and strategies for effective delivery of antisense and siRNA oligonucleotides. *Nucleic Acids Res* 2008; **36**: 4158–4171.
- [60] De Paula, D; Bentley, M.V; Mahato, R.I. Hydrophobization and bioconjugation for enhanced siRNA delivery and targeting. *RNA* 2007; **13**: 431–456.
- [61] Corey, R. D. Chemical modification: the key to clinical application of RNA interference? *J. Clin. Invest.* 2007; **117**:3615-3622.
- [62] Won, J.K; and Sung, W.K. Efficient siRNA delivery with Non-viral Polymeric Vehicles. *Pharmaceutical Research* 2009; **26**: 657-666.
- [63] Baigude, H.; Rana, T.M. Delivery of therapeutic RNAi by nanovehicles. *ChemBioChem* 2009; **10**: 2449-2454.
- [64] Sioud, M.; Sorensen, DR. Cationic liposome-mediated delivery of siRNAs in adult mice. *Biochem Biophys Res Commun* 2003; **312**: 1220-1225.
- [65] Bouxsein, NF.; McAllister, CS.; Ewert, KK.; Samuel, CE.; Safinya, CR. Structure and gene silencing activities of monovalent and pentavalent cationic lipid vectors complexed with siRNA. *Biochemistry* 2007; **46**: 4785-4792.
- [66] Spagnou S, Miller AD, Keller M. Lipidic carriers of siRNA: differences in the formulation, cellular uptake, and delivery with plasmid DNA. *Biochemistry* 2004; **43**: 13348-13356.
- [67] Zimmermann, TS. ; Lee, AC.; Akinc, A. et al. RNAi-mediated gene silencing in non-human primates. *Nature* 2006; **441**:111–114.
- [68] Landen, CN. Jr.; Chavez-Reyes, A. ; Bucana, C. et al. Therapeutic EphA2 gene targeting in vivo using neutral liposomal small interfering RNA delivery. *Cancer Res.* 2005; **65**: 6910–6918.
- [69] Wang, Y.; Gao, S.; Ye, W-H.; Yoon, HS; Yang, Y-Y. Co-delivery of drugs and DNA from cationic core-shell nanoparticles self-assembled from a biodegradable copolymer. *Nat. Mater.* 2006; **5**:791-796.
- [70] Kakizawa, Y.; Furukawa, S.; Kataoka, K. Block copolymer-coated calcium phosphate nanoparticles sensing intracellular environment for oligodeoxynucleotide and siRNA delivery. *J. Control Release* 2004; **97**:345-356.
- [71] Kataoka, K.; Itaka, K.; Nishiyama, N.; Yamasaki, Y.; Oishi, M.; Nagasaki, Y. Smart polymeric micelles as nanocarriers for oligonucleotides and siRNA delivery. *Nucleic Acids Res. Suppl* 2005; **49**: 17-18.
- [72] Katas, H.; Alpar, HO. Development and characterisation of chitosan nanoparticles for siRNA delivery. *J. Control Release* 2006; **115**: 216-225.

- [73] Gorbatyuk, M.; Justilien, V.; Liu, J.; Hauswirth, WW; Lewin, AS. Suppression of mouse rhodopsin expression in vivo by AAV mediated siRNA delivery. *Vision Res.* 2007; **47**:1202-1208.
- [74] Nedjma, T.; Jean-Rémi, B. ; Ali, T.; Hind, E.; Hervé, H. ; Andrei, M. et al. Efficacy of siRNA nanocapsules targeted against the EWS–Fli1 oncogene in Ewing sarcoma. *Pharm. Res.* 2006; **23**:892-900.
- [75] Lee, H.; Mok, H.; Lee, S.; Oh, YK; Park, TG. Target-specific intracellular delivery of siRNA using degradable hyaluronic acid nanogels. *J. Control Release* 2007; **119**:245-252.
- [76] Segura, T.; Hubbell, JA. Synthesis and in vitro characterization of an ABC triblock copolymer for siRNA delivery. *Bioconjug. Chem.* 2007; **18**:736-745.
- [77] Takeshita, F.; Minakuchi, Y.; Nagahara, S.; Honma, K.; Sasaki, H.; Hirai, K. et al. Efficient delivery of small interfering RNA to bone-metastatic tumors by using atelocollagen in vivo. *Proc Natl. Acad. Sci. U. S. A* 2005; **102**:12177-12182.
- [78] Svintradze, DV; Mrevlishvili, GM. Fiber molecular model of atelocollagen-small interfering RNA (siRNA) complex. *Int. J. Biol. Macromol.* 2005; **37**:283-286.
- [79] Minakuchi, Y.; Takeshita, F.; Kosaka, N.; Sasaki, H.; Yamamoto, Y.; Kouno, M. et al. Atelocollagen-mediated synthetic small interfering RNA delivery for effective gene silencing in vitro and in vivo. *Nucleic Acids Res.* 2004;**32**:e109
- [80] Crombez L, Charnet A, Morris MC, Aldrian-Herrada G, Heitz F, Divita G. A non-covalent peptide-based strategy for siRNA delivery. *Biochem. Soc. Trans.* 2007; **35**:44-46.
- [81] Vogel, V.; Lochmann, D.; Weyermann, J.; Mayer, G.; Tziatzios, C.; van den Broek, JA. et al. Oligonucleotide-protamine-albumin nanoparticles: preparation, physical properties, and intracellular distribution. *J. Control Release* 2005; **103**:99-111.
- [82] Chiu, Y. L., Ali, A., Chu, C. Y., Cao, H., and Rana, T. M. Visualizing a correlation between siRNA localization, cellular uptake, and RNAi in living cells. *Chem. Biol.* 2004; **11**: 1165– 1175.
- [83] Turner, J. J.; Jones, S.; Fabani, M. M.; Ivanova, G.; Arzumanov, A. A.; Gait. M. J. RNA targeting with peptide conjugates of oligonucleotides, siRNA and PNA. *Blood Cells Mol. Dis.* 2007; **38**:1–7.
- [84] Muratovska, A.; Eccles, M. R. Conjugate for efficient delivery of short interfering RNA (siRNA) into mammalian cells. *FEBS Lett.* 2004; **558**:63–68.
- [85] Davidson, T. J.; Harel, S.; Arboleda, V. A.; Prunell, G. F.; Shelanski, M. L.; Greene, L. A.; Troy, C. M. Highly efficient small interfering RNA delivery to primary mammalian neurons induces microRNA-like effects before mRNA degradation. *J. Neurosci.* 2004; **24**:10040–10046.

- [86] Chu, T. C., Twu, K. Y., Ellington, A. D., and Levy, M. Aptamer mediated siRNA delivery. *Nucleic Acids Res.* 2006; **34**: e73.
- [87] Hicke, B. J., and Stephens, A. W. Escort aptamers: a delivery service for diagnosis and therapy. *J. Clin. Invest.* 2000; **106**: 923–928.
- [88] Akerman, M. E., Chan, W. C., Laakkonen, P., Bhatia, S. N., and Ruoslahti, E. Nanocrystal targeting in vivo. *Proc. Natl. Acad. Sci. U.S.A.* 2002; **99**: 12617–12621.
- [89] Gupta, A. K., and Gupta, M. Synthesis and surface engineering of iron oxide nanoparticles for biomedical applications. *Biomaterials* 2005; **26**: 3995–4021.
- [90] Kam, N. W., Liu, Z., and Dai, H. Functionalization of carbon nanotubes via cleavable disulfide bonds for efficient intracellular delivery of siRNA and potent gene silencing. *J. Am. Chem. Soc.* 2005; **127**: 12492–12493.
- [91] Akhtar, S.; Hughes, M. D.; Khan, A.; Bibby, M.; Hussain, M.; Nawaz, Q.; Double, J.; Sayyed, P. The delivery of antisense therapeutics. *Adv. Drug Deliv. Rev.* 2000; **44**:3–21.
- [92] Hughes, M. D.; Hussain, M.; Nawaz, Q.; Sayyed, P.; Akhtar, S. The cellular delivery of antisense oligonucleotides and ribozymes. *Drug Discov. Today.* 2001; **6**:303–315.
- [93] Gilmore, I. R.; Fox, S. P.; Hollins, A. J.; Sohail, M.; Akhtar, S. The design and exogenous delivery of siRNA for post-transcriptional gene silencing. *J. Drug Target.* 2004; **12**:315–340.
- [94] Kawakami, S.; Hashida, M. Targeted delivery systems of small interfering RNA by systemic administration. *Drug Metab. Pharmacokinet.* 2007; **22**:142–151.
- [95] Davis, M. E. Non-viral gene delivery systems. *Curr. Opin. Biotechnol.* 2002; **13**: 128-131.
- [96] Zhao, Z.; Wang, J.; Mao, H. Q.; Leong, K. W. Polyphosphoesters in drug and gene delivery. *Adv. Drug Deliv. Rev.* 2003; **55**: 483-499.
- [97] Urban-Klein, B.; Werth, S.; Abuharbeid, S.; Czubayko, F.; Aigner, A. RNAi-mediated gene-targeting through systemic application of polyethylenimine (PEI)-complexed siRNA in vivo, *Gene Ther.* 2005; **12**: 461–466.
- [98] Read, L. M.; Singh, S.; Ahmed, Z.; Stevenson, M.; Briggs, S. S.; Oupicky, D.; Barrett, B. I.; Spice, R.; Kendall, M.; Berry, M.; Preece, A. J.; Logan, A.; Seymour, W. A versatile reducible polycation-based system for efficient delivery of a broad range of nucleic acid. *Nucleic Acids Res.* 2005; **33**:e86.
- [99] Thomas, M.; Lu, J. J.; Ge, Q.; Zhang, C.; Chen, J.; Klibanov, M. A. Full deacylation of polyethylenimine dramatically boosts its gene delivery efficiency and specificity to mouse lung. *Proc. Natl. Acad. Sci. USA* 2005; **102**:5679-5684.

- [100] Grayson, C. A.; Doody, M. A.; Putnam, D. Biophysical and structural characterization of polyethylenimine-mediated siRNA delivery *in vitro*. *Pharm. Res.* 2006; **23**:1868-1876.
- [101] Breunig, M.; Hozsa, C.; Lungwitz, U.; Watanabe, K.; Umeda, I.; Kato, H.; Goepferich, A. Mechanistic investigation of poly(ethyleneimine)-based siRNA delivery: disulfide bonds boost intracellular release of the cargo, *J. Control. Release* 2008; **130**: 57–63.
- [102] Merdan, T.; Kunath, K.; Fischer, D.; Kopecek, J.; Kissel, T. Intracellular processing of poly (ethylene imine)/ribozyme complexes can be observed in living cells by using confocal laser scanning microscopy and inhibitor experiments, *Pharm. Res.* 2002;**19**:140–146.
- [103] Akine, A.; Thomas, M.; Klibanov, A.M.; Langer, R. Exploring polyethylenimine mediated DNA transfection and the proton sponge hypothesis, *J. Gene Med.* 2005;**7**: 657–663.
- [104] Boussif, O. *et al.* A versatile vector for gene and oligonucleotide transfer into cells in culture and *in vivo*: polyethylenimine. *Proc. Natl Acad. Sci. USA* 1995; **92**: 7297–7301.
- [105] Godbey, W.T.; Barry, M.A.; Saggau, P.; Wu, K.K.; Mikos, A.G. Poly(ethylenimine)-mediated transfection: a new paradigm for gene delivery. *J. Biomed. Mater. Res.* 2000; **51**:321–328.
- [106] Grzelinski, M. *et al.*, RNA interference-mediated gene silencing of pleiotrophin through polyethylenimine-complexed small interfering RNAs *in vivo* exerts antitumoral effects in glioblastoma xenografts. *Hum. Gene Ther.* 2006; **17**:751–766.
- [107] Schiffelers, R.M. *et al.*, Cancer siRNA therapy by tumor selective delivery with ligand-targeted sterically stabilized nanoparticles. *Nucleic Acids Res.* 2004; **32**: e149.
- [108] Richards Grayson, A.C.; Doody, A.M.; Putnam, D. Biophysical and structural characterization of polyethylenimine-mediated siRNA delivery *in vitro*. *Pharm. Res.* 2006; **23**:1868–1876.
- [109] Kircheis, R.; Wightman, L.; Wagner, E. Design and gene delivery activity of modified polyethylenimines. *Adv. Drug Deliv. Rev.* 2001; **53**: 341– 358.
- [110] Nimesh, S. *et al.* Polyethylenimine nanoparticles as efficient transfecting agents for mammalian cells. *J. Control. Release* 2006; **110**: 457–468.
- [111] Swami, A. *et al.*, Imidazolyl-PEI modified nanoparticles for enhanced gene delivery. *Int. J. Pharm.* 2007; **335**:180–192.
- [112] Tietze, N.; Pelisek, J.; Philipp, A. *et al.* Induction of apoptosis in murine neuroblastoma by systemic delivery of transferrin-shielded siRNA polyplexes for down regulation of Ran. *Oligo-nucleotides* 2008; **18**: 161–74.

- [113] Hunter, AC. Molecular hurdles in polyfectin design and mechanistic background to polycation induced cytotoxicity. *Adv Drug Deliv. Rev.* 2006; **58**: 1523–1531.
- [114] Nimesh, S. et al. Influence of acyl chain length on transfection mediated by acylated PEI nanoparticles. *Int. J. Pharm.* 2007; **337**:265–274.
- [115] Zintchenko, A.; Philipp, A.; Dehshahri, A.; Wagner, E. Simple modifications of branched PEI lead to highly efficient siRNA carriers with low toxicity. *Bioconjug. Chem.* 2008; **19**:1448–1455.
- [116] Shim, M.S.; Kwon, Y.J. Controlled delivery of plasmid DNA and siRNA to intracellular targets using ketalized polyethylenimine. *Biomacromolecules* 2008; **9**:444–455.
- [117] Jeong Soon, J.; So Yeon, K.; Sang Bong, L.; Kyung Ok, K.; Joong Soo, H. Young Moo, L. Poly(ethylene glycol)/poly( $\epsilon$ -caprolactone) diblock copolymeric nanoparticles for non-viral gene delivery: the role of charge group and molecular weight in particle formation, cytotoxicity and transfection. *J Control Release* 2006; **113**:173-182.
- [118] Conner, S. D.; Schmid, S. L. Regulated portals of entry into the cell. *Nature* 2003; **422**: 37-44.
- [119] Mayor, S.; Pagano, R. E. Pathways of clathrin-independent endocytosis. *Nat. Rev. Mol. Cell Biol.* 2007; **8**: 603-612.
- [120] Chithrani, B. D.; Ghazani, A. A.; Chan, W. C. Determining the size and shape dependence of gold nanoparticle uptake into mammalian cells. *Nano Lett* 2006; **6**:662-668.
- [121] Gratton, S. E. A.; Ropp, P. A.; Pohlhaus, P. D.; Luft, J. C.; Madden, V. J.; Napier, M. E.; DeSimone, J. M. The effect of particle design on cellular internalization pathways. *Proc. Natl. Acad. Sci. U.S.A* 2008; **105**:11613-11618.
- [122] Jiang, W.; KimBetty, Y. S.; Rutka, J. T.; ChanWarren, C. W. Nanoparticle-mediated cellular response is size-dependent. *Nat Nano* 2008; **3**:145-150.
- [123] Aa,M.A.E.M.; Huth,U.S.; Haefele,S.Y.; Schubert,R.; Oosting,R.S.; Mastrobattista,E.; Hennink,W.E.; Peschka-Suess,R.; Koning,G.A.; Crommelin,D.J.A. Cellular uptake of cationic polymer-DNA complexes via caveolae plays a pivotal role in gene transfection in COS-7 cells. *Pharm. Res.* 2007; **24**:1590-1598.
- [124] Lundqvist, M.; Stigler, J.; Elia, G.; Lynch, I.; Cedervall, T.; Dawson, K. A. Nanoparticle size and surface properties determine the protein corona with possible implications for biological impacts. *Proc. Natl. Acad. Sci. U.S.A* 2008; **105**:14265-14270.
- [125] Giljohann, D. A.; Seferos, D. S.; Patel, P. C.; Millstone, J. E.; Rosi, N. L.; Mirkin, C. A. Oligonucleotide loading determines cellular uptake of DNA-modified gold nanoparticles. *Nano Lett* 2007; **7**:3818-3821.



- [126] Hauck, T. S.; Ghazani, A. A.; Chan, W. C. W. Assessing the effect of surface chemistry on gold nanorod uptake, toxicity, and gene expression in mammalian cells. *Small* 2008; **4**:153-159.
- [127] Neu, M.; Fischer, D.; Kissel, T. Recent advances in rational gene transfer vector design based on poly(ethylene imine) and its derivatives. *J. Gene Med.* 2005; **7**: 992–1009.
- [128] Pozharski, E. V.; MacDonald, R. C. Single lipoplex study of cationic lipid-DNA, self-assembled complexes. *Mol. Pharm.* 2007; **4**: 962–974.
- [129] Chesnoy, S.; Huang, L. Structure and function of lipid-DNA complexes for gene delivery. *Annu. Rev. Biophys. Biomol. Struct.* 2000; **29**: 27–47.
- [130] Ghosh, P.; Han, G.; De, M.; Kim, C. K.; Rotello, V. M. Gold nanoparticles in delivery applications. *Adv. Drug Delivery Rev.* 2008; **60**: 1307-1315.
- [131] Otsuka, H., Akiyama, Y. , Nagasaki, Y. , Kataoka, K. Quantitative and reversible lectin-induced association of gold nanoparticles modified with  $\alpha$  - lactosyl- $\omega$ - mercapto-poly(ethylene glycol). *J. Am. Chem. Soc.* 2001; **123**: 8226–8230.
- [132] Idegami, K.; Chikae, M.; Kerman, K.; Nagatani, N.; Yuhi, T.; Endo, T.; Tamiya, E. Gold nanoparticle-based redox signal enhancement for sensitive detection of human chorionic gonadotropin hormone. *Electroanalysis* 2007; **20**: 14-21.
- [133] Katti, K. V.; Kannan, R.; Katti, K.; Kattumori, V.; Pandrapraganda, R.; Rahing, V.; Cutler, C.; Boote, E. J.; Casteel, S. W.; Smith, C. J.; Robertson, J. D.; Jurrison, S. S. Hybrid gold nanoparticles in molecular imaging and radiotherapy. *Czechoslovak Journal of Physics* 2006; **56**: d23-d34.
- [134] Hainfeld, J. F.; Slatkin, D.; Smilowitz, H. M. The use of gold nanoparticles to enhance radiotherapy in mice. *Physics in Medicine & Biology* 2004; **49**: N309-N315.
- [135] Hirsch, L.R., Stafford, R.J., Bankson, J.A., Sershen, S.R., Rivera , B., Price, R.E., Hazle, J.D., Halas, N.J., West , J.L. Nanoshell-mediated near-infrared thermal therapy of tumors under magnetic resonance guidance. *Proc. Natl. Acad. Sci. U.S.A.* 2003; **100**: 13549–13554.
- [136] Sahoo, W.S. Y.; Swihart, M. T. Gold nanoparticles surface-terminated with bifunctional ligands. *Colloids and Surfaces, A: Physicochemical and Engineering Aspects* 2004; **246**: 109-113.
- [137] Thomas, M., Klibanov, A. M. Conjugation to gold nanoparticles enhances polyethylenimine's transfer of plasmid DNA into mammalian cells. *Proc. Natl. Acad. Sci. U.S.A.* 2003; **100**: 9138–9143.
- [138] Liu, Y.; Franzen, S. Factors determining the efficacy of nuclear delivery of antisense oligonucleotides by gold nanoparticles. *Bioconjug. Chem.* 2008; **19**: 1009-1016.

- [139] Rosi, N.L., Giljohann, D.A., Thaxton, C.S., Lytton-Jean, A .K., Han, M.S., Mirkin, C.A . Oligonucleotide-modified gold nanoparticles for intracellular gene regulation. *Science* 2006; **312**: 1027–1030.
- [140] Lee, S. H.; Bae, K. H.; Kim, S. H.; Lee, K. R.; Park, T. G. Amine-functionalized gold nanoparticles as non-cytotoxic and efficient intracellular siRNA delivery carriers. *Int. J. Pharm.* 2008; **364**: 94-101.
- [141] Giljohann, D. A.; Seferos, D. S.; Prigodich, A. E.; Patel, P. C.; Mirkin, C. A. Gene regulation with polyvalent siRNA-nanoparticle conjugates. *J. Am. Chem. Soc.* 2009; **131**: 2072-2073.
- [142] Boisselier, E.; Astruc, D. Gold nanoparticles in nanomedicine: preparations, imaging, diagnostics, therapies and toxicity. *Chem. Soc. Rev.* 2009; **38**: 1759-1782.
- [143] Storhoff, J.J., Elghanian, R., Mucic, R.C., Mirkin, C.A., Letsinger, R.L. One-pot colorimetric differentiation of polynucleotides with single base imperfections using gold nanoparticle probes. *J. Am. Chem. Soc.* 1998; **120**: 1959–1964.
- [144] Oishi, M.; Nakaogami, J.; Ishii, T.; Nagasaki, Y. Smart PEGylated gold nanoparticles for the cytoplasmic delivery of siRNA to induce enhanced gene silencing. *Chem. Lett.* 2006; **35**: 1046–1047.
- [145] Lee, J. S.; Green, J. J.; Love, K. T.; Sunshine, J.; Langer, R. D.; Anderson, G. Gold, poly( $\beta$ -amino ester) nanoparticles for small interfering RNA delivery. *Nano Lett.* 2009; **9**: 2402-2406.
- [146] Decher, G.; Schmitt, J. Fine-tuning of the film thickness of ultrathin multilayer films composed of consecutively alternating layers of anionic and cationic polyelectrolytes. *Prog. Colloid Polym. Sci.* 1992; **89**:160–164.
- [147] Decher, G. Fuzzy nanoassemblies: Toward layered polymeric multicomposites. *Science* 1997; **277**: 1232–1237.
- [148] Thierry, B.; Winnik, F.M.; Merhi, Y.; Silver, J.; Tabrizian, M. Bioactive coatings of endovascular stents based on polyelectrolyte multilayers. *Biomacromolecules* 2003; **4**:1564–1571.
- [149] Thierry, B. *et al.* Delivery platform for hydrophobic drugs: Prodrug approach combined with self-assembled multilayers. *J. Am. Chem. Soc.* 2005; **127**:1626–1627.
- [150] Berg, M.C.; Zhai, L.; Cohen, R.E.; Rubner, M.F. Controlled drug release from porous polyelectrolyte multilayers. *Biomacromolecules* 2006; **7**:357–364.
- [151] Wood, K.C.; Chuang, H.F.; Batten, R.D.; Lynn, D.M.; Hammond, P.T. Controlling interlayer diffusion to achieve sustained, multiagent delivery from layer-by-layer thin films. *Proc. Natl. Acad. Sci. U.S.A.* 2006; **103**:10207–10212.

- [152] Nguyen, PM.; Zacharia, NS.; Verploegen, E.; Hammond, PT. Extended release antibacterial layer-by-layer films incorporating linear-dendritic block copolymer micelles. *Chem. Mat* 2007; **19**:5524–5530.
- [153] Zhang, JT.; Chua, LS; Lynn, DM. Multilayered thin films that sustain the release of functional DNA under physiological conditions. *Langmuir* 2004; **20**:8015–8021.
- [154] Jewell, CM; Zhang, J.; Fredin, NJ; Lynn, DM. Multilayered polyelectrolyte films promote the direct and localized delivery of DNA to cells. *J Control Rel.* 2005; **106**:214–223.
- [155] Meyer, F.; Ball, V.; Schaaf, P.; Voegel, JC; Ogier, J. Polyplex-embedding in polyelectrolyte multilayers for gene delivery. *Biochim Biophys Acta* 2006; **1758**:419–422.
- [156] Jessel, N. *et al.* Multiple and time-scheduled in situ DNA delivery mediated by beta-cyclodextrin embedded in a polyelectrolyte multilayer. *Proc. Natl. Acad. Sci. U.S.A.* 2006; **103**:8618–8621.
- [157] Recksiedler, C.L.; Deore, B.A.; Freund, M.S.; A novel layer-by-layer approach for the fabrication of conducting polymer/RNA multilayer films for controlled release. *Langmuir* 2006; **22**: 2811–2815.
- [158] Dimitrova, M.; Affolter, C.; Meyer, F.; Nguyen, I.; Richard, D. G.; Schuster, C.; Bartenschlager, R.; Voegel, J. C.; Ogier, j.; Baumert, T. F. Sustained delivery of siRNAs targeting viral infection by cell-degradable multilayered polyelectrolyte films. *PNAS*. 2008; **105**:16320-16325.
- [159] Caruso, F. Nanoengineering of particle surfaces. *Adv. Mater.* 2001; **13**: 11-22.
- [160] Caruso, F. *Colloids and colloid assemblies: Synthesis, modification, organization and utilization of colloidal particles*; Ed.; Wiley-VCH, Weinheim, 2004.
- [161] Caruso, F.; Caruso, R. A.; Möhwald, H. Nanoengineering of inorganic and hybrid hollow spheres by colloidal templating. *Science* 1998; **282**: 1111-1114.
- [162] Donath, E.; Sukhorukov, G. B.; Caruso, F.; Davis, S. A.; Möhwald, H. Novel hollow polymer shells by colloid-templated assembly of polyelectrolytes. *Angew. Chem. Int. Ed.* 1998; **37**: 2201-2205.
- [163] Decher, G.; Schlenoff, J. *Multilayer thin films; Sequential assembly of nanocomposite materials*; Eds.; Wiley-VCH: Weinheim, 2003.
- [164] Gittins, D. I.; Caruso, F. Tailoring the polyelectrolyte coating of metal nanoparticles. *J. Phys. Chem. B* 2001; **105**: 6846-6852.
- [165] Mayya, K. S.; Shoeler, B.; Caruso, F. Preparation and organization of nanoscale polyelectrolyte-coated gold nanoparticles. *Adv. Funct. Mater.* 2003; **13**: 185-188.

- [166] Schneider, G.; Decher, G. Functional core/shell nanoparticles via Layer-by-Layer assembly. Investigation of the experimental parameters for controlling particle aggregation and for enhancing dispersion stability. *Langmuir* 2008; **24**:1778–1789.

## **Chapter 2**

### **Preparation, Characterization, and Stabilization of Gold Nanoparticles**

Asmaa Elbakry<sup>1</sup>, Alaa Zaky<sup>1</sup>, Renate Liebl<sup>1</sup>, Reinhard Rachel<sup>2</sup>, Miriam Breunig<sup>1</sup>,  
Achim Goepferich<sup>1</sup>

<sup>1</sup>Department of Pharmaceutical Technology, University of Regensburg,  
Universitätsstraße 31, 93040 Regensburg, Germany

<sup>2</sup>Centre for Electron Microscopy at the Institute for Anatomy, University of  
Regensburg, Universitätsstraße 31, 93040 Regensburg, Germany

**Abstract**

Gold colloids have fascinated scientists for over a century and are now widely used in chemistry, biology, physics and medicine. In particular, gold nanoparticles (AuNPs) play a vital role in nanoscience and nanotechnology. To date, a number of procedures utilizing both physical and chemical methods for the synthesis of AuNPs have been reported for the production of AuNPs of different sizes, shapes, and surface functionalities related to their practical applications. Due to their unique features (tuneable core size, monodispersity, large surface to volume ratio, and easy functionalization), AuNPs are also very promising candidates for nucleic acid delivery. The goal of this study was to prepare AuNPs that are stable under physiological conditions and can be coated with both positively charged polycation and negatively charged nucleic acid via Layer-by-Layer (LbL) technology in a subsequent step. First, AuNPs were prepared via the citrate reduction method, followed by thiol stabilization to obtain stabilized nanoparticles suitable for further coating steps. Afterwards, the mercaptoundecanoic acid stabilized AuNPs (MUA-AuNPs) were investigated at different pH values and ionic strengths to identify the optimum conditions for the production of stable monodisperse nanoparticles. MUA-AuNPs showed a good stability over time with low ionic strength (1-10 mM NaCl), and in a wide range of pH values, which allowed further coating at physiological pH. In summary, with these optimized conditions the MUA-AuNPs provide a good foundation for further coating by polyelectrolytes via LbL technology.

## 1. Introduction

Gold nanoparticles (AuNPs) play a key role in nanoscience and nanotechnology, with applications in fields as diverse as biology, medicine, physics, and chemistry [1]. The ability to control the size, shape, and surface functionalization in order to yield certain surface properties and manipulate the colloid stability of the AuNPs dispersions presents important issues related to practical applications of this technology [2, 3]. The synthesis of AuNPs has gained great interest in recent years, due to their unique electronic, optical, magnetic, chemical, and biological properties. The first synthesis of gold colloids was reported 150 years ago, when Michael Faraday used phosphorus to reduce  $\text{AuCl}_4^-$  ions [4]. Since then, a plethora of different synthetic procedures have been used to obtain AuNPs of different size, shape and dispersion media (either aqueous or non aqueous) according to their desired applications [5-7]. Aqueous gold nanoparticle dispersions are the most common preparation method, especially for biomedical and biological applications. The most popular and simplest method is the citrate reduction technique, which was introduced by Turkevitch in 1951 via reduction of hydrogen tetrachloroaurate ( $\text{HAuCl}_4$ ) in boiling sodium citrate solution [8]. Subsequently, Frens reported in 1973 that nanosized AuNPs from 15 to 150 nm can be obtained through an adequate control of the ratio of tri-sodium citrate to  $\text{HAuCl}_4$ , with higher ratios yielding smaller particles [9, 10]. The citrate anions have dual functions. Initially they act as the reducing agent to reduce  $\text{Au}^{+3}$  to  $\text{Au}^0$ , and they then act as a stabilizing agent by forming a layer of citrate anions on top of the nanoparticle surface, which repels the particles from contacting each other and thus preventing the aggregation of the particles [11,12]. Recently, Polte et al. described the mechanism of gold nanoparticle formation via the citrate reduction method, where four-step nucleation and growth process were proposed [13]. In this mechanism, particles are formed through a sequence of reaction steps with the fast initial formation of small nuclei of nanoparticles, followed by the coalescence of the nuclei into bigger nanoparticles. The third step comprises a slow growth of particles sustained by ongoing reduction of gold precursor as well as a further coalescence, and finally subsequent fast reduction ending with the complete consumption of the precursor species. Throughout these steps the colour of the solution changes from pale yellow to dark violet, eventually is ending in a brilliant deep red colour due to the formation of nanoparticles. This characteristic red colour of AuNPs is due to their strong light absorption in the visible region, caused by the collective oscillation of

surface electrons after exposure to light. This phenomenon is called surface plasmon resonance (SPR) [14]. The surface plasmon resonance depends mainly on the size (e.g AuNPs of 15 nm have a SPR of about 519 nm), shape, composition of particles, and the dielectric properties of the surrounding medium [15, 16]. Therefore, it is considered one of the most important parameters in the characterization of AuNPs. Consequently, particle aggregation, surface modification, and changes in the surrounding dielectric medium can be measured as either a peak broadening or peak shift in the absorbance spectra [17].

The adsorption of citrate anions on the gold surface negatively charges the particles and induces enough electrostatic repulsion between individual particles to keep them separately dispersed in the synthesis medium [18-21]. However, these molecules are weakly bound to the gold surface and form a loose shell of ligands, which is not suitable for further modification steps with polyelectrolytic coatings via the Layer-by-Layer (LbL) technique. It is proposed that the polycation/polyanion electrostatic attraction in multilayers is stronger than the one between the positive polyelectrolyte and the surface of the AuNPs. This would cause dewrapping of the positive polymer, resulting in a solution of bare gold particles and free polyelectrolyte [22]. This effect may be overcome by covalently immobilizing the surface charge on the nanoparticles by the use of a suitable molecule, instead of the chemisorbed surface charge from layers of citrate ions. Therefore, the use of ligands stronger than citrate was a major improvement for the synthesis and handling of AuNPs [15]. Thiols are the most important type of stabilizing agents for AuNPs of any size. This is because the thiol group is covalently attached to the nanoparticle surface, which forms strong covalent Au-S bonds as shown in Figure 1 [15]. This stabilization of AuNPs with thiol is an electrostatic stabilization.



**Figure 1:** Thiol stabilization of AuNPs



There are two basic modes to stabilize AuNPs [23]. The one already described is the electrostatic stabilization, based on the electrical double layer repulsion between the particles. The other is steric stabilization, achieved by the coordination of sterically bulky organic molecules such as polymers that act as protective shields on the metallic surface. The main differences between steric and electrostatic stabilization are summarized in (Table 1). An electrostatic-stabilized dispersion will not be stable and will coagulate on the addition of high concentrations of electrolytes. In contrast, with steric stabilization the dimensions of polymer chains (the steric hindrance of polymer chain) display no such dramatic sensitivity to polyelectrolytes; therefore sterically stabilized dispersions are relatively insensitive to the presence of electrolytes.

**Table 1:** Comparison between steric and electrostatic stabilization

Item	Steric stabilization	Electrostatic stabilization
Stability	Independent of the ionic strength and pH	Stabilization depends on the ionic strength and pH of the solvent
Electrolyte	Insensitive to electrolyte	Coagulate on addition of electrolyte
Media	Effective in both aqueous and non aqueous dispersion	Effective mainly in aqueous dispersion
Colloid	Effective at high and low colloid concentration	ineffective at high colloid concentration
Aggregation	Reversible flocculation possible	Coagulation usually irreversible

In addition, electrostatic stabilization is less effective in non aqueous dispersion media than it is in aqueous media. This is primarily due to the low relative dielectric constant of most non aqueous media. Moreover, the coagulation of electrostatic-stabilized particles induced by the addition of electrolyte is usually irreversible. In contrast, the flocculation of sterically stabilized dispersions can usually be reversed spontaneously.

Although steric stabilization has several advantages over electrostatic stabilization, we will focus on electrostatic stabilization. This is due to the fact that the charged surface of the AuNPs is necessary for the further deposition of the charged polymers (polyelectrolytes). This means that for the coating of AuNPs via the LbL technique, an electrostatic interaction between positively and negatively charged

polyelectrolytes is required for proper layer buildup. Therefore, we will focus on the factors that influence electrostatic stabilization of colloidal nanoparticles.

Most colloids will acquire a surface electric charge when dispersed in a polar medium such as water. This electric charge can be generated through the ionization of a surface functional group on the colloid, ion adsorption, or by the partial and unequal ion dissolution of the colloidal material [24]. An important consequence of the charge on the particle surface is that an electrical double layer around the colloid is produced in polar solutions. The double layer consists of two regions of charge as shown in (Figure 2).

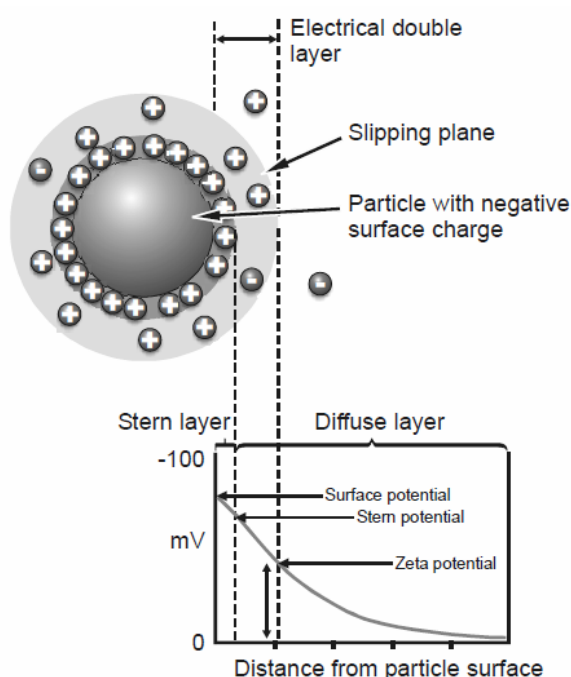


**Figure 2:** A schematic representation of the electrical double layer and Zeta potential of a charged particle in a polar environment [25]

Counterions in the region closest to the charged wall surface are strongly bound to the surface. This immobile layer is called the Stern or Helmholtz layer. The region adjacent to the Stern layer is called the diffuse layer and contains loosely and thus relatively mobile ions. Within the diffuse layer there is a notional boundary inside which the ions and particles form a stable entity. This boundary is called the surface of hydrodynamic shear, or slipping plane. The potential that exists at this boundary is known as the zeta potential ( $\xi$ -potential), which is very important parameter in the theory of interaction of colloidal particles [24]. The thickness of the electric double layer is known as the Debye-Huckel length  $K^{-1}$ . It is reciprocally proportional to the

square root of the ion concentration [24]. The electric potential associated with the double layer decreases as a reciprocal function of the distance from the particle and approaches zero as the counterions gradually reduce the effect of the field created by the surface. When two particles approach each other, the overlap of the counterions in the diffuse layer gives rise to Coulombic repulsion force between the particles and repulsion potential. With respect to particle-particle interactions, which determine colloid stability, the most widely accepted quantitative model (described by Derjaguin and Landau, and independently by Verwey and Overbeek) is known as (DLVO) theory [26]. This theory states that the total free energy of interaction is composed of two terms, Van der Waals and electrostatic interactions, as shown in equation 1.

$$V_T = V_A + V_R \quad (1)$$

In this equation,  $V_T$  is the total interaction energy,  $V_A$  is the attractive potential energy, and  $V_R$  is the repulsive potential energy.

Van der Waals forces ( $V_A$ ) between two identical particles are generally attractive. Electrostatic forces ( $V_R$ ) due to the overlapping of electrical double layers are generally repulsive. Figure 3 illustrates the potential energy between two particles as a function of interparticle distance. In brief, if the Coulombic repulsion force is high enough to counteract the Van der Waals force, then the electrostatic repulsion will prevent the particles from aggregation [26].

The combination of the two interactions typically generates an energy barrier. Hence, the height of the energy barrier determines whether a colloid will be stable or undergo coagulation. Factors such as the surface potential and the electrolyte concentration (ionic strength) influence the height of the energy barrier and can be used to control colloid stability.

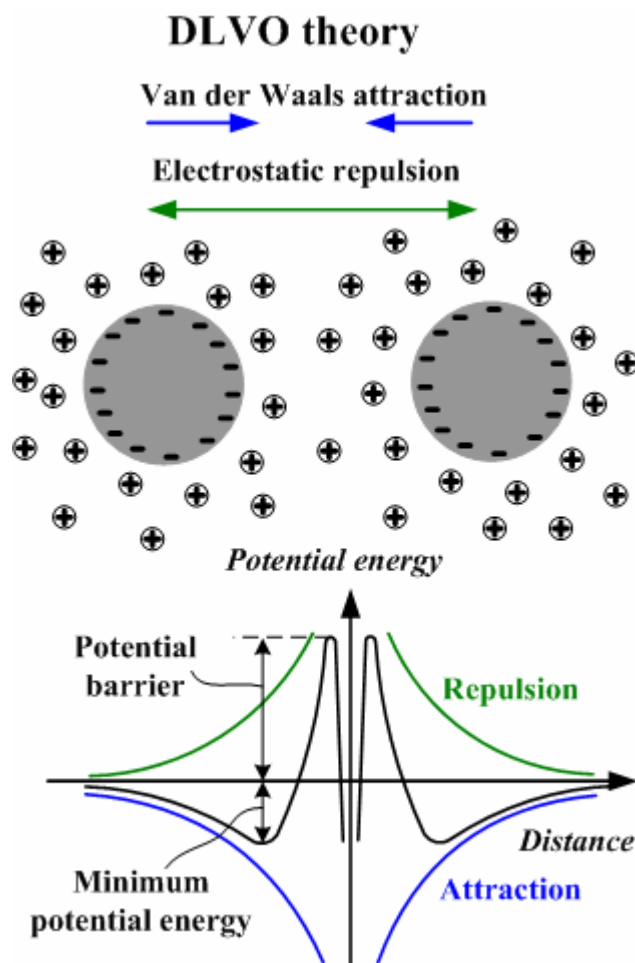


**Figure 3:** The potential energy of interaction as described by DLVO theory [27]

The higher the potential at the surface of a particle, the larger the electrostatic repulsion between the particles will be. The lower the concentration of indifferent electrolyte, the larger the distance from the surface at which repulsion is significant (e.g., the Debye–Huckel length is larger) (see Figure 4A). Therefore, both a higher potential at the particle surface and a lower concentration of inert electrolyte increase the height of the energy barrier and consequently the colloidal stability. However, increasing the ionic strength decreases the Debye-Huckel length [28], and this leads to a decreasing of the average distance of closest approach between particles (Figure 4). As this distance decreases, the repulsion due to double layer overlap declines.

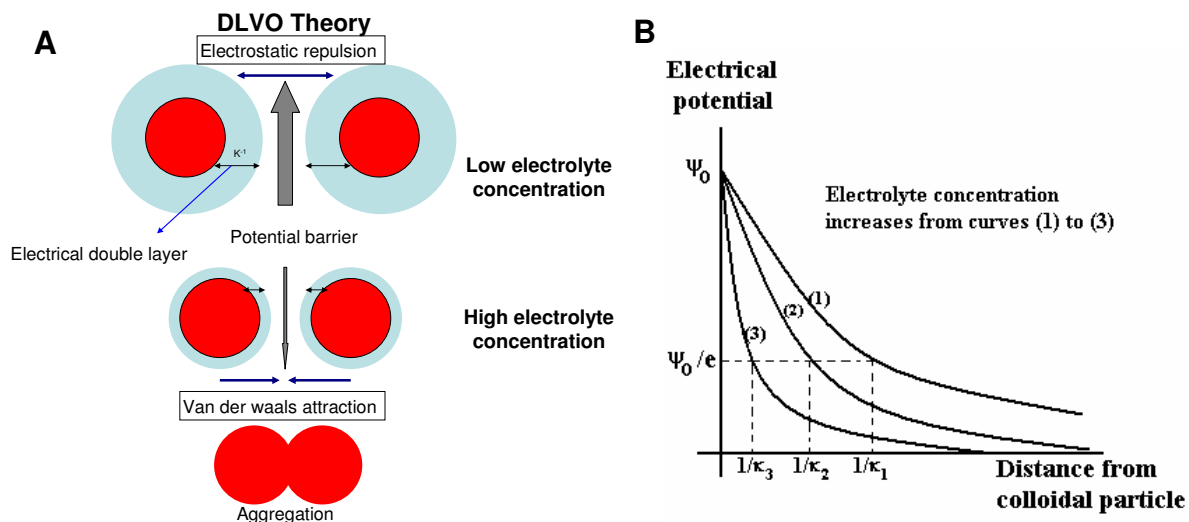


**Figure 4:** The relation between electrolyte concentration and double layer thickness (Debye-Huckel length) [picture B taken from 29]

Therefore, the degree of electrostatic screening (Debye-Huckel length) between two point charges in aqueous dispersion is directly proportional to the added salt concentration (ionic strength), as shown in equation 2.

$$k = \sqrt{8\pi l_b c} \quad (2)$$

Where  $k$  is the inverse Debye-Huckel screening length ( $\text{nm}^{-1}$ ),  $l_b$  is the Bjerrum length (for water it is approximately 0.7 nm), and  $c$  is the ionic strength of a monovalent salt ( $\text{mol dm}^{-3}$ ).

In summary, in order to obtain AuNPs suitable for coating with polyelectrolyte by the LbL strategy, the nanoparticles should first be stabilized with a strong ligand. In a next step important parameters that influence the stability of electrostatic stabilized nanoparticles should be addressed to achieve a high colloidal stability for the AuNPs. Therefore, the objective of this chapter was to describe the preparation and stabilization of AuNPs using 11-mercaptopundecanoic acid (11-MUA). Subsequently, the stabilized particles were optimized at different pH values and ionic strength to select the optimum conditions to produce stable monodisperse particles suitable for the subsequent coating steps with polyelectrolytes by the LbL technique.

## **2. Experimental**

### **2.1. Materials**

Hydrogen tetrachloroaurate tri-hydrate ( $\text{HAuCl}_4 \cdot 3\text{H}_2\text{O}$ ), and 11-Mercaptoundecanoic acid (11-MUA) were purchased from Sigma-Aldrich Chemical Company (Steinheim, Germany). Tri-sodium citrate dihydrate, sodium chloride, sodium hydroxide, nitric acid, hydrochloric acid, and absolute ethanol were purchased from Merck (Darmstadt, Germany). All glassware was thoroughly washed with freshly prepared aqua regia ( $\text{HCl}:\text{HNO}_3 = 3:1$ ) [Caution! Aqua regia is a strong acid], extensively rinsed with Millipore water several times and oven-dried at  $150\text{ }^\circ\text{C}$  for 2-3 h before use. All solutions were filtered through  $0.22\text{ }\mu\text{m}$  membrane filter (Corning Incorporated, Corning NY 14832, Germany) before use.

### **2.2. Preparation of gold nanoparticles**

AuNPs were prepared as previously described with slight modifications, using the standard reduction of tetrachloroauric(III) acid with tri-sodium citrate [9, 30]. Citrate gold nanoparticles (citrate-AuNPs) of approximately 18 nm in diameter were obtained using the following conditions: 1 ml of 1%  $\text{HAuCl}_4 \cdot 3\text{H}_2\text{O}$  solution was mixed with 100 ml of Millipore water in a 250 ml round flask and heated under reflux until boiling. 2.5 ml of a 1% tri-sodium citrate solution was added under vigorous stirring. Boiling was continued for 10 min, and then the reaction vessel was removed from the heating element. Stirring was continued for an additional 15 min. Larger aggregates were removed by centrifugation at  $2.450\text{ }xg$ . The produced nanoparticles were characterized by UV-vis spectroscopy, size and zeta potential measurements using photon correlation spectroscopy.

### **2.3. Stabilization of the produced citrate gold nanoparticles**

The pH of citrate-AuNPs was adjusted to 11 with 1N NaOH, followed by addition of differing amounts of 11-MUA which was sonicated in ethanol (to ensure complete dissolution) at a final concentration of 0.1 and 0.2 mg/ml. The gold sols were incubated under continuous stirring at room temperature overnight to allow sufficient exchange of citrate anions on the particle surface. The stabilized particles were purified two times at  $15.700\text{ }xg$  for 10 minutes for removal of excess 11-MUA, and resuspended in Millipore water [31].

## **2.4 Characterization of the gold nanoparticles**

### **2.4.1. UV-visible spectroscopy of AuNPs**

UV-vis absorbance spectra of the AuNPs were recorded using an Uvikon 941 spectrophotometer (Kontron Instruments GmbH).

### **2.4.2. Size and zeta potential measurements by dynamic light scattering (DLS)**

For the determination of size and  $\xi$ -potential, 0.5 ml of AuNPs was diluted with 1.5 ml Millipore water. The samples were adjusted to 25 °C and laser light scattering analysis was performed with an incident laser beam of 633 nm at a scattering angle of 90° using the Malvern ZetaSizer 3000 HSA (Malvern Instruments GmbH). The sampling time was set automatically. Three measurements each with 10 sub-runs were performed for each sample. The intensity of the autocorrelation function of the sample was deconvolved with the non-negatively constrained least squares (NNLS) algorithm because it provides a high resolution analysis and the quality of the fitting passed in all measurements. The  $\xi$ -potential measurements were performed in the standard capillary electrophoresis cell of the ZetaSizer 3000 HSA (Malvern Instruments GmbH), measuring the electrophoretic mobility at 25 °C. As described elsewhere, these mobilities ( $u$ ) were converted to the  $\xi$ -potential using the Smoluchowski relation  $\xi = u\eta/\epsilon$ , where  $\eta$  and  $\epsilon$  are the viscosity and permittivity of the solution respectively [32].

### **2.4.3. TEM image of the gold nanoparticles**

Transmission electron micrographs (TEM) of AuNPs were taken on a Philips CM12 microscope (FEI, Eindhoven, The Netherlands). Samples were prepared by depositing the colloidal gold solution onto a carbon-coated copper grid and then air-dried before analysis. Several micrographs of the sample were taken. For statistical evaluation, the diameter of 500 AuNPs cores was measured using Image J (NIH Image).

### **2.4.4. Determination of gold nanoparticles concentration by ICP-OES**

The concentration, and consequently the number of AuNPs per volume after synthesis, was determined by using inductively coupled plasma-optical emission spectroscopy (ICP-OES). 500  $\mu$ l of a sample containing AuNPs was mixed with 200  $\mu$ l of freshly prepared aqua regia [Caution! Aqua regia is a strong acid] and diluted to 5 ml with Millipore water. The  $\text{Au}^{3+}$  content of the solution was determined by ICP-OES analysis on a JY-70 PLUS (Jobin Yvon Instruments S.A.). The plasma flow was

16 L/min argon. All standards were made with gold (III) chloride at a concentration of 1, 10, 100 and 1000 ppm. The measured concentration of  $\text{Au}^{3+}$  was divided by the number of gold atoms per particle to obtain the concentration of AuNPs in solution [33].

## 2.5. Stability study of MUA-AuNPs

In order to determine the stability of different amounts of 11-MUA capped AuNPs to choose the optimum concentration for stabilization, a time scale experiment was performed and the stability of the colloidal dispersions was monitored by size determination,  $\xi$ -potential measurement and the changes in the UV-vis spectra of nanoparticle dispersions. In addition, the effect of different pH on the stability of the nanoparticles was studied by UV-vis spectroscopy, size determination and  $\xi$ -potential measurement. Finally, to study the influence of different ionic strength on the stability of MUA capped AuNPs, the purified particles were resuspended in different concentration of NaCl (1, 2, 5, 10, and 30 mM) and particle size distributions as well as  $\xi$ -potential and UV-vis absorbance were determined.

## 3. Results and discussion

### 3.1. Preparation, stabilization and characterization of gold nanoparticles

Small and monodisperse AuNPs were obtained using the citrate reduction method and a citrate: $\text{HAuCl}_4$  ratio of 2.5:1. The produced particles were mainly spherical and monodisperse as shown by the TEM (Figure 8). The hydrodynamic diameter of citrate gold nanoparticles (citrate-AuNPs) was  $18.2 \pm 0.5$  nm with low polydispersity index (0.182) as determined by dynamic light scattering. The AuNPs had a negative surface charge of citrate anions as investigated by  $\xi$ -potential. Because of the negative charge formed due to the adsorption of citrate anions which were weakly bound to the gold surface, it made them unsuitable for further coating steps as described earlier. A stronger stabilizing agent is required to achieve LbL coating. 11-MUA is one of the thiol compounds which form a strong covalent bond with the gold surface. Hence, citrate-AuNPs were further stabilized by 11-MUA. First, the pH of citrate-AuNPs was elevated to 11. This high basicity is important in reinforcing electrostatic stabilization, because at a high pH the carboxyl groups of 11-MUA are deprotonated and stabilize the particle dispersion through electrostatic repulsion [31,



34]. Two different concentrations of 11-MUA were added to the colloidal gold in order to determine the optimum concentration required for nanoparticle stabilization. The strong surface-plasmon band absorbance of AuNPs in the visible spectrum was used to characterize the AuNPs before and after coating (Figure 5). MUA stabilized gold nanoparticles (MUA-AuNPs) exhibited a surface plasmon resonance band at 522 nm, which is slightly broadened and red shifted compared to that of citrate-AuNPs, which had UV absorbance at 519 nm. The red shift in the surface plasmon band is attributed to the change in the dielectric constant of the medium surrounding the AuNPs [35-37], as well as the electron-withdrawing properties of the SH group [38].

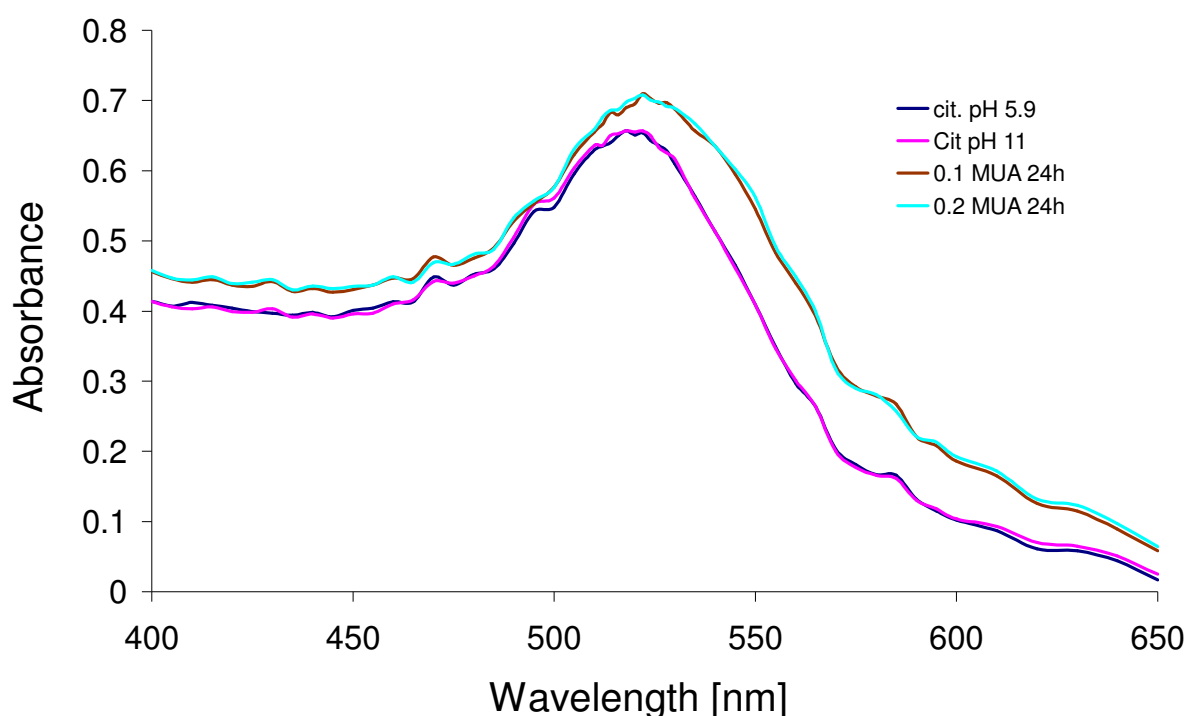


**Figure 5:** UV-vis spectra of citrate-AuNPs and different concentrations of 11-MUA stabilized AuNPs

In order to determine the optimal parameters for the stability of MUA-AuNPs, the size, polydispersity index, surface charge, and the change in surface plasmon resonance were determined at different time intervals. These time intervals were chosen since the literature states that the suitable time for stabilization of AuNPs with thiols may take anywhere between 20 hrs [31] to three days [22]. Figure 6 shows the effect of different concentrations of 11-MUA on the size and polydispersity index of the AuNPs compared to citrate-AuNPs. The size of citrate-AuNPs was  $18.2 \pm 0.5$  nm as determined by dynamic light scattering, while this size increased to  $22.0 \pm 0.4$

and  $29.0 \pm 1.2$  nm after stabilization with 0.1 and 0.2 mg/ml 11-MUA, respectively. The polydispersity index of 0.2 mg/ml MUA was higher than those of 0.1mg/ml MUA, which could be due to the presence of higher amount of free thiols.

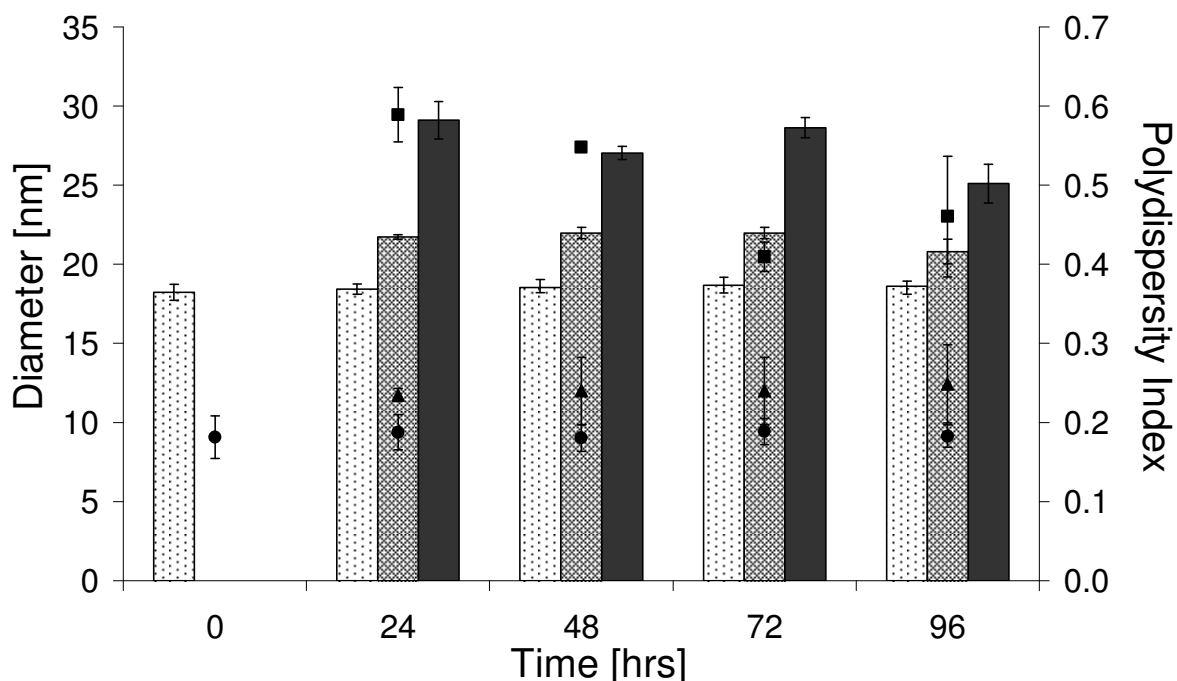


**Figure 6:** The hydrodynamic diameter of citrate (▤), 0.1mg/ml MUA (▨), 0.2mg/ml MUA (■) and the polydispersity index of citrate (●), 0.1mg/ml MUA (▲) and 0.2mg/ml MUA (■) AuNPs were measured at different time points

The surface charge plays an important role in the stability of the nanoparticles, and the magnitude of the zeta potential gives an indication of the potential stability of the colloidal system. Therefore, the  $\xi$ -potential of citrate and MUA-AuNPs was also measured as a function of time (Figure 7). The  $\xi$ -potential of citrate-AuNPs was  $-35.5 \pm 3.5$  mV, while it became more negative after stabilization with 11-MUA to be about  $-59.5 \pm 0.7$  and  $-64.3 \pm 6.6$  mV for 0.1 and 0.2 mg/ml, respectively. This increase in the  $\xi$ -potential could be due to the replacement of citrate anions with thiol. Furthermore, there was no significant difference between the two concentrations of MUA in the  $\xi$ -potential over 4 days, indicating satisfactory stability of the produced nanoparticles. Additionally, the surface plasmon resonance of stabilized particles did not change over time, again confirming the stability of the particles (data not shown), since any increase in the size of AuNPs would be accompanied by a red shift in the surface plasmon resonance [39].

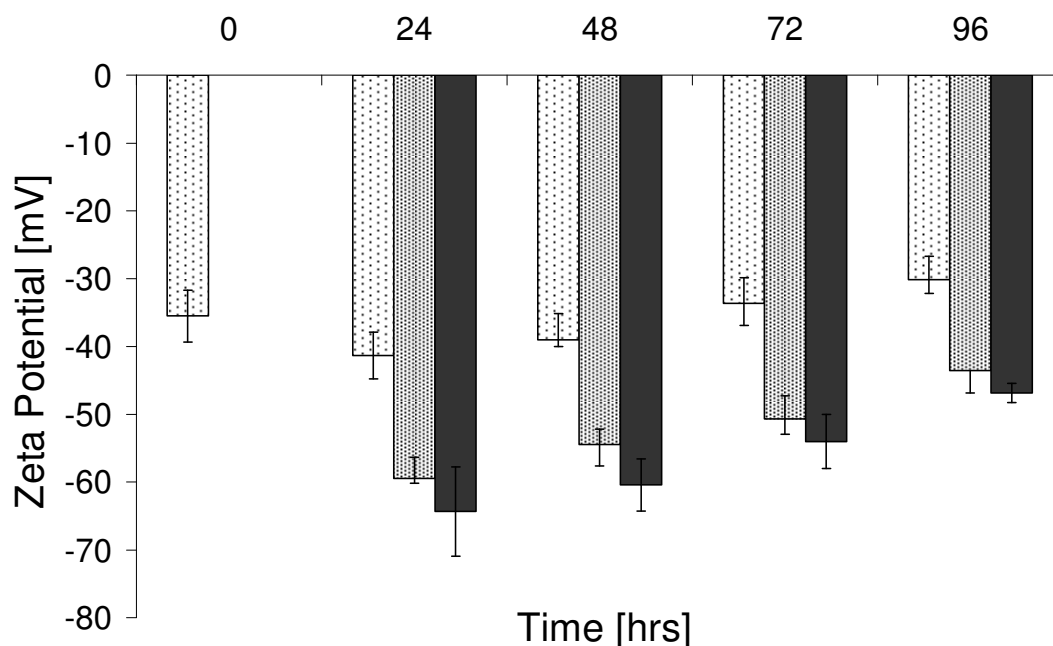


**Figure 7:** The zeta potential of citrate (●), 0.1 mg/ml MUA (■), and 0.2 mg/ml MUA (■) AuNPs were determined at different time points

It was found from the above results that there were no significant differences between 0.1 and 0.2 mg/ml MUA stabilized gold nanoparticles in the  $\xi$ -potential and surface plasmon resonance, and both concentrations showed good stability over the time. However, 0.1 mg/ml MUA-AuNPs showed smaller size and a lower polydispersity index than 0.2 mg/ml MUA-AuNPs. Therefore, 0.1 mg/ml MUA was chosen as optimum concentration for stabilization of AuNPs.

To further characterize the morphology and to verify the size of the prepared nanoparticles in comparison with the hydrodynamic diameter, imaging of the AuNPs by transmission electron microscopy (TEM) was applied. Both the citrate and MUA-AuNPs were spherical and highly monodisperse (Figure 8). The average core diameters of the AuNPs were  $18.3 \pm 1.4$  nm as calculated using Image J software counting of 500 AuNPs cores. In order to determine the concentration of AuNPs and to make a batch to batch characterization, the gold content of the nanoparticles was analyzed by ICP-OES.

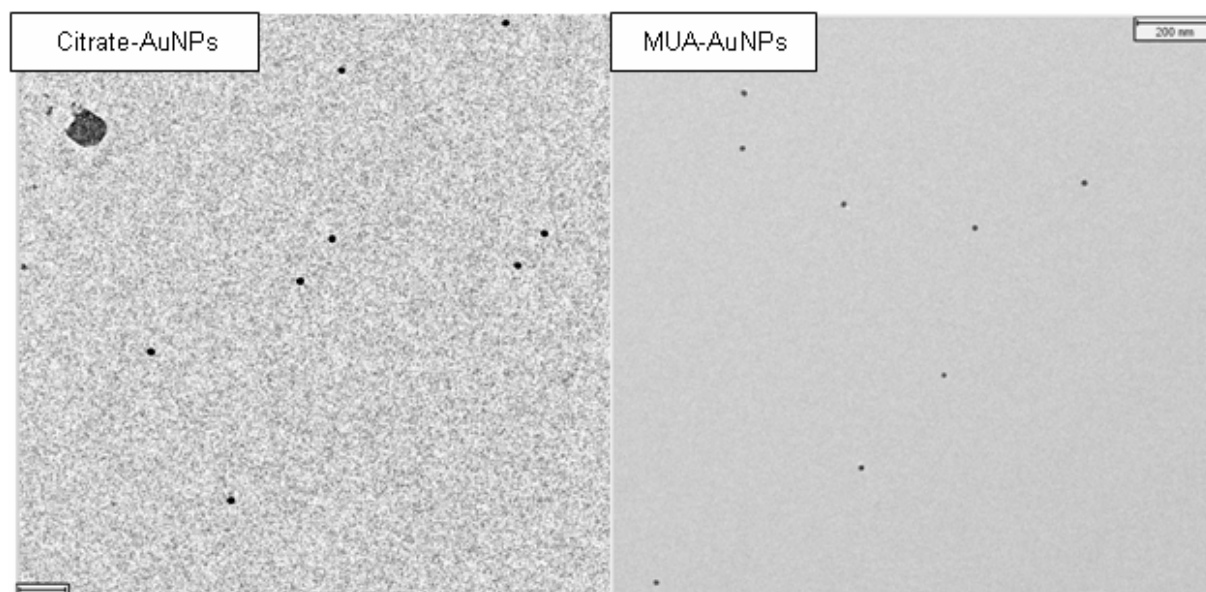


**Figure 8:** Transmission electron micrographs of citrate-AuNPs and MUA-AuNPs. The size is  $18.3 \pm 1.4$  nm calculated using Image J. The large crystal in the left image is from an excess of sodium citrate

The measured concentration of  $\text{Au}^{3+}$  was divided by the number of gold atoms per particle to obtain the concentration of AuNPs in solution. The number of gold atoms per particle was then calculated using the particle diameter, the density of bulk gold, and the molecular weight of gold. The value was determined to be  $18.9 \times 10^4$  atoms per particle. Additionally, the number of nanoparticles per ml was calculated based on the ICP-OES measurement and the TEM images, and found to be approximately  $1.31 \times 10^{12}$  particles/ ml [40].

### 3.2. Stability of MUA-AuNPs in different pH

It is important to study the stability of MUA-AuNPs in different pH values in order to control the environmental conditions around the particles and to select the optimum pH suitable for coating with polyelectrolytes via the LbL technique. A pH of 7 would be favored, since it is very near normal physiological pH; all cell culture systems of mammalian cells have this pH.

Decreasing the pH of the stabilized particles from 11 to 5 was done by the addition of HCl to the colloidal gold and the absorption spectrum of the nanoparticles was monitored. After the gradual pH decrease 11 to 5, there was no change in the surface plasmon resonance (data not shown). More interestingly, the surface plasmon resonance did not change even after re-elevation of the pH to 11 again using NaOH, which strongly agrees with the results reported by other authors who

studied the stability of different thiol capped AuNPs in different pH environments [41-43]. At pH values below the pKa of 11-MUA (pKa 4.6) the color of the nanoparticles changed rapidly from red to blue, indicating an aggregation of the particles. These aggregations are generated from the intermolecular hydrogen bonds created from the protonation of 11-MUA [32, 44]. In further experiments, the stability of MUA-AuNPs was studied at pHs of 7 and 11. The hydrodynamic diameter and polydispersity index, as well as  $\xi$ -potential of particles, was determined at different time scales. There was no difference in the size and polyindex of the stabilized particles at different pH values even after 3 days, which is shown in Figure 9.

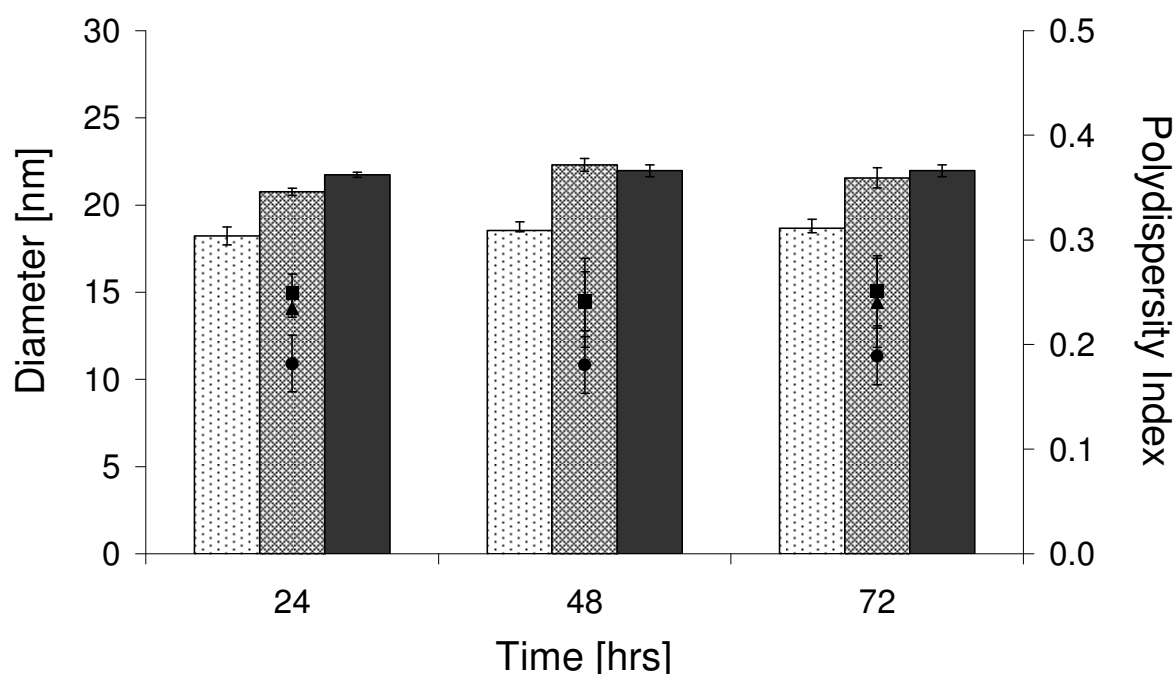


**Figure 9:** The hydrodynamic diameter of citrate (●), 0.1mg/ml MUA pH7 (▲), 0.1mg/ml MUA pH11 (■) and the polydispersity index of citrate (●), 0.1mg/ml MUA pH7 (▲) and 0.1mg/ml MUA pH11 (■) AuNPs were measured at different time points

Figure 10 shows the  $\xi$ -potential of MUA-AuNPs at pH 7 and 11 over 3 days, also here there was no significant difference in the  $\xi$ -potential of stabilized particles at different pH, it was  $-59.5 \pm 0.7$  and  $-55.6 \pm 2.8$  mV at pH 11 and 7, respectively. Furthermore, these particles were still stable after 3 days, with only a slight decrease in the  $\xi$ -potential (the  $\xi$ -potential did not decrease than about -50 mV). As known from the literature, aggregation is very unlikely for charged particles with optimum zeta potentials ( $\xi > 30$  mV) because of the electrostatic repulsion forces between

similarly charged particles [45]. Consequently, the charged particles stay dispersed, since the double layer repulsion caused by the charges can successfully counteract the attractive Van der Waal forces between two identical gold spheres [46].

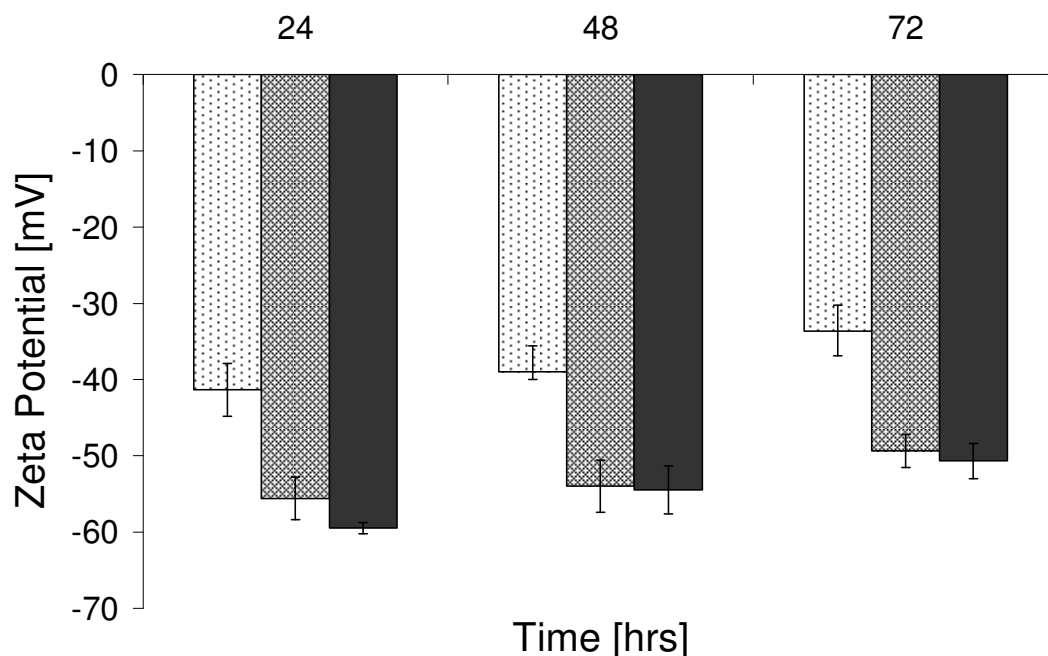


**Figure 10:** The zeta potential of citrate (dots), 0.1mg/ml MUA pH7 (cross-hatch), and 0.1mg/ml MUA pH11 (solid black) AuNPs were measured at different time scales

In summary, the stabilized particles did not show any significant difference in their hydrodynamic diameter, polydispersity index or  $\xi$ -potential at different pH values. Therefore, a pH of 7 was selected as the optimum pH for further experimentation, since the physiological pH (pH 7) is more favorable for nucleic acid assembly via LbL technology and it is important for internalization of the particles within the cell.

### 3.3. Effect of different ionic strength on MUA-AuNPs

Ionic strength plays an important role in the stability of a colloidal system, especially those stabilized via electrostatic interaction. Moreover, it is considered one of the most important parameters that influence the wrapping of the polymer around AuNPs in LbL technology, due to its ability to reduce the stiffness of the polymer. Therefore, the stability of the particles in different ionic strength was determined by monitoring the change in the surface plasmon resonance, particle size distribution, and zeta potential. Both the hydrodynamic diameter and polydispersity index serve as very

important indicators for the quality and stability of the nanoparticles. Figure 11 shows that the hydrodynamic diameter of the purified MUA-AuNPs in water, 1, and 2 mM NaCl did not differ from the crude MUA-particles. It was approximately 21 nm with the polydispersity index 0.25 (satisfactorily low), while the size and polyindex slightly increased with 5 and 10 mM NaCl to about 24 nm and 0.37. With 30 mM NaCl the size reached to 35.8 nm and the polydispersity index became 0.518, which indicates the beginning of particle instability and aggregation. This is attributed to a decrease in the Debye length between the particles because of the increased ionic strength.

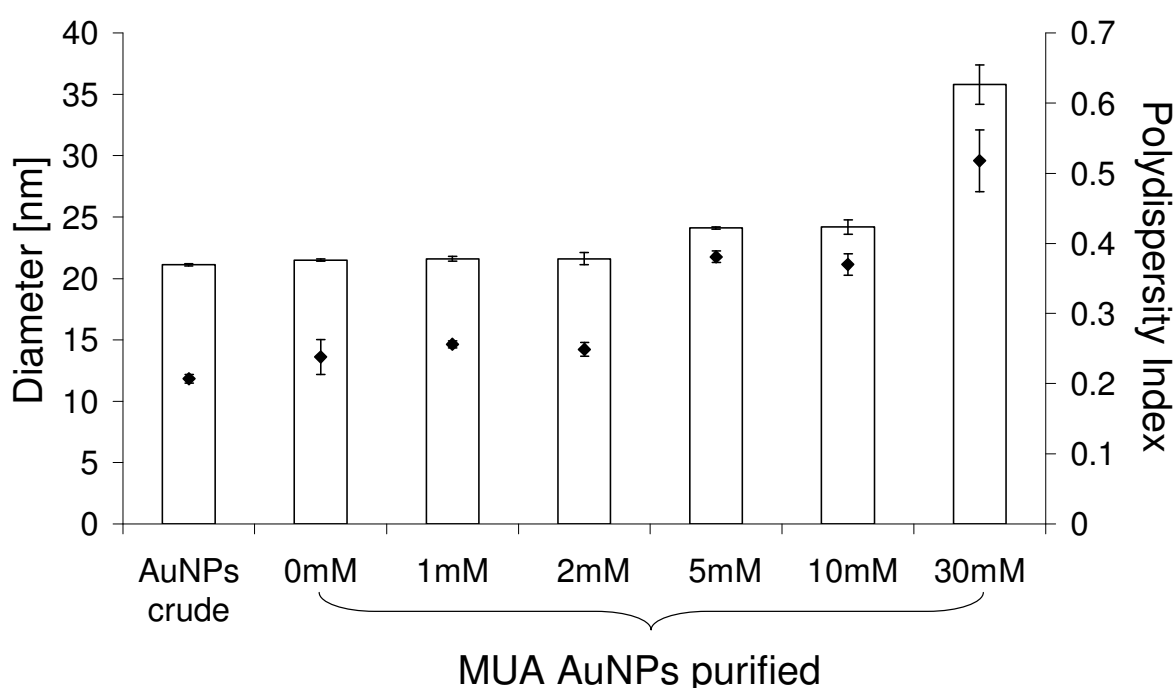


**Figure 11:** The hydrodynamic diameter (white columns) and the polydispersity index (rhombs) of MUA-AuNPs at different ionic strength of NaCl

Table 2 represents the  $\lambda_{\max}$  and  $\xi$ -potential at different ionic strength. The purified particles in 1 and 2 mM NaCl had the same  $\lambda_{\max}$  as the purified particles in water (522 nm). This could be attributed to the fact that the very low ionic strength did not have much influence on the surface plasmon resonance. While at higher ionic strength, little increase in the maximum absorbance was observed, which shifted to 524 nm in case of 5mM NaCl and then 525 and 526 nm at 10 and 30 mM NaCl, respectively. It is known from the literature that the ionic strength has an influence in the optical properties of AuNPs, where ionic strength should cause the nanoparticle's surface plasmon color change. This phenomenon is more pronounced at high ionic strength

and in divalent cations rather than monovalent ones [47]. At ionic strength higher than 30 mM NaCl the color of the nanoparticles rapidly changed from red to blue, which indicates the aggregation of the nanoparticles. This aggregation is generated from the reduction of electrostatic repulsion between surface-charged nanoparticles by the added ions and the decreasing distance between the particles, thereby favoring the interactions felt by the Van der Waals forces [16, 48]. It is also clear from this table that there was no significant difference in the  $\xi$ -potential at lower ionic strength, which is also attributed to very low salt concentration not altering the  $\xi$ -potential. Only slight reduction was observed from 5 to 30 mM NaCl.

**Table 2:** Effect of ionic strength on the surface plasmon resonance and zeta potential of purified MUA-AuNPs

Ionic strength	$\lambda_{\max}$	$\xi$ - Potential
0 mM	522 nm	$-53.6 \pm 2.7$ mV
1 mM	522 nm	$-60.2 \pm 2.3$ mV
2 mM	522 nm	$-56.2 \pm 1.3$ mV
5 mM	524 nm	$-61.1 \pm 1.5$ mV
10 mM	525 nm	$-59.2 \pm 1.4$ mV
30 mM	526 nm	$-53.0 \pm 1.0$ mV



#### 4. Summary and conclusion

Monodisperse and uniform AuNPs of  $18.2 \pm 0.5$  nm were prepared in aqueous solution using the citrate reduction method according to [9, 30] with slight modification. The stabilization of AuNPs with 0.1 mg/ml 11-MUA was found to be suitable for subsequent coating via LbL technique. After stabilization, the size of the stabilized particles only slightly increased compared to citrate stabilized particles, and also had a narrow particle size distribution and low polydispersity index. In addition, the zeta potential became more negative, possibly due to the replacement of citrate anions with thiol. Furthermore, the stabilized particles showed a good stabilization over time and in a wide range of pH values, which allows further coating at physiological pH. Additionally, MUA-AuNPs had good stability in low ionic strength (1-10 mM NaCl) which is important for the flexibility of the polymer chain, which reduces the chain stiffness and allows for the complete wrapping of the polymer around nanoparticles. However, at higher ionic strength the particles aggregated. In summary, the MUA-AuNPs presented here provide a valuable tool for further coating by polyelectrolytes via LbL technology.

## 5. References

- [1] Daniel, MC; Astruc, D. Gold nanoparticles: assembly, supramolecular chemistry, quantum-size-related properties, and applications toward biology, catalysis, and nanotechnology. *Chem. Rev.* 2004; **104**: 293-346.
- [2] Long, N. N.; Vu, LV.; Kiem, D.C.; Doanh, C. S.; Nguyet, T. C.; Hang, T. P.; Thien, D. N.; Quynh, M. L. Synthesis and optical properties of colloidal gold nanoparticles. *Journal of Physics: Conference Series* 2009; **187**: 012026.
- [3] Zhou, J.; Ralston, j.; Sedev, R.; Beattie, D.A. Functionalized gold nanoparticles: synthesis, structure and colloid stability. *Journal of Colloid and Interface Science* 2009; **331**: 251-262.
- [4] Faraday, M. Experimental relations of gold (and other metals) to light. *Philos. Trans. R. Soc. London* 1857; **147**: 145-181.
- [5] Yang, SY.; Cheng, FY.; Yeh, CS.; Lee, GB. Size-controlled synthesis of gold nanoparticles using a micro-mixing system. *Microfluid Nanofluid* 2010; **8**: 303-311.
- [6] Hori, M.; Pagnoux, C.; Baumard, JF.; Nogami, M. Preparation of gold nanoparticles (GNP) aqueous suspensions by a new method involving Tiron. *J. Mat. Sci.* 2007; **42**: 80-86.
- [7] Lu, X.; Tuan, HY.; Korgel, BA.; Xia, Y. Facile synthesis of gold nanoparticles with narrow size distribution by using AuCl or AuBr as the precursor. *Chem. Eur. J.* 2008; **14**: 1584-1591.
- [8] Turkevitch, J.; Stevenson, P. C.; Hillier, J. Nucleation and Growth Process in the Synthesis of Colloidal Gold. *Discuss. Faraday Soc.* 1951; **11**: 55-75.
- [9] Frens, G. Controlled nucleation for the regulation of the particle size in monodisperse gold suspensions. *Nature (London), Physical Science* 1973; **241**: 20-22.
- [10] Handley, D. A. in *Colloidal Gold. Principles, Methods, and Applications*, Vol.1, Ed.; M.A. Hayat, Academic Press, New York, 1989, pp.13-32.
- [11] Ji, X.; Song, X.; Li, J.; Bai, Y.; Yang, W.; Peng, X. Size control of gold nanocrystals in citrate reduction: the third role of citrate. *J. Am. Chem. Soc.* 2007; **129**: 13939-13948.
- [12] Kumar, S.; Gandhi, K. S.; Kumar, R. Modeling of formation of gold nanoparticles by citrate method. *Industrial & Engineering Chemistry Research* 2007; **46**: 3128- 3136.
- [13] Polte, J.; Ahner, TT.; Delissen, F.; Sokolov, S.; Emmerling, F.; Thünemann, AF.; Kraehnert, R. Mechanism of gold nanoparticle formation in the classical citrate synthesis method derived from coupled in situ XANES and SAXS evaluation. *J. Am. Chem. Soc.* 2010; **132**: 1296-1301.

- [14] Liz-Marzan, LM. Nanometals formation and color. *Materialstoday* 2004; **7**: 26-31.
- [15] Schmid, G.; Corain, B. Nanoparticulated gold: synthesis, structures, electronic, and reactivities. *Eur. J. Inorg. Chem.* 2003; 3081-3098.
- [16] Wang, G.; Sun, W. Optical limiting of gold nanoparticles aggregates induced by electrolytes. *J. Phys. Chem. B* 2006; **110**: 20901-20905.
- [17] Mulvaney, P.; Liz-Marzan, L. M.; Giersig, M.; Ung, T. Silica encapsulation of quantum dots and metal clusters. *J. Mater. Chem.* 2000; **10**: 1259-1270.
- [18] Pong, BK.; Elim, HI.; Chong, J. X.; Ji, W.; Trout, BL.; Lee, JY. New insights on the nanoparticle growth mechanism in the citrate reduction of gold(III) salt: Formation of the Au nanowire intermediate and its nonlinear optical properties. *J. Phys. Chem. C* 2007; **111**: 6281-6287.
- [19] Yang, T.; Li, Z.; Wang, L.; Guo, C.; Sun, Y. Synthesis, characterization, and self-assembly of protein lysozyme monolayer-stabilized gold nanoparticles. *Langmuir* 2007; **23**: 10533-10538.
- [20] Sugunan, A.; Thanachayanont, C.; Dutta, J.; Hilborn, J. G. Heavy-metal ion sensors using chitosan-capped gold nanoparticles. *Science and Technology of Advanced Materials* 2005; **6**: 335-340.
- [21] Andrew, N.; Shipway, E. K.; Itamar, W. Nanoparticle arrays on surfaces for electronic, optical, and sensor applications. *ChemPhysChem* 2000; **1**: 18-52.
- [22] Gittins, D. I.; Caruso, F. Tailoring the polyelectrolyte coating of metal nanoparticles. *J. Phys. Chem. B* 2001; **105**: 6846-6852.
- [23] Bradley, J. S. *Clusters and Colloids*; Ed.; G. Schmid, VCH, Weinheim, 1994.
- [24] Caruso, F. *Colloids and colloid assemblies: Synthesis, modification, organization and utilization of colloid particles*; Eds.; Wiley-VCH: Weinheim, 2004.
- [25] Zetasizer Nano User Manual, man0137, issue 4.0 May 2008, chapter 16.
- [26] Hiemenz, P.C.; Rajagopalan, R. *Principles of Colloid and Surface Chemistry*, third ed., Marcel Dekker, New York, 1997.
- [27] [www.substech.com/dokuwiki/doku](http://www.substech.com/dokuwiki/doku) accessed on May 21th, 2010.
- [28] Hunter, R.J. *Foundations of Colloid Science*, vol. 1, Clarendon Press, Oxford, 1993, pp. 329-341, 415-418.
- [29] [www.dur.ac.uk/sharon.cooper/lectures/colloids/interfaces](http://www.dur.ac.uk/sharon.cooper/lectures/colloids/interfaces) accessed on July 10th, 2007.
- [30] Grabar, KC.; Freeman, RG.; Hommer, MB.; Natan, MJ. Preparation and characterization of Au colloid monolayers. *Anal. Chem.* 1995; **67**: 735-743.

- [31] Lin, S-Y.; Tsai, Y-T.; Chen, C-C.; Lin, C-M.; Chen, C-H. Two-step functionalization of neutral and positively charged thiols onto citrate-stabilized Au nanoparticles. *J. phys. Chem. B* 2004; **108**: 2134-2139.
- [32] Mayya, K.S.; Schoeler, B.; Caruso, F. Preparation and organization of nanoscale polyelectrolyte-coated gold nanoparticles. *Adv. Funct. Mater.* 2003; **13**: 183-188.
- [33] Chithrani, B. D.; Ghazani, A. A.; Chan, W. C. Determining the size and shape dependence of gold nanoparticle uptake into mammalian cells. *Nano Lett.* 2006; **6**: 662-668.
- [34] Laaksonen, T.; Ahonen, P.; Johans, C.; Kontturi, K. Stability and electrostatics of mercaptoundecanoic acid-capped gold nanoparticles with varying counterion size. *Chem Phys Chem* 2006; **7**: 2143-2149.
- [35] Kamat, P.V. Photophysical, photochemical and photocatalytic aspects of metal nanoparticles. *J. Phys. Chem. B* 2002; **106**: 7729-7744.
- [36] Underwood, S.; Mulvaney, P. Effect of the solution refractive index of the color of gold colloid. *Langmuir* 1994; **10**: 3427-3430.
- [37] Elghanian, R.; Storhoff, J.J.; Mucic, R.C.; Letsinger, R.L. Mirkin, C.A. Selective colorimetric detection of polynucleotides based on the distance-dependent optical properties of gold nanoparticles. *Science* 1997; **277**: 1078-1081.
- [38] Sendroiu, I E.; L.Mertens, SF.; Schiffrin, DJ. Plasmon interactions between gold nanoparticles in aqueous solution with controlled spatial separation. *J. Phys. Chem. Chem. Phys.* 2006; **8**: 1430-1436.
- [39] Haiss, W.; Thanh, NT. K.; Aveyard, J.; Fernig, DG. Determination of size and concentration of gold nanoparticles from UV-Vis spectra. *Anal. Chem.* 2007; **79**: 4215-4221.
- [40] Liu, X.; Atwater, M.; Wang, J.; Huo, Q. Extinction coefficient of gold nanoparticles with different sizes and different capping ligands. *Colloids and Surfaces, B: Biointerfaces* 2007; **58**: 3-7.
- [41] Mayya, K. S.; Patil, V.; Sastry, M. On the stability of carboxylic acid derivatized gold colloidal particles: the role of colloidal solution pH studied by optical absorption spectroscopy. *Langmuir* 1997; **13**: 3944-3947.
- [42] Shiraishi, Y.; Arakawa, D.; Toshima, N. pH-dependent color change of colloidal dispersions of gold nanoclusters: effect of stabilizer. *Eur. Phys. J. E* 2002; **8**: 377-383.
- [43] Li, G.; Wang, T.; Bhosale, S.; Zhang, Y.; Fuhrhop, J-H. Completely reversible aggregation of nanoparticles by varying the pH. *Colloid Polym. Sci.* 2003; **281**: 1099-1103.
- [44] Simard, J.; Briggs, C.; Boal, AK.; Rotello, VM. Formation and pH-controlled assembly of amphiphilic gold nanoparticles. *Chem.Comm.* 2000; 1943-1944.

- [45] Bhumkar, DR.; Joshi, HM.; Sastry, M .; Pokharkar, VB. Chitosan reduced gold nanoparticles as novel carriers for transmucosal delivery of insulin. *Pharmaceutical Research* 2007; **24**: 1415-1426.
- [46] Zhou, J.; Beattie, D A.; Ralston, J.; Sedev, R. Colloid stability of thymine-functionalized gold nanoparticles. *Langmuir* 2007; **23**: 12096-12103.
- [47] Burns, C.; Spendel, W.U.; Puckett, S.; Pacey, G.E. Solution ionic strength effect on gold nanoparticle solution color transition. *Talanta* 2006; **69**: 873-876.
- [48] Aryal, S.; Bahadur, K. C.; R. Bhattarai, N.; Kim, CK.; Kim, HY. Study of electrolyte induced aggregation of gold nanoparticles capped by amino acids. *Journal of Colloid and Interface Science* 2006; **299**: 191-197.



# **Chapter 3**

## **Polyelectrolyte Coated Gold Nanoparticles Via LbL Technology**

Asmaa Elbakry<sup>1</sup>, Alaa Zaky<sup>1</sup>, Renate Liebl<sup>1</sup>, Reinhard Rachel<sup>2</sup>, Miriam Breunig<sup>1</sup>,  
Achim Goepferich<sup>1</sup>

<sup>1</sup>Department of Pharmaceutical Technology, University of Regensburg,  
Universitätsstraße 31, 93040 Regensburg, Germany

<sup>2</sup>Centre for Electron Microscopy at the Institute for Anatomy, University of  
Regensburg, Universitätsstraße 31, 93040 Regensburg, Germany

**Abstract**

The design of advanced nanostructured materials is of great interest, with broad applications in the biomedical field. Among the available techniques, the Layer-by-Layer (LbL) assembly method has attracted extensive attention. LbL assembly is a simple, versatile, and comparatively inexpensive approach with the capability of achieving high loads with numerous types of biomolecules. Gold nanoparticles (AuNPs) are the most commonly used nanocore for the LbL deposition of polyelectrolytes and are considered a good model for understanding the parameters controlling polymer multilayer formation on nanoparticles. In order to coat AuNPs with polyelectrolytes via the LbL technique for nucleic acid delivery, appropriate parameters had to be identified. First, the suitability of the polycations protamine sulfate (~ 5 KDa) and poly(ethylene imine) (PEI) 25 KDa for LbL assembly for nucleic acid delivery using 21 base pair DNA as a model was investigated. Additionally, other important parameters (such as polyelectrolyte concentration, ionic strength, and the purity of the nanoparticles after a subsequent coating step) were also determined. Having optimized the conditions, AuNPs were successfully coated with 1 mg/ml PEI at 1 mM NaCl and 1.5  $\mu$ M 21 bp DNA at 10 mM NaCl in alternative order via the LbL approach. Moreover, the LbL-coated AuNPs showed good stability in a culture medium containing serum and were taken up by CHO-K1 cells. Thus, nucleic acid delivery can be achieved via LbL technology using these optimized parameters.



## 1. Introduction

Controlling the surface properties of colloidal materials is a major research interest in the field of nanomedicine for biomedical applications, such as the delivery of small drug molecules or large biomolecules, like proteins and nucleic acids, into cells. There are several ways to modify the surface of a colloidal particle, including the attachment of small ligands or polymers via either covalent or non-covalent binding [1]. In particular, the coating of colloidal particles with polymers is a favorable method to modify surface properties, with the polymer type determining the final surface characteristics of the particles. Among polymers, polyelectrolytes (charged polymers) are frequently used to modify flat surfaces [2-5] and colloids (curved surfaces) [6, 7]. Polyelectrolytes have an advantage over uncharged polymers, since they can be self-assembled onto the surface and contain certain charged functional groups that may be directly attached by electrostatic interaction onto the particles. A technique exploiting this mechanism is the Layer-by-Layer (LbL) deposition of polyelectrolytes on colloidal surfaces, which enables the total polymer thickness to be determined by the number of layers deposited [4]. This alleviates the need for chemical routes to modify particles [8].

The adsorption of polyelectrolytes onto oppositely charged spherical particles depends on various parameters, including the polyelectrolyte chain length, type, and concentration, particle diameter and concentration, and the ionic strength of the adsorption solution [9]. The main problems in transferring the LbL technique from macroscopic flat substrates to the surface of colloidal particles lies in the separation of the coated colloids from free, excess polyelectrolyte prior to the next deposition cycle. In addition, flocculation instead of layer growth is often induced by the added polyelectrolyte, as shown in Figure 1a. In this case, the two ends of the long chain polyelectrolyte may adsorb onto different colloidal particles and then draw them together, leading to bridging flocculation. To prevent these undesirable effects, the initial colloidal substrate and each of the employed polyelectrolyte species has to be sufficiently charged. Moreover, it has to be ensured that the particles are added to the polyelectrolyte solution and not vice versa, and that the amount of the adsorbing polyelectrolyte is large enough to provide a complete surface coverage. If this requirement is not met, incomplete layer growth and aggregation arising from the coexistence of particles having different charge density occurs [10]. Recently, Decher et al. investigated the appropriate parameters required to prevent bridging

flocculation during polyelectrolyte adsorption and enhance the stability of the colloidal dispersion. They used gold nanoparticles (AuNPs) as a core and poly(allylamine hydrochloride) (PAH) and poly(styrene sulfonate) (PSS) as the polycation and polyanion, respectively. They concluded that by controlling the experimental parameters such as nanoparticle concentration, polymer charge density, concentration, and length and the concentration of added salt, AuNPs can be coated with up to 10 layers of polyelectrolytes (five pairs of PAH/PSS layers). Under these selected conditions the recovery yield of individual particles was higher than 90% per adsorption cycle accompanied only by very small amounts of oligomeric aggregates (for review see [11]).

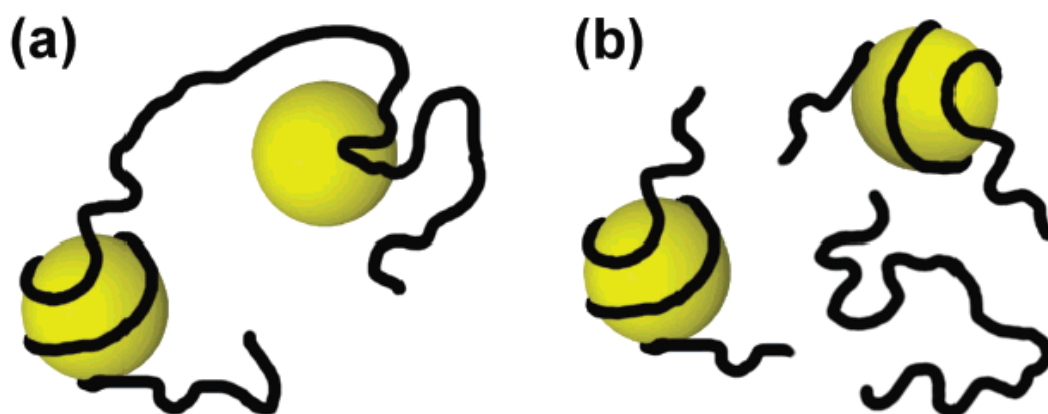


**Figure 1:** Simple representations of nanoparticles being aggregated by bridging flocculation (a) and being individually wrapped by polymer chains (b) [10]

The ionic strength plays an important role in the colloidal stability of nanoparticles and is considered one of the most important parameters in LbL technology. The choice of the ionic strength during LbL build-up is made with consideration to the Debye-Huckel screening length ( $\text{nm}^{-1}$ ) (see [chapter 2]). The Debye-Huckel length is given by  $k = c^{0.5}/0.304$ , where  $c$  is the ionic strength of monovalent salt solution [12]. It is known that the ionic strength required to reduce the chain stiffness of the polymer in order to coat particles with polyelectrolytes of a given length increases with decreasing particle size [13, 14]. In addition, shorter polymer chains need higher salt concentrations to be flexible enough to wrap around the colloid. However, a high ionic strength may cause aggregation of the AuNPs, whereas high molecular weight polymers induce flocculation through bridging [15]. Therefore, a low molecular weight

polymer and a low salt concentration are desired to successfully coat small nanoparticles.

Although the fabrication of multilayered polyelectrolyte films is a well-established method for nucleic acid delivery [16-20], after a comprehensive literature search we determined that the delivery of nucleic acid via LbL technique using AuNPs as a template has not been performed. This is due to the fact that biomacromolecules such as DNA and short interfering RNA (siRNA) are stiff and rodlike molecules that do not easily wrap around of high surface curvature small nanoparticles [21]. Therefore, in order to coat AuNPs with polyelectrolyte for nucleic acid delivery via the LbL technique, it is important to choose an appropriate combination of polycation and nucleic acid. In addition, identifying the suitable parameters required for successful assembly, such as polyelectrolyte concentration and ionic strength of the adsorption medium, will be a major issue.

Both nature and polymer chemistry provide an enormous wealth of materials potentially suitable as polycations for the coating. Unfortunately, very few synthetic couples have been studied so far with regard to their properties concerning LbL formation [22]. A plethora of materials have been used as polycations for the LbL assembly process such as poly(diallyldimethylammonium chloride) (PDDA), polyallylamine hydrochloride (PAH), poly-L-lysine (PLL), poly-L-arginine (PLA), poly(ethylene imine) (PEI), and protamine [10, 22]. In particular, PEI and protamine have additionally been shown to form complexes with nucleic acids that are delivered into cells [23, 24]. Protamine is a natural polymer and a highly basic peptide which is constituted of 75% arginine. It is available in large quantities from fish sperm. One of its biological functions is to ensure compaction of DNA [25, 26]. Regarding the possible use of LbL multilayers containing protamine, it is interesting to note that protamine slows down the release of insulin when insulin/protamine complexes are used [27]. Both these features of protamine are based on polyelectrolyte complex formation. Hence, protamine should be a suitable candidate for LbL formation with a wide range of anionic biopolymers [28, 29]. On the other hand, PEI has already been used for nucleic acid delivery via LbL technique using flat surfaces [30]. Although PEI is a synthetic polymer and has pronounced cytotoxicity [31], it is considered the gold standard for nucleic acid delivery, due to its high transfection efficiency and endosomal escape through the proposed proton sponge effect [32-34]. Therefore, the goal of this chapter was to investigate if mercaptoundecanoic acid stabilized gold

nanoparticles (MUA-AuNPs) [from chapter 2] can be coated with either protamine or PEI as a polycation and DNA as a polyanion via the LbL technique.

First, the suitability of the polycations protamine and PEI for LbL assembly for nucleic acid delivery using 21 base pair DNA as a model was investigated. In addition, the appropriate parameters of polyelectrolyte required for assembly, such as the concentration of polyelectrolyte, the ionic strength required to achieve complete wrapping of polyelectrolyte around nanoparticles, and purification of AuNPs after subsequent coating, were determined. The toxicity of the produced LbL-coated nanoparticles was also measured in a cell culture model. Moreover, the stability of the resulting LbL nanoparticles after the whole fabrication was determined in a culture medium to examine if these nanoparticles are still monodispersed or aggregated after exposure to culture medium. Subsequently, the cellular uptake of the produced nanoparticles was investigated.

## 2. Experimental

### 2.1. Materials

Hydrogen tetrachloroaurate tri-hydrate ( $\text{HAuCl}_4 \cdot 3\text{H}_2\text{O}$ ), protamine sulfate salt from salmon grade X, poly(ethylene imine) (PEI)  $\text{Mw} = 25,000 \text{ g/mol}^{-1}$ , and 11-Mercaptoundecanoic acid (11-MUA) were purchased from Sigma-Aldrich Chemical Company (Steinheim, Germany). 21 base pair DNA was synthesized by Eurofins MWG Operon (sense strand: 5'-ATGAACTTCAGGGTCAGCTTGC-3' and antisense strand: 5'-GCAAGCTGACCCTGAAGTTCAT-3'). Picryl sulfonic acid solution was purchased from Fluka (Steinheim, Germany). Tri-sodium citrate dihydrate, sodium chloride, sodium hydroxide, nitric acid, hydrochloric acid, and absolute ethanol were purchased from Merck (Darmstadt, Germany). Chinese hamster ovarian cells (CHO-K1 cells) (ATCC No. CCL-61) were grown in  $75\text{cm}^2$  culture flasks to 90% confluency. Dulbecco's Phosphate buffer saline 1x (DPBS) and Leibovitz's L-15 medium 1x without phenol red were purchased from (GIBCO) Invitrogen (Germany). Fetal bovine serum was purchased from Biochrom AG (Germany). All glassware was thoroughly washed with freshly prepared aqua regia ( $\text{HCl}:\text{HNO}_3 = 3:1$ ) [Caution! Aqua regia is a strong acid], extensively rinsed with Millipore water several times, and oven-dried at  $150^\circ\text{C}$  for 2-3 h before use. All used solutions filtered through  $0.22 \mu\text{m}$  membrane filter (Corning Incorporated, Corning NY 14832, Germany) before use.

## 2.2. Preparation and stabilization of gold nanoparticles

AuNPs were prepared as described previously using the standard reduction of tetrachloroauric(III) acid with sodium citrate [35,36]. Briefly, 1.0 ml of 1%  $\text{HAuCl}_4 \cdot 3\text{H}_2\text{O}$  solution was added to 100 ml of Millipore water and heated under reflux until boiling. 2.5 ml of a 1% tri-sodium citrate solution was added under vigorous stirring. Boiling was continued for 10 min; after that, the heating mantle was removed, and stirring was continued for an additional 15 min. Larger aggregates of nanoparticles were removed by centrifugation at 2,450  $\times g$ . The pH of AuNPs was adjusted to 11 with 1N NaOH, followed by the addition of 11-MUA at a final concentration of 0.1 mg/ml. The stabilized particles were purified two times at 15,700  $\times g$  for 10 minutes, and resuspended in 1 mM NaCl [37].

## 2.3. Layer-by-Layer (LbL) deposition of polyelectrolytes onto MUA-stabilized gold nanoparticles (MUA-AuNPs)

First layer: the purified MUA-AuNPs were added drop-wise to different concentrations of protamine sulfate or PEI 25 KDa to determine the optimum concentration of polycation required for coating. The solution was stirred for 30 minutes. The nanoparticles were characterized via UV-vis spectroscopy, TEM imaging, size, and zeta potential measurement. PEI coated gold nanoparticles (PEI-AuNPs) were purified three times at 15,700  $\times g$  for 15 minutes.

Second layer: the purified PEI-AuNPs were added to different concentrations of 21 bp DNA. After 30 minutes of stirring, the size and  $\xi$ -potential of coated particles were measured and the optimum concentration for coating was chosen. After that, excess DNA was removed by two steps of centrifugation at 15,700  $\times g$  for 15 minutes and the particles were resuspended in 10 mM NaCl.

Third layer: the purified DNA/PEI-AuNPs were added to 1mg/ml PEI 25 KDa and the solution of nanoparticles was stirred for 30 minutes. The PEI/DNA/PEI-AuNPs were purified three times at 15,700  $\times g$  for 15 minutes for the removal of excess PEI, and resuspended in 10mM NaCl.

## **2.4. Characterization of the LbL-coated gold nanoparticles**

### **2.4.1. UV-visible spectroscopy of AuNPs**

UV-vis absorbance spectra of the AuNPs after each coating step were recorded using an Uvikon 941 spectrophotometer (Kontron Instruments GmbH).

### **2.4.2. Size and zeta potential measurements by dynamic light scattering (DLS)**

For the determination of size and  $\xi$ -potential, 0.5 ml of AuNPs was diluted with 1.5 ml Millipore water. The samples were thermostated to 25 °C and laser light scattering analysis was performed with an incident laser beam of 633 nm at a scattering angle of 90° using the Malvern ZetaSizer 3000 HSA (Malvern Instruments GmbH). The  $\xi$ -potential measurements were performed in the standard capillary electrophoresis cell of the ZetaSizer 3000 HSA (Malvern Instruments GmbH), measuring the electrophoretic mobility at 25 °C.

### **2.4.3. TEM image of the gold nanoparticles**

Transmission electron micrographs (TEM) of AuNPs were taken on a Philips CM12 microscope (FEI, Eindhoven, The Netherlands). Samples were prepared by depositing the colloidal gold solution onto a carbon-coated copper grid and air-dried before analysis. Several micrographs for sample were taken.

### **2.4.4. Stability of LbL-coated AuNPs in different ionic strength**

The effect of different ionic strength on the properties of nanoparticles coated with the optimum concentration of protamine was determined. In addition, the stability of purified PEI-AuNPs was examined in different ionic strength in order to determine the suitable ionic strength for further coating steps with the polyanion (DNA). The purified particles were resuspended in different concentrations of NaCl (1, 5, 10, 20, and 30 mM), and particle size distribution,  $\xi$ -potential, and UV-vis absorbance were determined.

### **2.4.5. Determination of excess polyelectrolyte after purification**

The amount of free polyelectrolytes (PEI and DNA) in the supernatant after purification was determined. This was in order to ensure that only a minimal amount of PEI was detected in the supernatant. The amount of PEI in the supernatant was determined according to the method established by Snyder et al. [38] that uses 2,4,6 Trinitrobenzenesulfonic acid (TNBS) for the detection of amines. In brief, 25  $\mu$ l of a 0.03 M TNBS solution were added to 1 ml of the supernatant containing PEI. After 30 minutes at room temperature, the absorbance was read at 420 nm using a Uvikon

941 spectrophotometer. The concentration of PEI was calculated using a standard calibration curve. The amount of free DNA in the supernatant was determined by UV measurement at 260 nm using a standard calibration curve.

## **2.5. Cell culture experiments**

### **2.5.1. Stability of LbL-coated nanoparticles in cell culture medium**

The stability of AuNPs after each coating step was investigated in serum-free and serum-containing culture media. The change in UV-vis spectra, hydrodynamic diameter, and  $\xi$ -potential were monitored.

### **2.5.2. Toxicity experiments**

PEI-, DNA/PEI-, and PEI/DNA/PEI-AuNPs (both crude or purified) were incubated with CHO-K1 cells for 4 hours and the cells were then visualized by light scanning microscopy for toxicity determination. For the quantitative determination of cell viability, CHO-K1 cells were grown in 24-well plates at an initial density of 38,000 cells per well. 20 hours after plating, the culture medium was removed, the cells were washed with PBS, and a certain volume of purified PEI-AuNPs was added to the different volumes of culture media containing serum. After 4 hours, the medium was replaced with fresh culture medium. 48 hours later, cells were prepared for flow cytometry analysis as described previously [39]. In brief, floating cells were collected and combined with adherent cells after trypsinization. The pooled cells were washed twice with PBS, resuspended in 500  $\mu$ l PBS, and propidium iodide was added at a concentration of 1  $\mu$ g/ml to stain the dead cells. Measurements were taken on a FACS Calibur (Becton Dickinson, Germany) using CellQuest Pro software (Becton Dickinson, Germany) and evaluated by WinMDI 2.8 software (©1993–2000 Joseph Trotter). 20,000 cells were counted for each sample. The propidium iodide emission was measured with a 670 nm longpass filter. The fraction of propidium iodide negative cells was used to calculate cell viability. The cell population and the number of propidium iodide negative cells in the samples were normalized to the untreated CHO-K1 cells.

### **2.5.3. Cellular uptake experiments**

CHO-K1 cells were incubated with culture medium and serum containing DNA/PEI- and PEI/DNA/PEI-AuNPs for 6 hours. Thereafter, the cells contained in three flasks were washed two times with PBS, detached from the flask by trypsinization, pelleted,

and again washed with PBS. For the determination of the  $\text{Au}^{3+}$  content via inductively coupled plasma-optical emission spectroscopy (ICP-OES) the cell pellet was air dried, dissolved in 500  $\mu\text{l}$  of freshly prepared aqua regia [Caution! Aqua regia is a strong acid] and diluted to 5 ml with Millipore water. ICP-OES analysis of the samples was performed on a JY-70 PLUS (Jobin Yvon Instruments S.A.) with a plasma flow of 16 L/min argon. All standards were made with gold (III) chloride at concentrations of 1, 10, 100 and 1,000 ppm. The measured number of  $\text{Au}^{3+}$  was used to calculate the number of AuNPs, as described by Cumberland et al. [40] and related to the total number of cells. The number of total cells was determined by counting the cells of one 75cm<sup>2</sup> culture flasks in a Neubauer Chamber. The samples for cell counting were incubated with AuNPs in the same way as samples for ICP-OES measurements. Cell samples treated as described above but without addition of AuNPs were used as controls for background subtraction.

### 3. Results and discussion

#### 3.1. Coating of stabilized MUA-AuNPs with different polycations

##### 3.1.1. Coating and characterization of stabilized MUA-AuNPs with protamine

Protamine sulfate was used as a positive polyelectrolyte that could coat the negatively charged MUA-AuNPs. A uniform polyelectrolyte coating is desired, since such a coating is favorable for the formation of colloiddally stable coated nanoparticles. It has been shown previously that a low concentration of added polyelectrolyte causes particle aggregation due to the electrostatic attraction of partially coated and uncoated colloids [41-43]. At the same time, polyelectrolyte excess should be limited, as to maintain conditions that are practical for synthesis and handling. Therefore, the determination of the optimal concentration is a necessary step in overcoming this obstacle. Figure 2 shows the hydrodynamic diameter and polydispersity index (PI) of purified MUA-AuNPs suspended in 1mM NaCl coated with different concentrations of protamine sulfate. The hydrodynamic diameter of MUA-AuNPs increased from  $21.6 \pm 0.2$  to  $25.2 \pm 0.6$  nm after being coated with 6  $\mu\text{g/ml}$  protamine. The diameter further increased with increasing protamine concentration. The highest hydrodynamic diameter was observed with 1000  $\mu\text{g/ml}$  protamine ( $35.4 \pm 0.5$  nm). With respect to the polydispersity index, considerable differences were observed with different concentrations of protamine.



The PI of MUA-AuNPs coated with 6 and 10  $\mu\text{g/ml}$  protamine was about 0.6, which indicates the presence of polydispersed particles in the preparation. With a higher concentration of protamine (100 and 500  $\mu\text{g/ml}$ ), the PI reduced to about 0.4 but it increased again with 1000  $\mu\text{g/ml}$  to about 0.55.

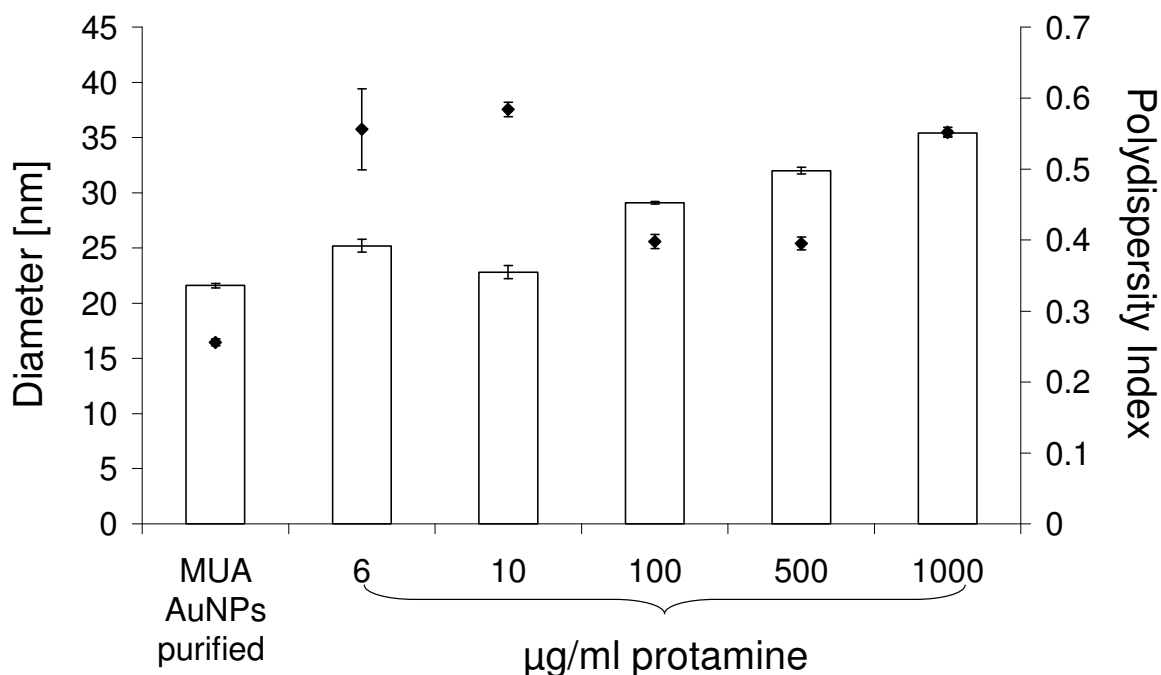


**Figure 2:** The hydrodynamic diameter (white columns) and the polydispersity index (rhombs) of different protamine concentrations coated MUA-AuNPs at 1mM NaCl

Several methods are applied to characterize particles, especially in terms of size, but none of them is ever fully satisfactory. Therefore, a combination of at least two methods is highly recommended, with one of the methods being microscopic in nature [44]. Therefore, the produced particles were further characterized via TEM imaging. Figure 3 shows the TEM images of two different concentrations of protamine sulfate coated MUA-AuNPs. The image of 10  $\mu\text{g/ml}$  protamine coated nanoparticles shows both single and aggregated particles. These aggregated particles could be attributed to incomplete surface coverage of the nanoparticles with protamine. The presence of these different species of partially coated and uncoated particles causes the aggregation which is reflected by the high PI readings. In contrast, particles coated with 100  $\mu\text{g/ml}$  protamine were mostly spherical and monodispersed, indicating complete surface coverage of nanoparticles. These TEM micrographs agreed very well with the measurement of the hydrodynamic diameter.

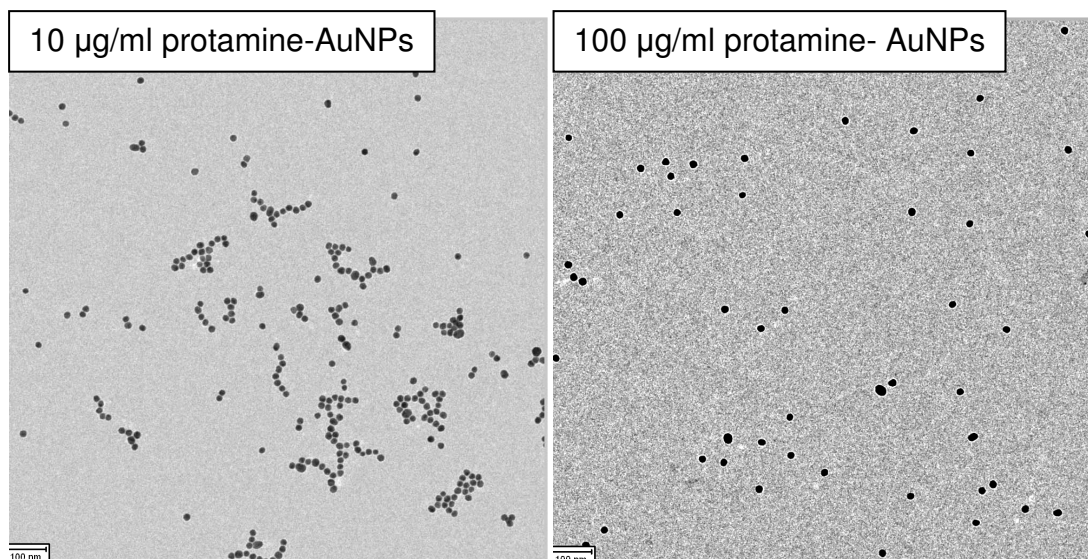


**Figure 3:** TEM images of 10 and 100 µg/ml protamine coated AuNPs

The zeta potential ( $\xi$ -potential) not only plays an important role in the stability of nanoparticles, but is also considered one of the most important parameters characterizing successful deposition of polyelectrolytes on colloidal surfaces. Therefore, to establish the successful coating of nanoparticles with protamine and the cause of aggregation at lower protamine concentrations, zeta potential measurements were carried out. The  $\xi$ -potentials of lower concentrations of protamine coated nanoparticles were about 15.8 and 29 mV for 6 and 10 µg/ml protamine, respectively. However, the highest  $\xi$ -potential (45.2 mV) was observed with 100 µg/ml protamine, as shown in Figure 4. Particle aggregation is less likely to occur for charged particles with a zeta potential higher than 30 mV, due to electrostatic repulsion forces between similarly charged particles [15]. From the particle size distribution, TEM image, and  $\xi$ -potential results, 100 µg/ml protamine was chosen as the optimum concentration for coating of MUA-AuNPs.

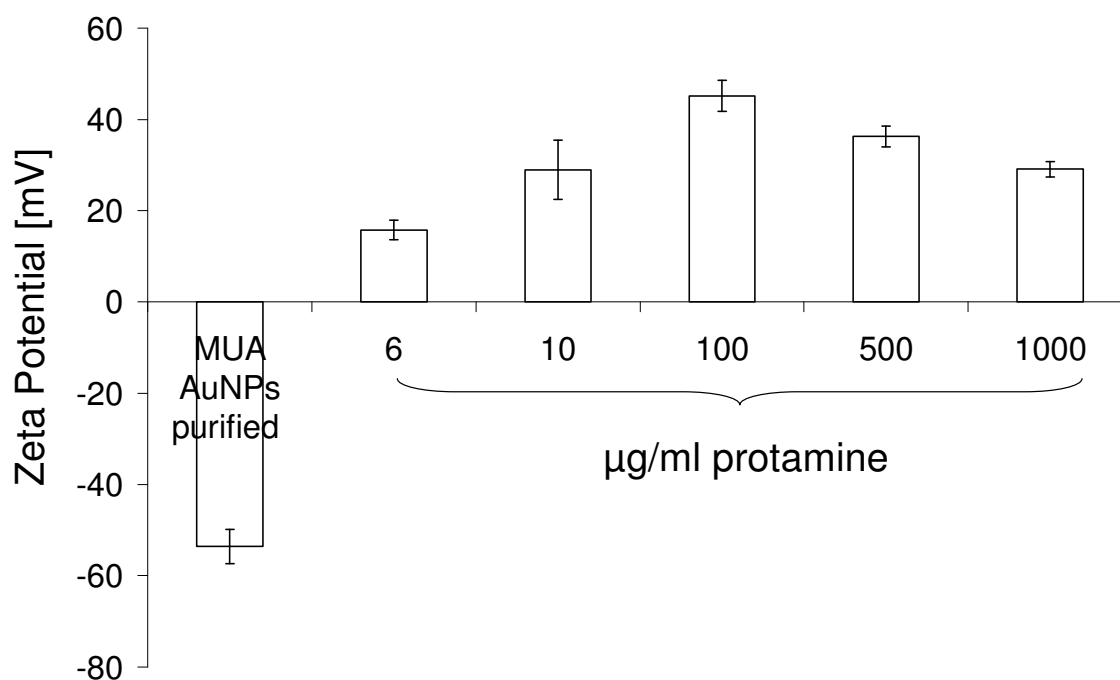


**Figure 4:** Zeta potential of different concentrations of protamine coated MUA-AuNPs at 1 mM NaCl

It is known that the ionic strength of a solution is important in order to reduce the stiffness of a polymer, allowing it to wrap around nanoparticles. Unfortunately increasing the ionic strength also causes an aggregation of nanoparticles [14, 45]. It is therefore necessary to find a balance between chain flexibility and the stability of nanoparticles. We determined the stability of 100  $\mu\text{g/ml}$  protamine coated MUA-AuNPs at different ionic strength by monitoring particle size distribution, zeta potential measurements, and changes in surface plasmon resonance (SPR). The hydrodynamic diameter of protamine coated nanoparticles increased from 29 nm to approximately 58 nm, with increasing ionic strength from 1 to 30 mM NaCl (data not shown). In contrast, there was no significant difference in the  $\xi$ -potential of coated nanoparticles at different ionic strength (data not shown). Figure 5 shows the change in the SPR of MUA-AuNPs before and after coating with protamine at different ionic strength. Only a slight red shift in SPR after coating with protamine at 1, 5, and 10 mM NaCl was observed, which is due to a change in the refractive index of the environment surrounding the nanoparticles. This change is a result of an attached polymer layer around the particles, and is also an indication of the successful coating of nanoparticles with the polymers [46, 47]. However, the SPR shifted about 10 nm after the coating of nanoparticles at 30 mM NaCl, which is considered a sign of

aggregation, reflected by the increased hydrodynamic diameter. The reported increase in size could be attributed to instability and the aggregation of particles at higher ionic strength (30 mM NaCl), since increasing the ionic strength decreases the Debye-Hückel length, allowing the Van der Waals attractive forces to become more pronounced and thereby counteract the repulsive forces [48]. Therefore, 1 mM NaCl was chosen as suitable ionic strength for coating of MUA-AuNPs, since it was sufficient for wrapping protamine around nanoparticles. For the reasons previously mentioned, it is recommended to work at the lowest possible ionic strength when coating nanoparticles with polyelectrolyte via LbL approach [49].

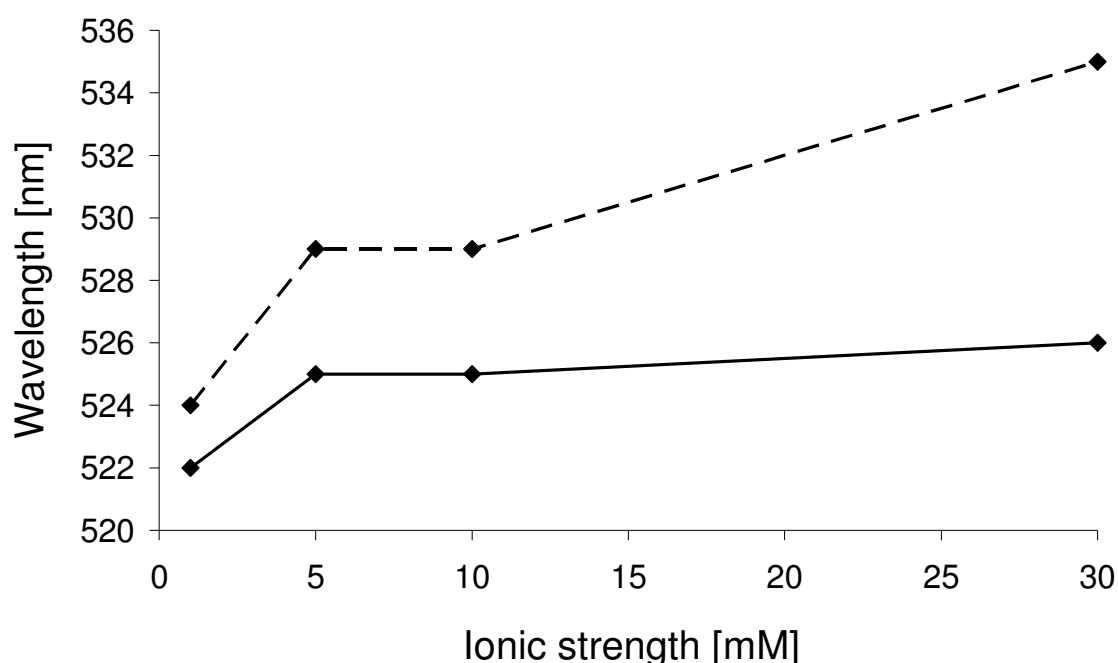


**Figure 5:** Effect of different ionic strength on UV-vis absorbance of MUA-AuNPs (solid line) and protamine-AuNPs (dashed line)

The major challenge in the use of LbL technology on colloidal particles is the purification and removal of excess polyelectrolyte before subsequent coating steps, as to avoid the formation of polyelectrolyte complexes and aggregations in bulk solution [9, 10]. Therefore, several methods, such as centrifugation at high speed (about 15,700  $\times g$ ) and ultrafiltration, were evaluated to purify protamine-AuNPs from free unbound protamine before coating with the polyanion. Unfortunately, the particles aggregated during the purification process and there was no suitable method for the removal of excess protamine. This could be attributed to the low

molecular weight of protamine (only about 5 KDa). Hence, it could be that protamine is not large enough to maintain nanoparticle stabilization during purification, since the polymer length must be long enough to achieve colloidal stability while being short enough to minimize interparticle cross-bridging and flocculation [11, 49, 50]. Due to the difficulty of the purification of nanoparticles with protamine, it was decided that protamine was not suitable for the coating of small AuNPs via the LbL technique.

### 3.1.2. Coating and characterization of stabilized MUA-AuNPs with PEI 25 KDa

In the next step PEI was chosen for coating MUA-AuNPs. In contrast to protamine, PEI is a branched polymer with high molecular weight (25 KDa). Therefore, it could be better for the coating of nanoparticles via the LbL technique than protamine. An ionic strength of 1 mM NaCl was chosen as suitable ionic strength for the coating of purified MUA-AuNPs with PEI 25 KDa in accordance with previous results and reported by Caruso et al. [49, 50]. Figure 6 shows the hydrodynamic diameter and polydispersity index of MUA-AuNPs coated with different concentrations of PEI before (crude) and after purification. The particles were coated well with three different concentrations, as observed from size and  $\xi$ -potential measurements. However, the nanoparticles coated with 0.1 mg/ml PEI aggregated during the purification process and the hydrodynamic diameter increased to about 50 nm with a high PI of about 0.7, which indicates that this concentration failed to stabilize the particles. However, both 0.5 and 1 mg/ml PEI worked well during coating and purification. 1 mg/ml was chosen as the optimum concentration for coating because PEI coated AuNPs (PEI-AuNPs) at this concentration had lower hydrodynamic diameters after purification (about 20 nm) and a PI approximately 0.2, while the PI after coating with 0.5 mg/ml PEI was about 0.4. In addition, 1 mg/ml PEI-AuNPs had higher  $\xi$ -potentials, even after purification. It was 35.8 mV, as shown in Figure 7.

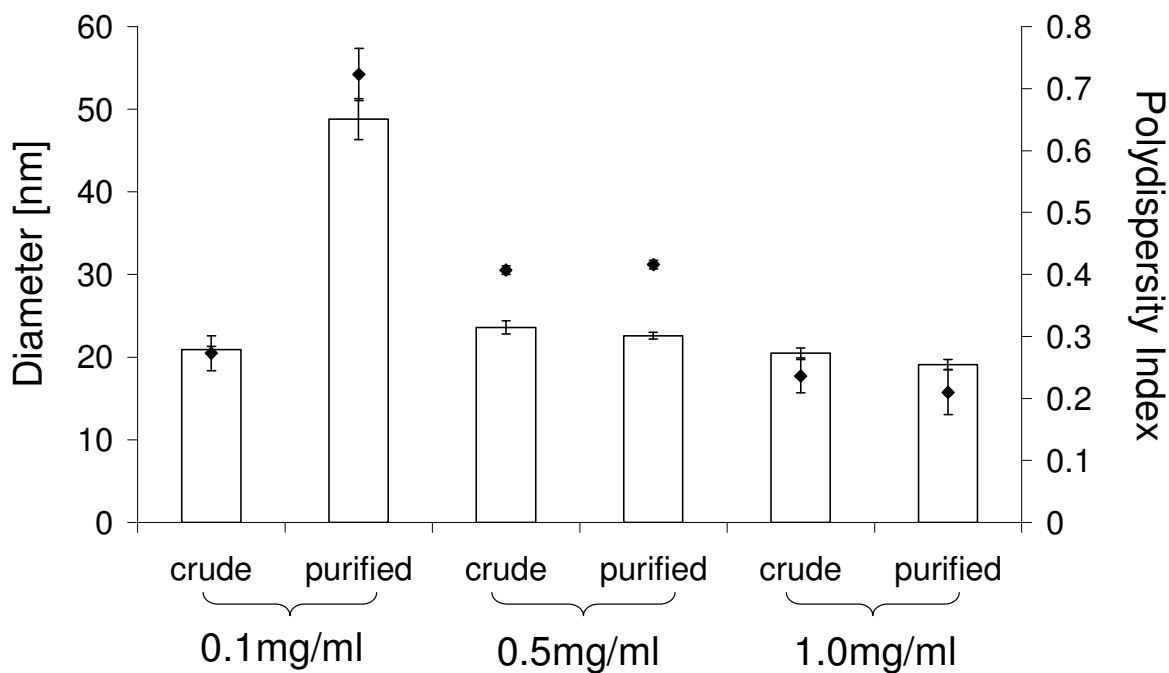


**Figure 6:** The hydrodynamic diameter (white columns) and the polydispersity index (rhombs) of different concentrations of PEI coated MUA-AuNPs at 1 mM NaCl

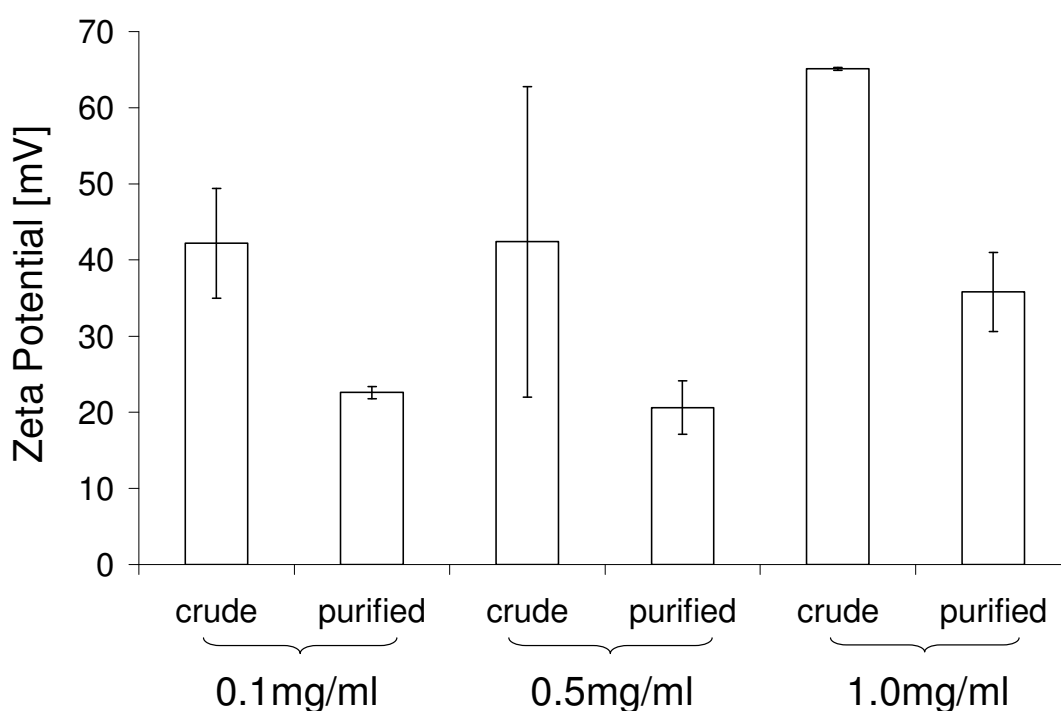


**Figure 7:** Zeta potential of different concentrations of PEI coated MUA-AuNPs at 1 mM NaCl

In order to rule out the formation of nanoparticle aggregates on adsorption of the polyelectrolytes, the coated particles were also characterized by using TEM. Figure 8 shows representative TEM images of 1 mg/ml PEI coated MUA-AuNPs. It can be

seen that the particles were well separated, with no apparent signs of aggregation. It should also be noted that no broadening of the SPR peak of PEI-AuNPs occurred as a result of coating with PEI, suggesting the absence of aggregated nanoparticles (data not shown). Furthermore, the PEI-AuNPs were found to be colloidal stable for more than one month (data not shown).

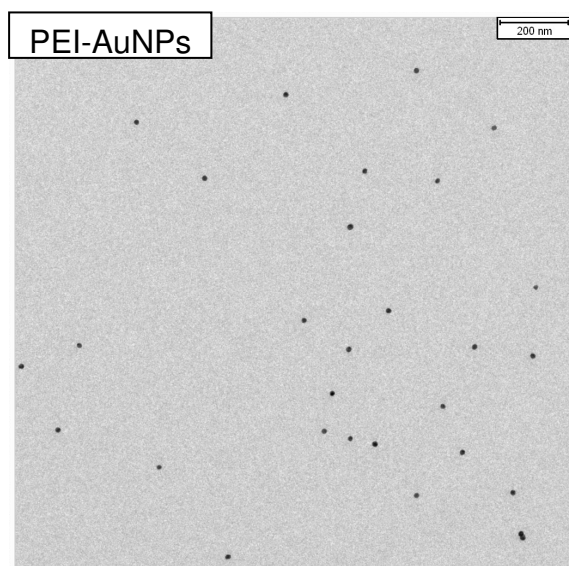


**Figure 8:** TEM image of 1.0 mg/ml PEI-AuNPs

Because successful removal of the excess polyelectrolyte is a critical obstacle for LbL coating, the amount of free PEI in the supernatant after purification was determined. Table 1 shows that after three purification steps only a negligible amount of free PEI was observed, which indicates the removal of the free PEI from the colloid.

**Table 1:** Initial concentration of PEI-AuNPs and its concentration in the discarded supernatant after purification

Layer	Initial polyelectrolyte concentration	Purification step	Polyelectrolyte concentration in supernatant
PEI	1.0 mg/ml	1	0.7312 mg/ml
		2	0.0138 mg/ml
		3	0.0005 mg/ml

Furthermore, the purified particles did not show any signs of toxicity within the CHO-K1 cell as shown in Figure 9. The cells were flat and spreaded, as were the control

cells that were treated with buffer only. The cells that were incubated with crude (unpurified) PEI-AuNPs shrunk and died due to the presence of free PEI, which is considered the main cause of cell death [31]. This result was further confirmed by FACS analysis to determine the viability of CHO-K1 cells after incubation with different volumes of purified PEI-AuNPs. Figure 10 showed nearly no toxic effects on the viability of CHO-K1 cells at different  $\text{Au}^{3+}$  concentrations.

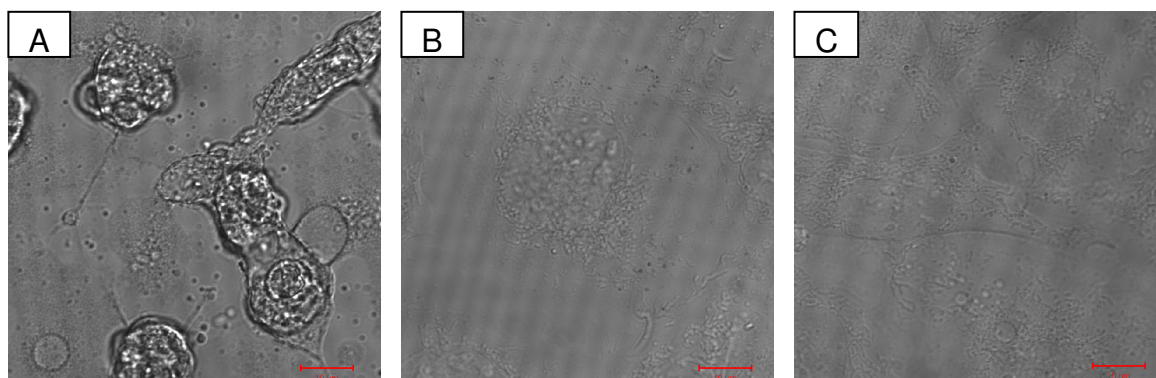


**Figure 9:** Light microscopy images of CHO-K1 cell after incubation with crude (A) and purified (B) PEI-AuNPs at  $\text{Au}^{3+}$  23.3  $\mu\text{M}$  and control cell without particles (C), each bar indicates 10  $\mu\text{m}$

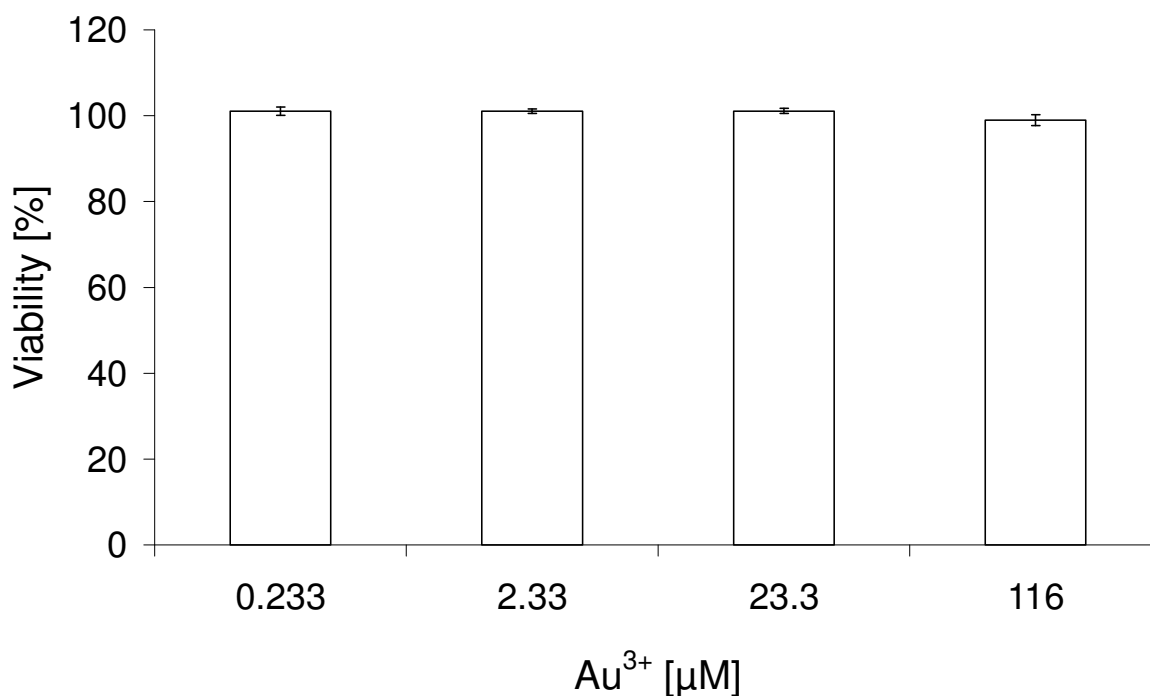


**Figure 10:** Relative viability of CHO-K1 cells after incubation with purified PEI-AuNPs, determined with propidium iodide staining followed by FACS analysis



Nucleic acids like DNA and siRNA are negatively charged, rigid, and stiff biopolymers [21]. Therefore, in order to coat PEI-AuNPs with this stiff nucleic acid and achieve the complete wrapping of nucleic acid around the small AuNPs, it is important to choose a suitable ionic strength that will allow for a reduction in the stiffness of DNA or siRNA, yet still maintain colloidal stability. We determined the stability of purified PEI-AuNPs at different ionic strength by monitoring the nanoparticle's change in size and zeta potential. Figure 11 shows the hydrodynamic diameter and polydispersity index of crude PEI-AuNPs, as well as the values after purification and resuspension in a different concentration of NaCl. The particles showed good stability in different ionic strength, with only a slight increase in PI of purified particles suspended in 30 mM NaCl, which was about 0.4. The  $\xi$ -potential of purified particles slightly decreased with increasing ionic strength, as shown in Figure 12.

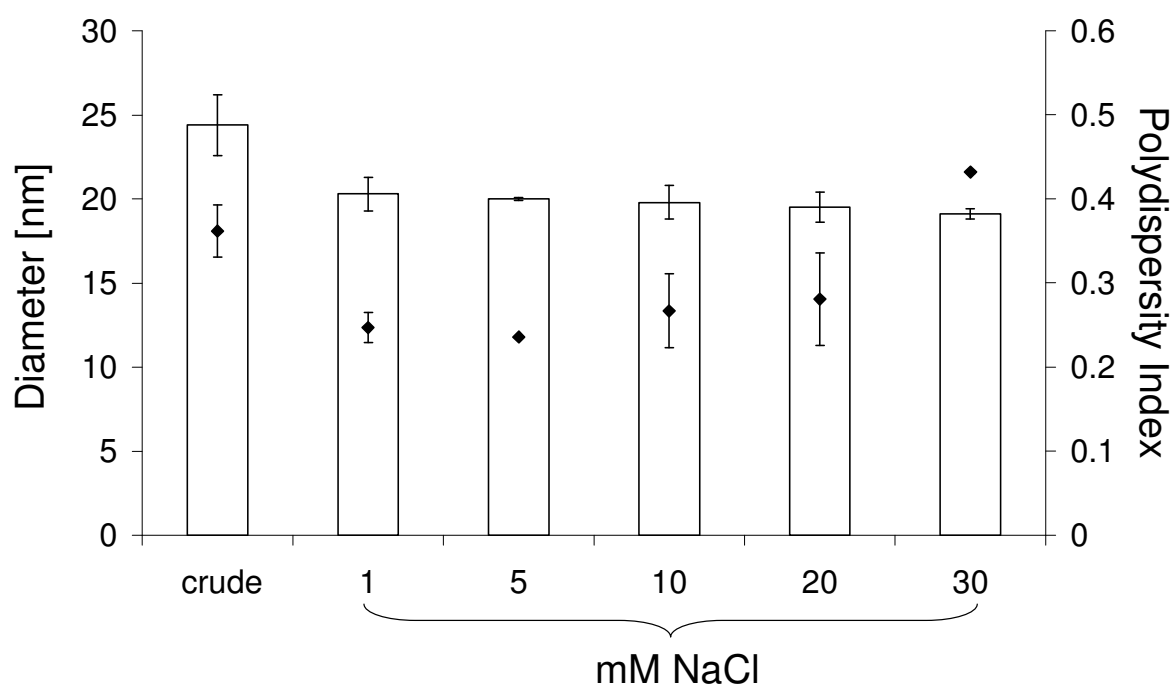


**Figure 11:** Influence of the ionic strength on the hydrodynamic diameter (columns) and polydispersity index (rhombs) of 1.0 mg/ml PEI-AuNPs after purification

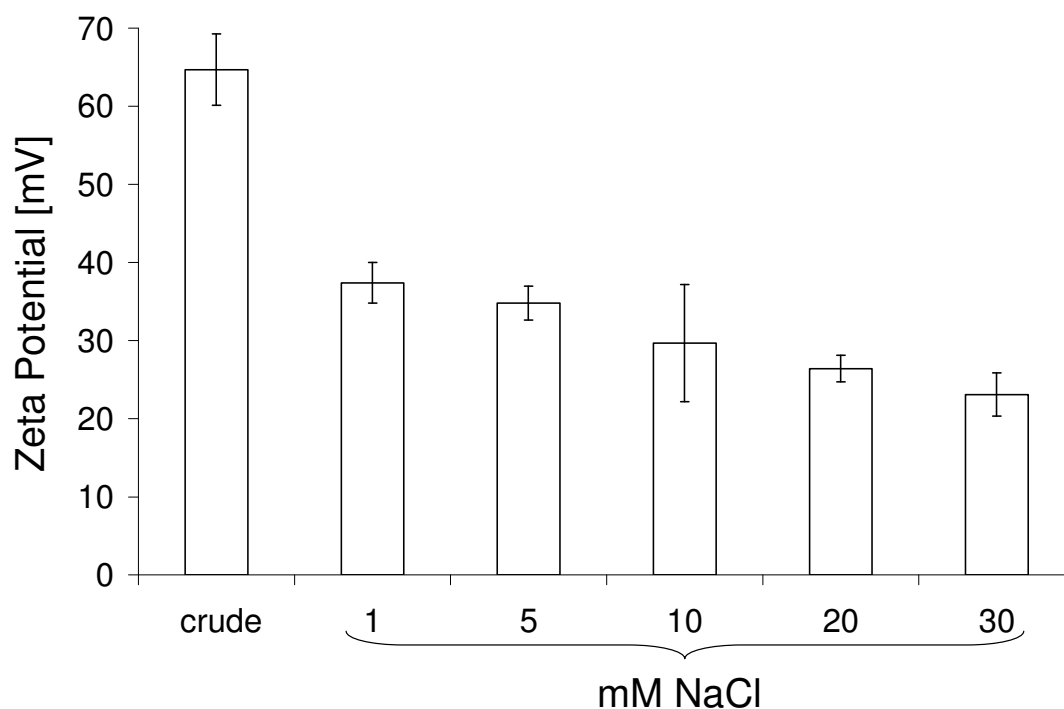


**Figure 12:** Influence of the ionic strength on the  $\xi$ -potential of 1.0 mg/ml PEI-AuNPs after purification

These results show that the purified PEI-AuNPs has good stability at different ionic strength (1-30 mM NaCl). The lowest possible ionic strength (10mM NaCl) required for reducing DNA stiffness and allowing for complete wrapping around AuNPs was selected.

### 3.3. Coating and characterization of purified PEI-AuNPs with polyanion (21 bp DNA)

It is known that full DNA wrapping is obtained for salt concentrations corresponding to the Debye-Hückel screening length larger than  $0.2 \text{ nm}^{-1}$ , as calculated by Kunze and Netz on the salt-induced DNA-histone complexation [12]. Therefore, 10 mM NaCl, which is equivalent to a Debye-Hückel screening length  $0.32 \text{ nm}^{-1}$ , was chosen as the ionic strength able to reduce the stiffness of DNA and cause complete wrapping of it around AuNPs. Purified PEI-AuNPs coated with different concentrations of DNA were characterized by determining particle size distribution and zeta potential. Figure 13 revealed that DNA at concentration of 0.5, 1 and  $1.5 \mu\text{M}$  DNA successfully coated nanoparticles. However, the particles coated with  $0.5 \mu\text{M}$  DNA aggregated during purification, with a dramatic increase in size (100 nm). This aggregation indicates that  $0.5 \mu\text{M}$  DNA is not concentrated enough to keep the

particle stable during purification, while particles coated with 1 and 1.5  $\mu\text{M}$  DNA showed good stability after purification. However, 1  $\mu\text{M}$  DNA had a high PI before and after purification.

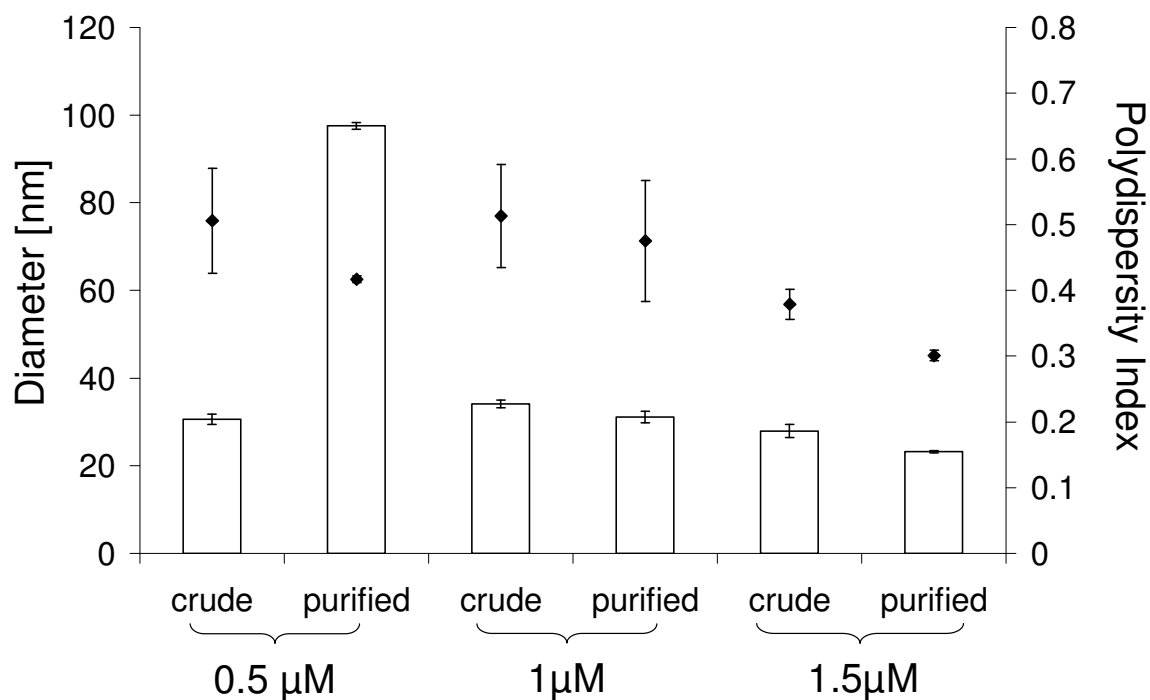


**Figure 13:** The hydrodynamic diameter (white columns) and the polydispersity index (rhombs) of different concentrations of DNA coated PEI-AuNPs before (crude) and after purification (purified)

In addition, the  $\xi$ -potential of 0.5 and 1  $\mu\text{M}$  DNA after purification significantly decreased and became nearly neutral, as shown in Figure 14. 1.5  $\mu\text{M}$  DNA showed the highest  $\xi$ -potential before and after purification,  $-67.2 \pm 1.7$  and  $-37.6 \pm 1.7$  mV respectively, which indicates the stability of coated particles. This also demonstrates the inversion of  $\xi$ -potential from positive to negative, signifying the successful wrapping of DNA around nanoparticles. Therefore, 1.5  $\mu\text{M}$  DNA was chosen as suitable concentration for coating of PEI-AuNPs and the produced DNA/PEI-AuNPs were monodispersed and free from aggregate, as shown in TEM images in Figure 15.

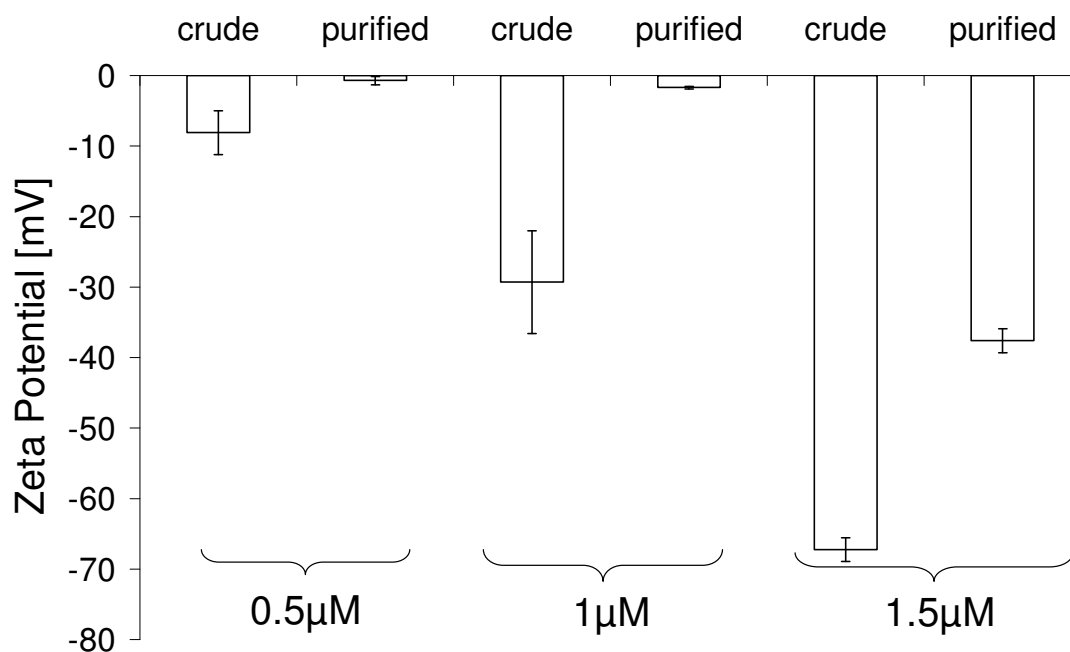


**Figure 14:** The  $\xi$ -potential of different concentrations of DNA coated PEI-AuNPs before (crude) and after purification (purified)

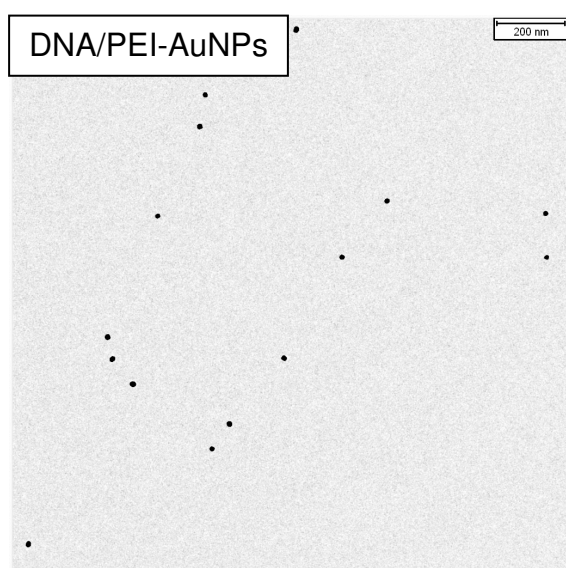


**Figure 15:** TEM image of 1.5  $\mu$ M DNA/PEI-AuNPs

In order to confirm successful purification, the amount of free DNA in the supernatant was determined. Table 2 shows only trace amounts of DNA remained after the second purification step. Hence, there was no chance of polyelectrolyte complex formation during the last step of coating with PEI. In addition, both crude and purified particles did not show any signs of toxicity when incubated with CHO-K1 cell for 4

hours (data not shown). The absence of toxicity with crude particles could be attributed to the fact that DNA is a biopolymer and not toxic to the cells.

**Table 2:** Initial concentration of DNA coated PEI-AuNPs and the concentration in the discarded supernatant after purification.

Layer	Initial polyelectrolyte concentration	Purification step	Polyelectrolyte concentration in supernatant
DNA	1.5 $\mu$ M	1	1.30 $\mu$ M
		2	0.07 $\mu$ M

### 3.4. Fabrication of polyelectrolyte coated gold nanoparticles via LbL technology

According to the optimal parameters identified earlier, MUA-AuNPs were assembled via the LbL technique. The first layer polycation was PEI, the second layer was negatively charged DNA, and the third was again PEI, which formed LbL-coated PEI/DNA/PEI-AuNPs. The successful polyelectrolyte deposition was monitored by dynamic light scattering (DLS),  $\xi$ -potential measurement, UV-vis absorbance spectroscopy, and TEM. Figure 16 shows that the hydrodynamic diameter increased during coating from  $21.6 \pm 0.5$  nm (MUA-AuNPs) to  $25.5 \pm 0.8$  nm (PEI/DNA/PEI-AuNPs). Additionally, a reversal in  $\xi$ -potential signified the deposition of each polyelectrolyte layer (Figure 17). The  $\xi$ -potential slightly decreased after purification due to the removal of free unbound polyelectrolyte.

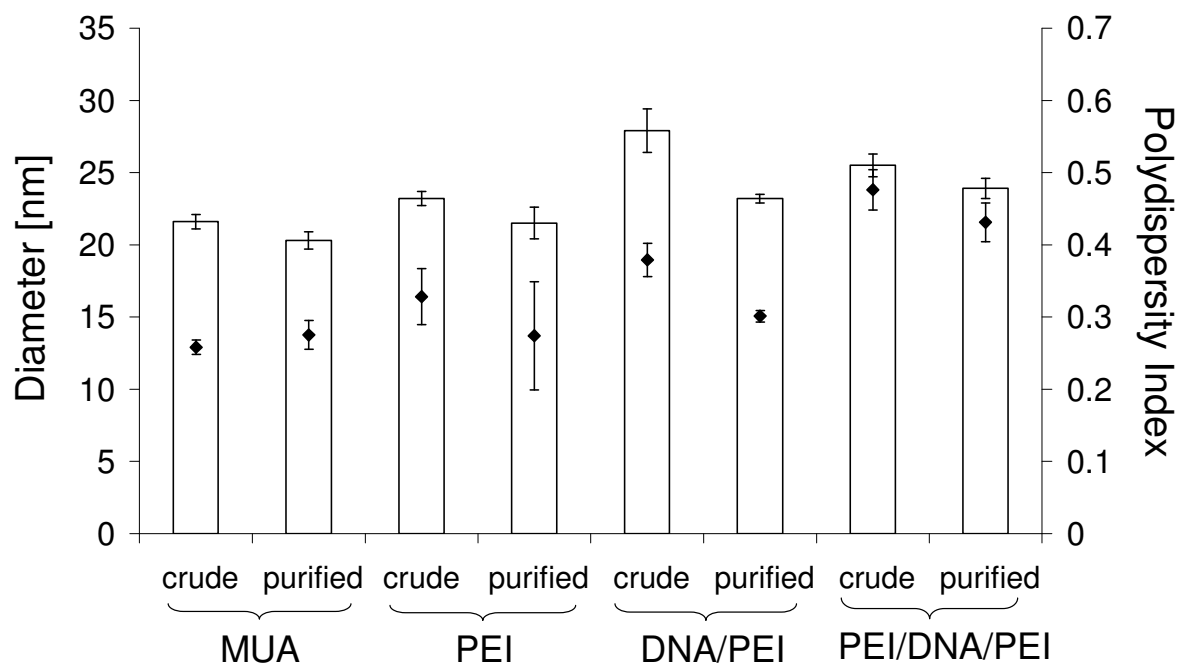


**Figure 16:** Effect of subsequent coating steps of AuNPs during LbL build-up on the hydrodynamic diameter (white columns) and the polydispersity index (rhombs) of AuNPs before (crude) and after purification (purified)

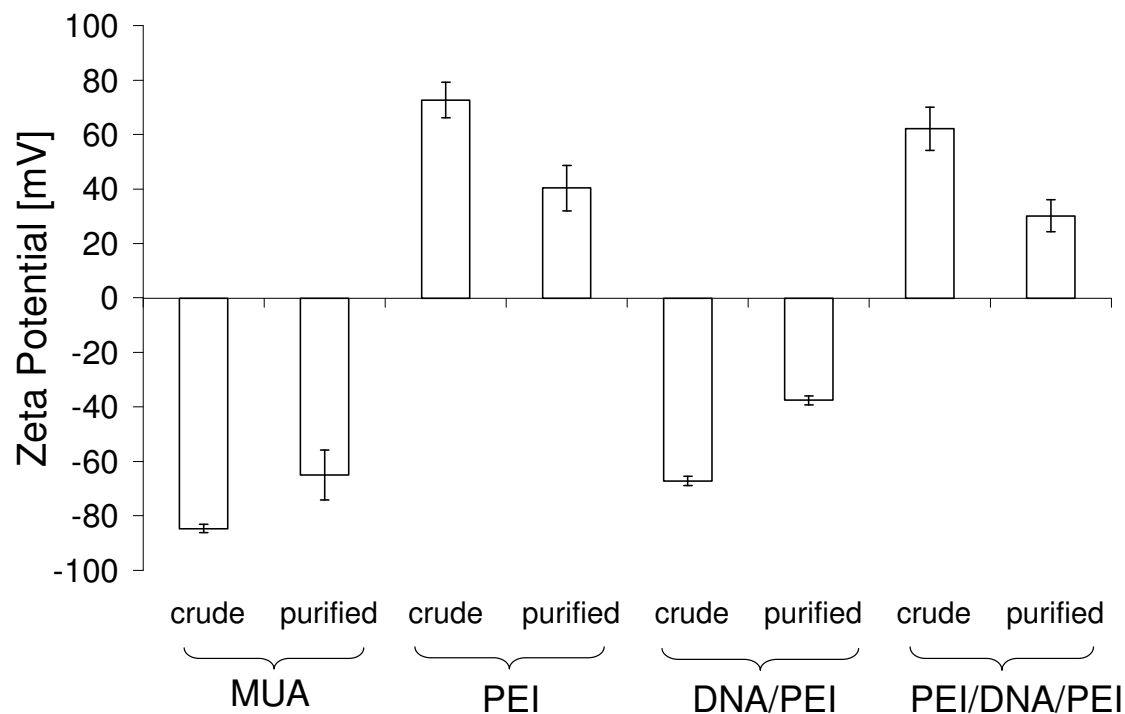


**Figure 17:** Effect of subsequent coating steps of AuNPs during LbL build-up on the  $\xi$ -potential of AuNPs before (crude) and after purification (purified)

The change in the surface plasmon resonance of gold nanoparticles was used to differentiate between polymer adsorption onto the AuNPs surface and interparticulate bridging and aggregation [49, 51]. The UV-vis spectra of AuNPs on Figure 18 shows only a small red shift (1 and 2 nm) in the SPR, which is attributed to subsequent layer deposition and increases in nanoparticle size, along with an overall decrease in the maximum absorbance intensity. This decrease is attributed to dilution effects during purification steps. To further characterize the LbL buildup, TEM images of the nanoparticles were taken after the completion of LbL coating. Figure 19 revealed that the nanoparticles were mainly spherical and well separated from each other, without any signs of aggregation. The polyelectrolyte coating around the nanoparticles could not be seen, which is due to the lack of contrast between the nanoparticles and the background at the given magnification.

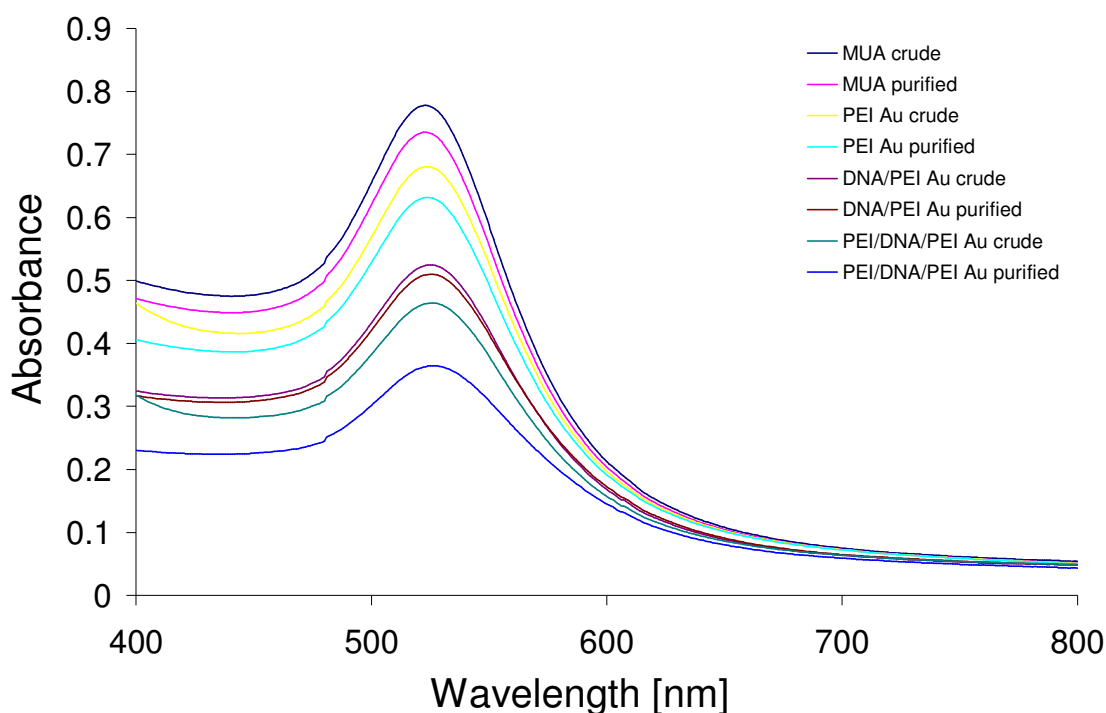


**Figure 18:** UV-vis spectra of AuNPs coated with polyelectrolyte

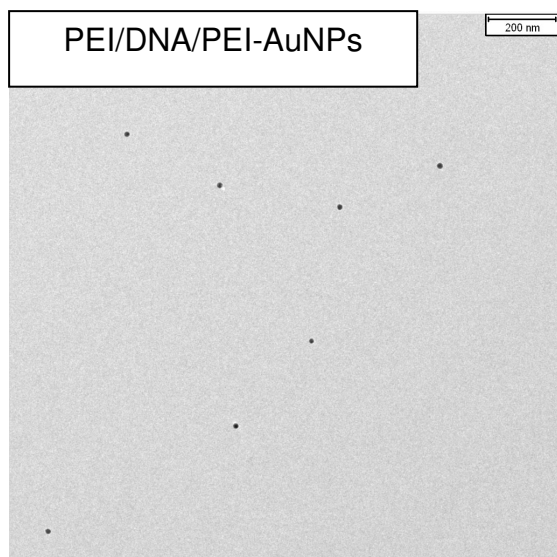


**Figure 19:** TEM images of PEI/DNA/PEI-AuNPs

In most cases, self assembled aggregates of PEI and nucleic acid suffer from severe aggregation when subjected to the high ionic strength of biological fluids [33, 52], and the initial size of these complexes may increase to several micrometers [33]. This feature would make the fabrication of LbL-coated nanoparticles tedious and would render their application in cell culture pointless, because the nanoparticles would no longer be monodisperse. Therefore, the AuNPs were exposed to cell culture medium with and without fetal bovine serum, and the hydrodynamic diameter,  $\xi$ -potential, and the change in SPR were monitored. Regardless of the type of the outer layer (PEI or DNA) the hydrodynamic diameter of AuNPs only increased by a factor of 2.1 to 2.5 in culture medium containing serum. This increase in size would be attributed to the adsorption of proteins on the surface of AuNPs, as already demonstrated with unmodified and other oligonucleotide-modified AuNPs [53, 54]. In contrast, the particle size increased by a factor of 7 to 10 in serum-free culture medium as shown in Figure 20. This change in the hydrodynamic diameter was also reflected in the red shift of the SPR. The maximum plasmon peak ( $\lambda_{\max}$ ) was 530, 531, and 535 nm for PEI-, DNA/PEI-, and PEI/DNA/PEI-AuNPs in culture medium containing serum (data not shown). In serum-free culture medium, the individuality of AuNPs was lost, as demonstrated with  $\lambda_{\max}$  values of 573, 579, and 583 nm for PEI-, DNA/PEI-, and PEI/DNA/PEI-AuNPs, respectively (data not shown). These results corroborate the hypothesis that serum proteins are necessary for the nanoparticles stabilization.



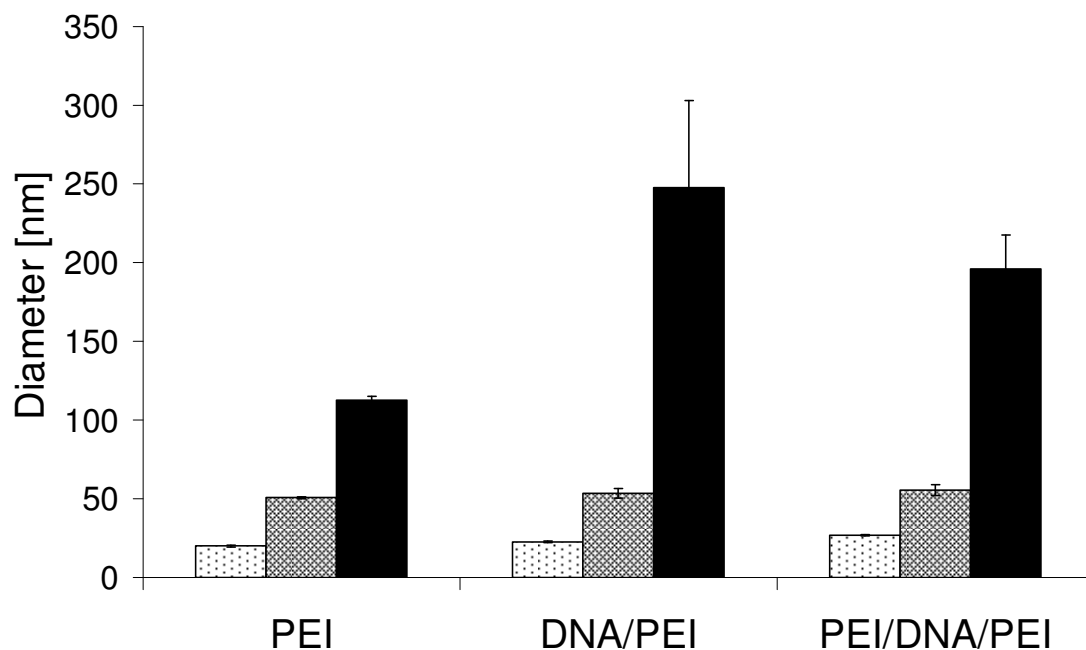


**Figure 20:** The hydrodynamic diameter of subsequent coating steps of AuNPs layers in water (▨), serum containing culture medium (▩), and serum free culture medium (■)

Moreover, the  $\xi$ -potential of all particle types was negative after incubation in culture medium (Figure 21). More specifically, the negative  $\xi$ -potential of DNA/PEI-AuNPs became more positive, while PEI- and PEI/DNA/PEI-AuNPs showed a reversal of the charge. In addition, the purified PEI/DNA/PEI-AuNPs did not show any signs of toxicity after incubation with CHO-K1 cells, while crude unpurified particles caused severe toxicity to the cells from the presence of free unbound PEI (Figure 22).

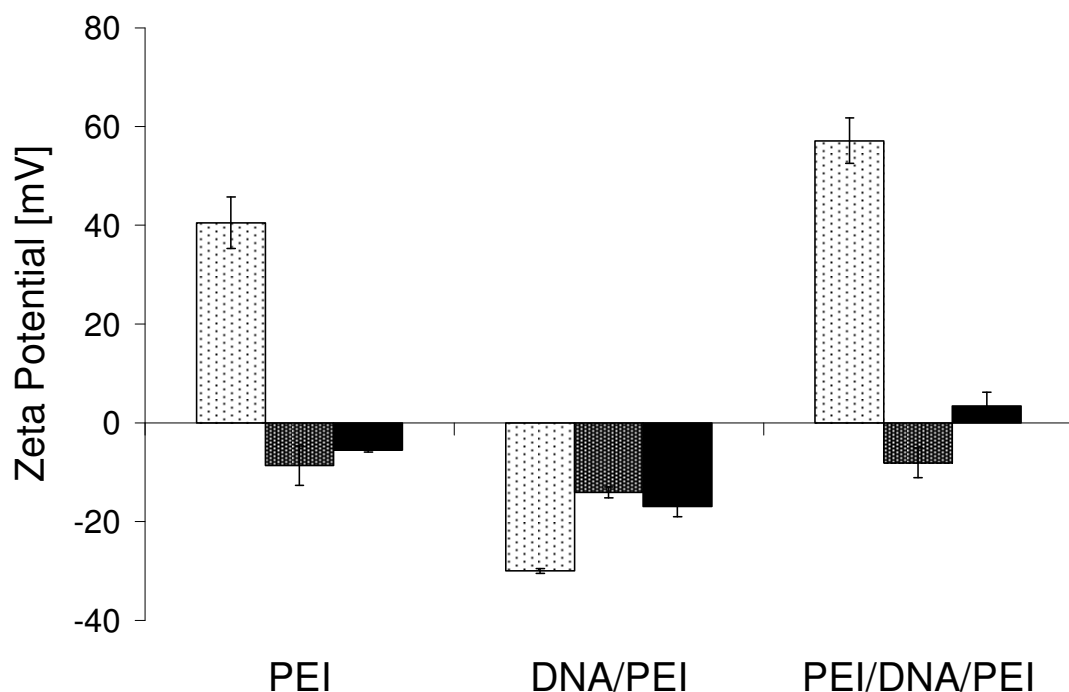


**Figure 21:** The  $\xi$ -Potential of subsequent coating steps of AuNPs in water (▨), serum-containing culture medium (▩), and serum-free culture medium (■)

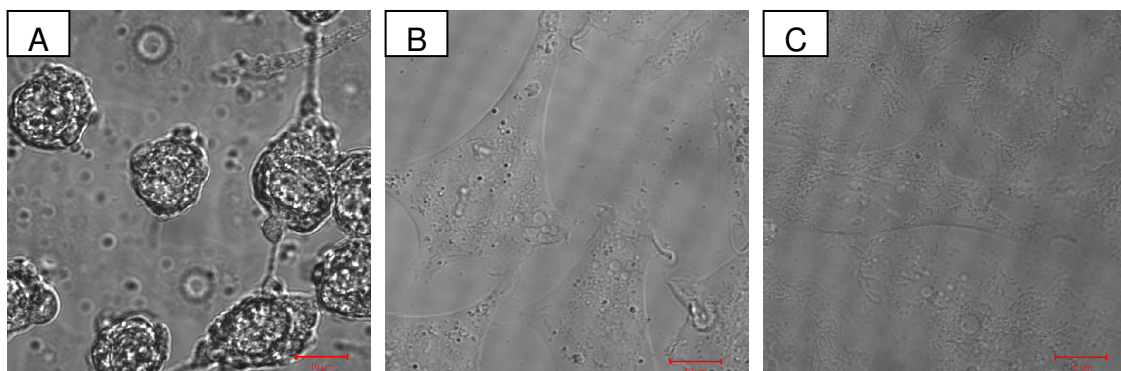


**Figure 22:** Light microscopy images of a CHO-K1 cell after incubation with crude (A) and purified (B) PEI/DNA/PEI-AuNPs at  $\text{Au}^{+3}$   $23.3 \mu\text{M}$  and control cell without particles (C). Each bar indicates  $10 \mu\text{m}$

In order to determine if the particles are taken up by cells and to obtain quantitative data for the number of AuNPs per cell, CHO-K1 cells were incubated with DNA/PEI- and PEI/DNA/PEI-AuNPs for 6 hrs in culture medium containing serum, and the  $\text{Au}^{+3}$  content was determined by ICP-OES. Both types of particles were successfully taken up by the cells, and the amount of the particles per cell strongly depended on the type of the top layer. CHO-K1 cells internalized more DNA/PEI-AuNPs ( $66.1 \times 10^3$ ) in relation to PEI/DNA/PEI-AuNPs ( $37.7 \times 10^3$ ) (Figure 23). This significant difference in

the cellular uptake of AuNPs that are of nearly similar size but has different outer layers suggests that surface properties may strongly influence internalization of the nanoparticles within cells.

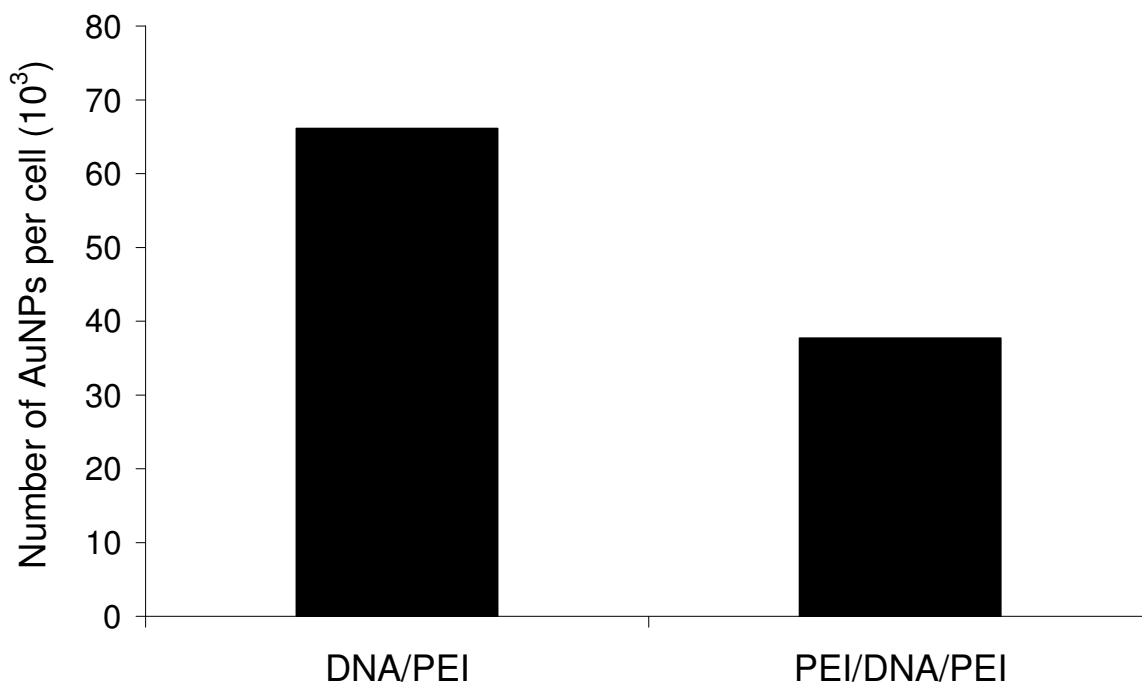


**Figure 23:** The cellular uptake of AuNPs. The number of AuNPs per cell as determined by ICP-OES and cell counting after 6 hours of incubation in serum containing culture medium as a function of surface modification. For each measurement cells from 3 culture flasks ( $75\text{ cm}^2$  each) were pooled to obtain values within the calibration range, bars are averages of two measurements of one representative experiment of two independent ones.

#### 4. Summary and conclusion

By controlling the polyelectrolyte type, concentration, ionic strength of the surrounding medium, and particle surface properties, AuNPs were successfully assembled with polyelectrolytes via the LbL approach for nucleic acid delivery. 1.0 mg/ml PEI 25 KDa was chosen as the positively charged polyelectrolyte at 1 mM NaCl, while 1.5  $\mu$ M of 21 bp DNA was selected as a model negatively charged polyelectrolyte at 10 mM NaCl. The resulting particles were small ( $\sim$  26 nm), and had a narrow size distribution with a polydispersity index of about 0.4. Although a high toxicity was observed with the formulation containing branched PEI 25 KDa, our purified particles did not show any visible signs of toxicity after incubation with CHO-K1 cells, due to removal of free unbound PEI from the particles. Moreover, the produced particles showed good stability in culture medium containing serum, which is attributed to the stabilization of the nanoparticles by serum proteins. This is considered a prerequisite for successful cellular uptake of monodisperse particles. In addition, both types of particles (DNA/PEI- and PEI/DNA/PEI-AuNPs) were successfully taken up by CHO-K1 cells and the amount of AuNPs per cell depended on the type of the top layer. Overall, these results demonstrated that delivery of nucleic acid can be achieved via LbL technology with colloidal gold as a template. These established parameters bring to fruition the successful fabrication of well defined and homogeneously distributed nano-carriers for siRNA delivery via the LbL technique.

## 5. References

- [1] Sperling, R. A.; Parak, W. J. Surface modification, functionalization and bioconjugation of colloidal inorganic nanoparticles. *Phil. Trans. R. Soc. A* 2010; **368**: 1333-1383.
- [2] Seo, J.; Schattling, P.; Lang, T.; Jochum, F.; Nilles, K.; Theato, P.; Char, K. Covalently bonded layer-by-layer assembly of multifunctional thin films based on activated esters. *Langmuir* 2010; **26**: 1830-1836.
- [3] Decher, G., Schlenoff, J. B. *Multilayer thin films: Sequential assembly of nanocomposite materials*; Eds.; Wiley-VCH: Weinheim, 2003.
- [4] Decher, G. Fuzzy nanoassemblies: Toward layered polymeric multicomposites. *Science* 1997; **277**: 1232-1237.
- [5] Hammond, P.; T. Recent explorations in electrostatic multilayer thin film assembly. *Curr. Opin. Colloid Interface Sci.* 2000; **4**: 430-442.
- [6] Boyer, C.; Bousquet, A.; Rondolo, J.; Whittaker, MR.; Stenzel, MH.; Davis, TP. Glycopolymer decoration of gold nanoparticles using a LbL approach. *Macromolecules* 2010; **43**: 3775-3784.
- [7] Dorris, A.; Rucareanu, S.; Reven, I.; Barrett, CJ.; Lennox, R.B. Preparation and characterization of polyelectrolyte-coated gold nanoparticles. *Langmuir* 2008; **24**: 2532-2538.
- [8] Caruso, F. *Colloids and colloid assemblies: Synthesis, modification, organization and utilization of colloid particles*; Eds.; Wiley-VCH: Weinheim, 2004.
- [9] Mayya, K.S.; Schoeler, B.; Caruso, F. Preparation and organization of nanoscale polyelectrolyte-coated gold nanoparticles. *Adv. Funct. Mater.* 2003; **13**: 183-188.
- [10] Dähne, L.; Peyratout, C.S. Tailor-made polyelectrolyte microcapsules: from multilayer to smart containers. *Angew. Chem. Int. Ed.* 2004; **43**: 3762-3783.
- [11] Schneider, G.; Decher, G. Functional core/shell nanoparticles via Layer-by-Layer assembly. Investigation of the experimental parameters for controlling particle aggregation and for enhancing dispersion stability. *Langmuir* 2008; **24**: 1778-1789.
- [12] Israelachvili, J. *Intermolecular & Surface Forces*; second ed., Academic Press Limited, London, 1991.
- [13] Kunze, K.-K.; Netz, R. R. Salt-induced DNA-histone complexation. *Phys. Rev. Lett.* 2000; **85**: 4389-4392.
- [14] Netz, R. R.; Joanny, J.-F. Complexation between a semiflexible polyelectrolyte and an oppositely charged sphere. *Macromolecules* 1999; **32**: 9026-9040.

- [15] Hayat, M. A. *Colloidal gold: principles, methods and applications*: Academic Press: San Diego, 1989.
- [16] Jewell, CM.; Zhang, J.; Fredin, NJ.; Lynn, DM. Multilayered polyelectrolyte films promote the direct and localized delivery of DNA to cells. *J. Control. Rel.* 2005; **106**:214–223.
- [17] Meyer, F.; Ball, V.; Schaaf, P.; Voegel, JC.; Ogier, J. Polyplex-embedding in polyelectrolyte multilayers for gene delivery. *Biochim. Biophys. Acta* 2006; **1758**:419–422.
- [18] Jessel, N.; *et al.* Multiple and time-scheduled in situ DNA delivery mediated by beta-cyclodextrin embedded in a polyelectrolyte multilayer. *Proc. Natl. Acad. Sci. U.S.A.* 2006; **103**:8618–8621.
- [19] Recksiedler, C.L.; Deore, B.A.; Freund, M.S. A novel layer-by-layer approach for the fabrication of conducting polymer/RNA multilayer films for controlled release. *Langmuir* 2006; **22**: 2811–2815.
- [20] Dimitrova, M.; Affolter, C.; Meyer, F.; Nguyen, I.; Richard, D. G.; Schuster, C.; Bartenschlager, R.; Voegel, J. C.; Ogier, j.; Baumert, T. F. Sustained delivery of siRNAs targeting viral infection by cell-degradable multilayered polyelectrolyte films. *PNAS*. 2008; **105**: 16320-16325.
- [21] Gary, D. j.; Puri, N.; Won, Y. Y. Polymer-based siRNA delivery: perspectives on the fundamental and phenomenological distinctions from polymer-based DNA delivery. *J. Control. Rel.* 2007; **121**: 64-73.
- [22] Srivastava, S.; Kotov, N A. Composite Layer-by-Layer (LBL) assembly with inorganic nanoparticles and nanowires. *Accounts of Chemical Research* 2008; **41**: 1831-1841.
- [23] Kerkmann, M.; Lochmann, D.; Weyermann, J.; Marchner, A.; Poeck, H.; Wagner, M.; Battiany, J.; Zimmer, A.; Enderes, S.; Hartman, G. Immunostimulatory properties of CpG-oligonucleotides are enhanced by the use of protamine nanoparticles. *Oligonucleotides* 2006; **16**: 313-322.
- [24] Kabanov, A V.; Kabanov, V A. DNA complexes with polycations for the delivery of genetic material into cells. *Bioconjugate Chem.* 1995; **6**: 7-20.
- [25] Brewer, L.; Corzett, M.; Lau, E. Y.; Balhorn, R. Dynamics of protamine 1 binding to single DNA molecules. *J. Biol. Chem.* 2003; **278**:42403-42408.
- [26] Dunne, M.; Bibby, D. C.; Jones, J. C.; Cudmore, S. Encapsulation of protamine sulphate compacted DNA in polylactide and polylactide-co-glycolide microparticles. *J. Control. Rel.* 2003; **92**: 209-219.
- [27] Yip, C. M.; Brader, M. L.; Frank, B. H.; DeFelippis, M. R.; Ward, M. D. Structural studies of a crystalline insulin analogue complex with protamine by atomic force microscopy. *Biophys. J.* 2000; **78**: 466-473.
- [28] Balabushevich, N. G.; Tiourina, O. P.; Volodkin, D. V.; Larionova, N. I.; Sukhorukov, G. B. Loading the multilayer dextran sulfate/protamine

- microsized capsules With peroxidase. *Biomacromolecules* 2003; **4**: 1191-1197.
- [29] Hiller, S.; Leporatti, S.; Schnäckel, A.; Typlt, E.; Donath, E. Protamine assembled in multilayers on colloidal particles can be exchanged and released. *Biomacromolecules* 2004; **5**: 1580-1587.
- [30] Yamauchi, F.; Kato, K.; Iwata, H. Layer-by-Layer assembly of poly(ethyleneimine) and plasmid DNA onto transparent indium-tin oxide electrodes for temporally and spatially specific gene transfer. *Langmuir* 2005; **21**: 8360-8367.
- [31] Lv, H.; Zhang, S.; Wang, B.; Cui, S.; Yan, J. Toxicity of cationic lipids and cationic polymers in gene delivery. *J. Control. Rel.* 2006; **114**: 100-109.
- [32] Boussif, O.; Lezoualch, F.; Zanta, M.A.; Mergny, M.D.; Scherman, D. Demeneix, B.; Behr, J. A versatile vector for gene and oligonucleotide transfer into cells in culture and in vivo: polyethylenimine. *Proc. Natl. Acad. Sci. U. S. A.* 1995; **92**: 7297-7301.
- [33] Lungwitz, U.; Breunig, M.; Blunk, T.; Goepferich, A. Polyethylenimine-based non-viral gene delivery systems, *Eur. J. Pharm. Biopharm.* 2005; **60**: 247-266.
- [34] Akine, A., Thomas, M.; Klibanov, A.M.; Langer, R. Exploring polyethylenimine-mediated DNA transfection and the proton sponge hypothesis, *J. Gene Med.* 2005; **7**: 657-663.
- [35] Frens, G. Controlled nucleation for the regulation of the particle size in monodisperse gold suspensions. *Nature (London), Physical Science* 1973; **241**: 20-22.
- [36] Grabar, KC.; Freeman, RG.; Hommer, MB.; Natan, MJ. Preparation and characterization of Au colloid monolayers. *Anal. Chem.* 1995; **67**: 735-743.
- [37] Lin, S-Y.; Tsai, Y-T.; Chen, C-C.; Lin, C-M.; Chen, C-H. Two-step functionalization of neutral and positively charged thiols onto citrate-stabilized Au nanoparticles. *J. phys. Chem. B* 2004; **108**: 2134-2139.
- [38] Snyder, S. L.; Sobocinski, P. Z. An improved 2,4,6-trinitrobenzenesulfonic acid method for the determination of amines. *Anal. Biochem.* 1975; **64**: 284-288.
- [39] Breunig, M.; Hozsa, C.; Lungwitz, U.; Watanabe, K.; Umeda, I.; Kato, H.; Goepferich, A. Mechanistic investigation of poly(ethylene imine)-based siRNA delivery: Disulfide bonds boost intracellular release of the cargo. *J. Control. Rel.* 2008; **130**: 57-63.
- [40] Cumberland, S. L.; Strouse, G. F. Analysis of the nature of oxyanion adsorption on gold nanomaterial surfaces. *Langmuir* 2002; **18**: 269-276.
- [41] Hiemenz, P. C. *Principles of Colloids, Surface Chemistry, 2nd ed.*; Marcel Dekker, Inc.: New York, 1989.

- [42] Caruso, F. Nanoengineering of particle surfaces. *Adv. Mater.* 2001; **13**: 11-22.
- [43] Heller, W.; Pugh, T. L. Steric stabilization of colloidal solutions by adsorption of flexible macromolecules. *J. Polym. Sci.* 1960; **47**: 203-217.
- [44] Gaumet, M.; Vargas, A.; Gurny, R.; Delie, F. Nanoparticles for drug delivery: The need for precision in reporting particle size parameters. *Eur. J. Pharm. Biopharm.* 2008; **69**: 1-9.
- [45] Wang, G.; Sun, W. Optical limiting of gold nanoparticles aggregates induced by electrolytes. *J. Phys. Chem. B* 2006; **110**: 20901-20905.
- [46] Eck, D.; Helm, C. A.; Wagner, N. J.; Vaynberg, A. Plasmon resonance measurements of the adsorption and adsorption kinetics of a biopolymer onto gold nanocolloids. *Langmuir* 2007; **23**: 9522.
- [47] Dixit, V.; Bossche, J. Vd.; Sherman, D. M.; Thompson, D. H. Andres, R. P. Synthesis and grafting of thioctic acid-PEG-folate conjugates onto Au nanoparticles for selective targeting of folate receptor-positive tumor cells. *Bioconjugate Chem.* 2006; **17**: 603-609.
- [48] Hunter, R.J. *Foundations of Colloid Science*, vol. 1, Clarendon Press, Oxford, 1993, pp. 329–341, 415–418.
- [49] Gittins, D.I.; Caruso, F. Tailoring the polyelectrolyte coating of metal nanoparticles. *J. Phys. Chem. B* 2001; **105**: 6846-6852.
- [50] Gittins, D.I.; Caruso, F. Multilayered polymer nanocapsules derived from gold nanoparticle templates. *Adv. Mater.* 2000; **12**: 1947-1949.
- [51] Schneider, G.; Decher, G. From functional core/shell nanoparticles prepared via layer-by-layer deposition to empty nanospheres. *Nano Lett.* 2004; **4**: 1833-1839.
- [52] Neu, M.; Fischer, D.; Kissel, T. Recent advances in rational gene transfer vector design based on poly(ethylene imine) and its derivatives. *J. Gene Med.* 2005; **7**: 992-1009.
- [53] Chithrani, B. D.; Ghazani, A. A.; Chan, W. C. Determining the size and shape dependence of gold nanoparticle uptake into mammalian cells. *Nano Lett.* 2006; **6**: 662-668.
- [54] Giljohann, D. A.; Seferos, D.S.; Patel, P.C.; Millstone, J. E.; Rosi, N. L.; Mirkin, C. A. Oligonucleotide loading determines cellular uptake of DNA-modified gold nanoparticles. *Nano Lett.* 2007; **7**: 3818-3821.



## **Chapter 4**

### **Layer-by-Layer Assembled Gold Nanoparticles for siRNA Delivery**

Asmaa Elbakry<sup>1</sup>, Alaa Zaky<sup>1</sup>, Renate Liebl<sup>1</sup>, Reinhard Rachel<sup>2</sup>, Achim Goepperich<sup>1</sup>,  
Miriam Breunig<sup>1</sup>

<sup>1</sup>Department of Pharmaceutical Technology, university of Regensburg,  
Regensburg, Universitätsstraße 31, 93040 Regensburg, Germany

<sup>2</sup>Centre for Electron Microscopy at the Institute for Anatomy, University of  
Regensburg, Universitätsstraße 31, 93040 Regensburg, Germany

**Abstract**

Although uptake into cells is highly complex and regulated, heterogeneous particle collectives are usually employed to deliver small interfering RNA (siRNA) to cells. Within these collectives, it is difficult to accurately identify the active species, and a decrease in efficacy is inherent to such preparations. Here, we demonstrate the manufacture of uniform nanoparticles with the deposition of siRNA on gold in a Layer-by-Layer approach, and we further report on the cellular delivery and siRNA activity as functions of surface properties.

## Introduction

The creation and design of nano-sized carriers for the delivery of nucleic acids such as small interfering RNAs (siRNAs) have recently gained interest because of their possible clinical applications [1, 2]. The interaction with cell membranes is of central importance for these delivery systems, because this represents the key event in the regulation of the uptake process. The multiple portals of entry into mammalian cells strongly vary with regard to the nature and size of the cargo, as do their intracellular destination and fate [3]. Consequently, the pathway of cellular entry will determine if the respective nucleic acid is unloaded at its site of action and if it is effective or not. Therefore, in order to deliver siRNA-loaded nanoparticles to specific intracellular destinations to elicit a distinctive biological effect, it is optimal to apply small, monodisperse nanoparticles with a defined zeta potential and surface chemistry.

Although the field of siRNA therapeutics has made significant progress, the effective delivery of siRNA remains a challenge that must be addressed before clinical use of siRNA becomes a preferred technique [1, 4, 5]. A plethora of materials that can form nano-sized complexes with siRNA have previously been intensively investigated [6, 7]. Most studies have focused on cationic lipids and polymers, which form random self-assembled aggregates with nucleic acids that are often larger than 100 nm. These systems are generally heterogeneous and poorly-defined particle collectives [8-11]. For example, a commonly used system involves forming nanoparticles with poly(ethylene imine) (PEI) and nucleic acids. The resulting collective contains different particle species that are in equilibrium with free polymer (about 86%) [12]. The heterogeneity of this system and the existence of different sub-populations in such random preparations lead to a decrease in efficacy, and this also complicates the interpretation of experimental results tremendously since it is not evident which particular sub-species of the preparation is responsible for the overall biological effect. Furthermore, toxic effects that may be exhibited by only a fraction of the preparation may appear to be intrinsic properties of the whole collective. Because endocytosis is governed by highly sophisticated and well-regulated principles and because heterogeneous particle collectives are associated with all of the aforementioned disadvantages, it is clear that new strategies for the fabrication of efficient nanocarriers are essential to advance the field.

While current approaches, which have focused on adjusting the size and surface properties of nanoparticles, are excellent models to help understand drug targeting

principles and cellular uptake [13-17], they are not ideally suited to transport highly charged macromolecules such as siRNA. Still, gold nanoparticles (AuNPs) have previously been used to deliver oligonucleotides or plasmid DNA [18-20] and even siRNA [21, 22] into cells. Very recently, Mirkin and co-workers attached siRNA molecules to the surface of AuNPs via a thiol group [22]. The polyvalent siRNA/nanoparticle conjugates showed a 6 times greater half-life and prolonged gene knock down compared to free RNA duplexes. While these approaches demonstrate the general applicability of AuNPs as delivery vehicle, in some cases, AuNPs seemed to aggregate after assembly with nucleic acids [18, 21], the delivered nucleic acid showed low activity inside cells [20], or the efficacy of the nucleic acid relied on an additional transfection reagent [19].

We hypothesized that a Layer-by-Layer (LbL) strategy would allow us to use monodisperse AuNPs as a template for the manufacture of a carrier that remains monodisperse during assembly and delivers active siRNA into cells, thereby circumventing the limitations of previous systems. Although the LbL deposition of oppositely charged polyelectrolytes is an established method for the fabrication of thin films on flat solid surfaces and microparticles [23, 24], the coating of nanoparticles presents a tremendous challenge. This is because many problems are associated with the wrapping of polyelectrolytes around nanoparticles with high curvature such as aggregation due to crosslinking of the particles by the polyelectrolyte chains and the separation of the unbound polyelectrolyte from the coated particles [25-27]. Here, we present a first proof of concept that even small nanoparticles can be modified with therapeutically relevant siRNA molecules in a LbL approach, and we report on the experimental parameters of their fabrication as well as their cellular delivery.

AuNPs as a core bear several advantages including straightforward synthesis, easy surface modification, availability in different size ranges with narrow size distribution, and finally high biocompatibility with cells or tissues [28-30].

## **Materials and method**

Polyelectrolytes used for multilayer deposition were poly(ethylene imine) (PEI)  $M_w = 25,000 \text{ g/mol}^{-1}$  (Sigma-Aldrich) and siRNA synthesized by Eurofins MWG Operon (siRNA against EGFP, sense strand: 5'-GAACUUCAGGGUCAGCUUGCCG-3' and antisense strand: 5'-GCAAGCUGACCCUGAAGUUCAU-3', non-targeted siRNA,

sense strand: 5'- GCAAGCTGACCCTGAAGTTCAT-3' and antisense strand: 5'- ATGAACTTCAGGGTCAGCTTGC-3'). AuNPs were prepared as described previously using the standard reduction of tetrachloroauric(III) acid with sodium citrate [31, 32]. Briefly, 1.0 ml of 1% AuCl<sub>4</sub>·3H<sub>2</sub>O solution was condensed to 100 ml and heated under reflux until boiling. 2.5 ml of a 1% trisodium citrate solution were added under vigorous stirring. Boiling was continued for 10 min. Larger aggregates were removed by centrifugation at 2,450 *xg*. The pH of AuNPs was adjusted to 11 with 1N NaOH, followed by the addition of 11-MUA at a final concentration of 0.1 mg/ml. The stabilized particles were purified two times at 15,700 *xg* for 10 minutes, and resuspended in 1 mM NaCl. Each coating step with PEI or siRNA was performed for 30 min after the addition of the gold nanoparticles to the respective, stirring polyelectrolyte solution. For the assembly of the first and third layer, PEI was used at a final concentration of 1.0 mg/ml. siRNA was added at a final concentration of 2.0 μM to purified PEI-AuNPs particles. Purification of the crude AuNPs was performed two or three times at 15,700 *xg* for 15 min, and the AuNPs were resuspended in 10 mM NaCl. The amount of PEI in the supernatant was determined according to the method of Snyder et al. [33] that uses 2,4,6-Trinitrobenzenesulfonic acid (TNBS) for the detection of amines. In brief, 25 μl of a 0.03 M TNBS solution were added to 1 ml of the supernatant containing PEI. After 30 minutes at room temperature, the absorbance was read at 420 nm using an Uvikon 941 spectrophotometer (Kontron Instruments GmbH). The concentration of PEI was calculated using a standard calibration curve. The amount of siRNA was determined by UV measurements (Uvikon 941 spectrophotometer) at 260 nm using a standard calibration curve.

For the determination of the size and zeta potential, 0.5 ml of AuNPs were either diluted with 1.5 ml millipore water or culture medium (Leibovitz's without phenolred, Invitrogen) with or without fetal bovine serum (Sigma-Aldrich). The samples were thermostated to 25 °C and laser light scattering analysis was performed with an incident laser beam of 633 nm at a scattering angle of 90° using the Malvern ZetaSizer 3000 HSA software (Malvern Instruments GmbH). The sampling time was set automatically. Three measurements each with 10 sub-runs were performed for each sample. The count rate for all dispersants was lower than 10 Kcps. The intensity of the autocorrelation function of the sample was deconvolved with the non-negatively constrained least squares (NNLS) algorithm because it provides a high resolution analysis and the quality of the fitting passed in all measurements during

each coating step. The zeta potential measurements were performed in the standard capillary electrophoresis cell of the ZetaSizer 3000 HSA (Malvern Instruments GmbH), measuring the electrophoretic mobility at 25 °C. UV-vis absorbance spectra of the AuNPs were recorded using an Uvikon 941 spectrophotometer (Kontron Instruments GmbH). Transmission electron micrographs (TEM) of AuNPs were taken on a Philips CM12 microscope (FEI, Eindhoven, The Netherlands). Samples were prepared by depositing the colloidal gold solution onto a carbon-coated copper grid and air-dried before analysis. Several micrographs of one sample were taken. For statistical evaluation, the diameter of 500 AuNP cores was measured using Image J for microscopy (NIH Image). For the determination of the concentration of AuNPs in solution, 500 µl of a sample containing AuNPs was mixed with 200 µl freshly prepared aqua regia [Caution! Aqua regia is a strong acid] and diluted to 5 ml with Millipore water. The  $\text{Au}^{3+}$  content of the solution was determined by ICP-OES analysis on a JY-70 PLUS (Jobin Yvon Instruments S.A.). The plasma flow was 16 L/min argon. All standards were made with gold(III) chloride at a concentration of 1, 10, 100 and 1,000 ppm. The measured concentration of  $\text{Au}^{3+}$  was divided by the number of gold atoms per particle to obtain the concentration of AuNPs in solution. The number of gold atoms per particle was calculated using the particle diameter, the density of bulk gold and the molecular weight of gold, the value was  $11.5 \times 10^4$  atoms per particle. The number of siRNA molecules per particle was calculated using the amount of siRNA adsorbed on the AuNP surface (amount of siRNA added - amount siRNA removed during purification (Table 1) and the concentration of particles in solution.

For cellular uptake studies (ICP-OES and TEM), CHO-K1 cells (ATCC No. CCL-61) were used. The cells were grown in 75cm<sup>2</sup> culture flasks to 90% confluency. Cells were incubated with culture medium with serum containing siRNA/PEI- and PEI/siRNA/PEI-AuNPs for 6 hours. The applied concentration of AuNPs is indicated in the figure legends. Thereafter, cells of three flasks were washed two times with PBS, detached from the flask by trypsinization, pelleted, and again washed with PBS. For the determination of the  $\text{Au}^{3+}$  content by ICP-OES the cell pellet was air dried, dissolved in 500 µl of freshly prepared aqua regia [Caution! Aqua regia is a strong acid] and diluted to 5 ml with Millipore water. ICP-OES analysis of the samples was performed on a JY-70 PLUS (Jobin Yvon Instruments S.A.) with a plasma flow of 16 L/min argon. All standards were made with gold(III) chloride at a concentration of 1,

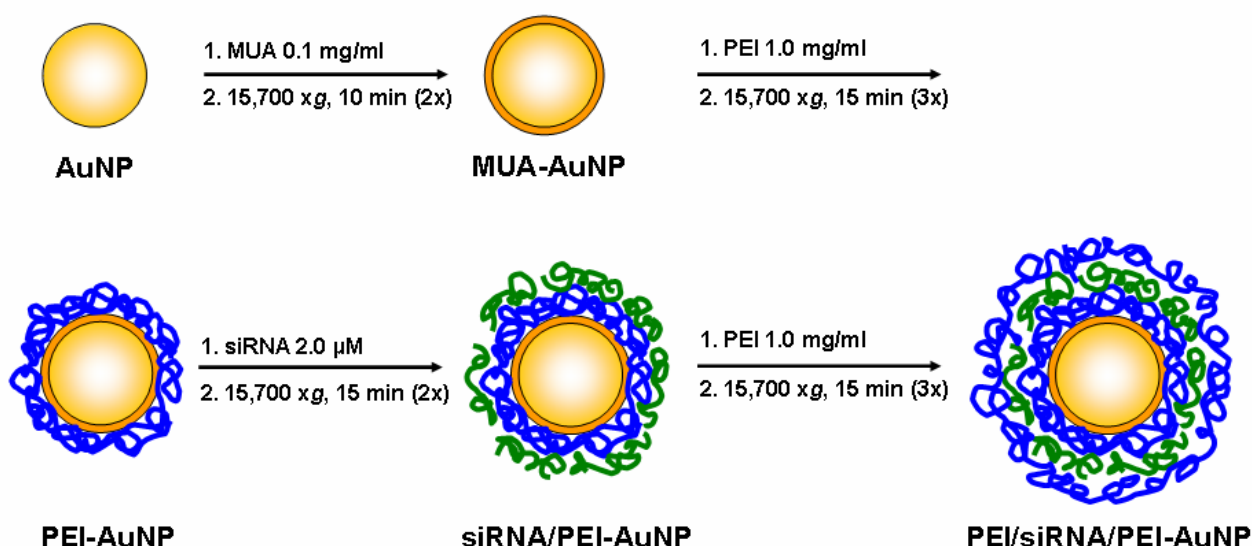
10, 100 and 1,000 ppm. The measured number of  $\text{Au}^{3+}$  was used to calculate the number of AuNPs as described above and related to the total number of cells. The number of total cells was determined by counting the cells of one  $75\text{cm}^2$  culture flasks in a Neubauer Chamber. The samples for cell counting were incubated with AuNPs in the same way as samples for ICP-OES measurements. Cell samples treated as described above but without addition of AuNPs were used as controls for background subtraction. One representative experiment of two independent ones is shown. For TEM experiments, the cell pellet was prepared as described above, then fixed with 2% glutaraldehyde in cacodylate buffer over night, and rinsed with 0.1 M cacodylate buffer. Postfixation was performed for 1h 45 min in 1% osmium tetroxide [Caution! Extremely toxic] at  $4^\circ\text{C}$ . After several washing steps with 0.1 M cacodylate buffer, the sample was embedded in agarose, and dehydrated in a graded series of ethanol (70, 80, 90, 95, and 100%). Thereafter, the sample was embedded in Epon. Ultrathin sections with a thickness of about 70 nm were imaged without further contrasting at 120 keV using a Philips CM12 microscope (FEI, Eindhoven, The Netherlands).

For gene silencing experiments, CHO-K1 cells stably expressing EGFP (CHO-K1/EGFP) were applied. These cells were generated by transfecting linearized pEGFP-N1 vector into CHO-K1 cells as described previously [34]. CHO-K1/EGFP cells were grown in 24-well plates at an initial density of 38,000 cells per well. 20 hours after plating, the culture medium was removed, cells were washed with PBS, and siRNA/PEI- or PEI/siRNA/PEI-AuNPs were added in various concentrations to the culture medium containing serum as indicated in the figure legends. After 6 hours, the medium was replaced with fresh culture medium. 48 hours later, cells were prepared for flow cytometry analysis on a FACS Calibur (Beckton Dickinson) and measurements of the mean fluorescence intensity (MFI) of EGFP and cell viability were performed as described previously [34]. The values of the MFI were used to calculate the knock-down of EGFP relative to untreated cells. All experiments were performed in triplicate and expressed as mean  $\pm$  standard deviation. One representative experiment of three independent ones is shown.

## Results and discussion

In this study, AuNPs were synthesized as spherical, homogeneous, and free of aggregates. They had a size of  $15.5 \pm 1.2$  nm as determined by transmission electron microscopy (TEM) (Figure 3).

For the LbL coating of the nanoparticles we envisioned a strategy that is illustrated in scheme 1. First, 11-mercaptoundecanoic acid (MUA) was to be deposited on the gold surface to facilitate the binding of the subsequent layers. Thereafter, the nanoparticles were to be consecutively added to oppositely charged polyelectrolyte solutions, first to PEI with a molecular weight of 25 kDa and then to double stranded 21-mer siRNA. Finally, PEI was to complete the shell as a last layer.



**Scheme 1:** Flowchart illustrating the LbL deposition applied to AuNPs. After each coating step, AuNPs were purified by centrifugation as indicated and resuspended in unbuffered 10 mM NaCl.

The major challenge involved identifying the appropriate parameters such that the coating and purification of AuNPs were possible. Although various polyelectrolytes have been applied for LbL deposition onto nanoparticles, siRNA was not expected to easily wrap around small AuNPs because it is a stiff, rod-like molecule [35]. In order to obtain well-defined particles onto which the polyelectrolyte can be adsorbed with high yield and to avoid interparticle bridging and flocculation, it was important to choose the appropriate polyelectrolyte concentration and ionic strength [25-27, 36]. More specifically, smaller particles need a higher salt concentration to overcome the repulsive forces and to wrap the polymer around themselves. However, a high ionic



strength may cause aggregation of gold nanoparticles [37]. The optimal concentrations of PEI (as determined in chapter 3, Figure 6 and 7) and siRNA during coating were determined to be 1.0 mg/ml and 2.0  $\mu$ M, respectively (Figure 1).

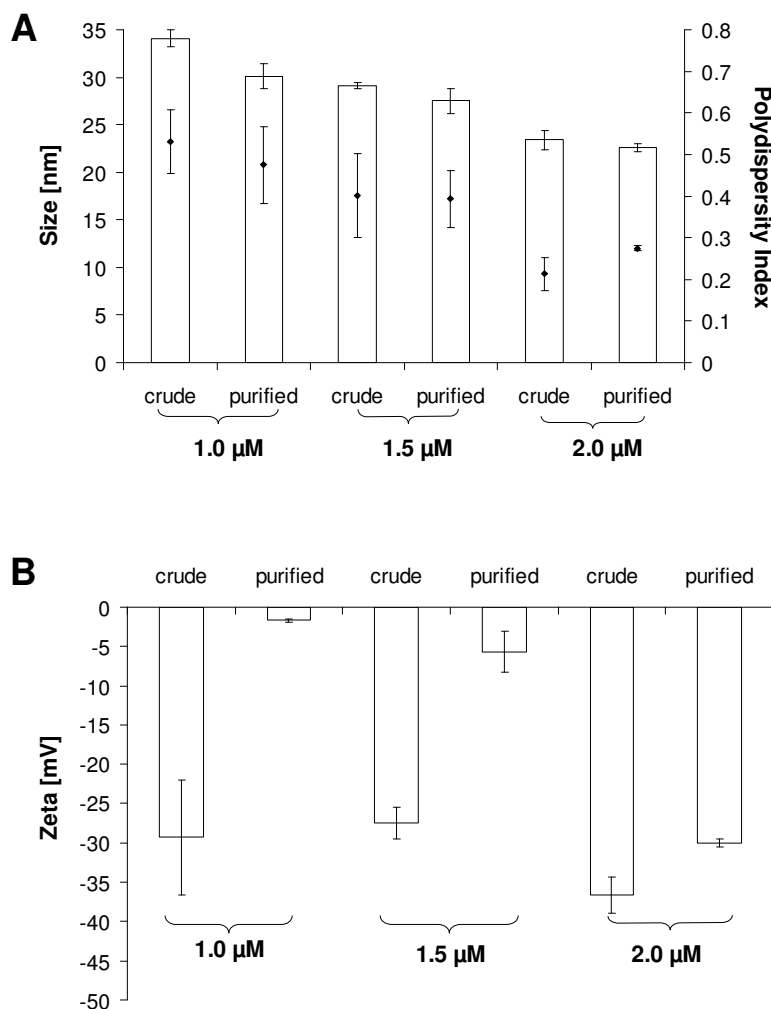


**Figure 1:** Determination of the optimal siRNA concentration for the LbL coating of purified PEI-AuNPs. (A) the hydrodynamic diameter (white columns) and the polydispersity index (rhombs) of siRNA/PEI-AuNPs before (crude) and after purification (purified) were determined along with the corresponding zeta potential (B). The values represent the mean  $\pm$  standard deviation of three sub-runs of one sample. The optimal concentration of siRNA was determined to be 2.0  $\mu$ M. It was chosen according to the following parameters: (1) hydrodynamic diameter and polydispersity index as low as possible, (2) no agglomeration or increase in the hydrodynamic diameter during the purification, and (3) a high value for the zeta potential before and after purification.

A final concentration of 10 mM NaCl proved to be suitable for maintaining a small hydrodynamic diameter and low polydispersity index of AuNPs during all coating and purification steps (see Figure 11, chapter 3, exemplified for the resuspension of PEI-AuNPs after the second purification step). After each coating step, unbound polyelectrolyte was removed by centrifugation in order to avoid formation of nano-

aggregates between free PEI and free siRNA, which would give rise to different, co-existing particle species. Two or three purification steps were necessary after coating with siRNA or PEI to ensure that only a minimal amount of polyelectrolyte was detectable in the supernatant (Table 1).

**Table 1:** The initial concentration of the polyelectrolytes for LbL assembly and the concentration of the respective polyelectrolytes in the discarded supernatant after purification.

Layer	Initial polyelectrolyte concentration	Purification step	Polyelectrolyte concentration in supernatant
PEI	1.0 mg/ml	1	0.7312 mg/ml
		2	0.0138 mg/ml
		3	0.0005 mg/ml
siRNA	2.0 $\mu$ M	1	1.157 $\mu$ M
		2	0.019 $\mu$ M

The optimal parameters were applied to assemble the LbL particles with PEI and siRNA, and the successful polyelectrolyte deposition was monitored by dynamic light scattering (DLS), zeta potential measurements, UV-vis absorbance spectra and TEM. Figure 2A details the change in the hydrodynamic diameter, including the polydispersity index as determined by DLS. The size of AuNPs increased during coating from  $18.5 \pm 0.2$  nm (MUA-AuNPs) to  $26.8 \pm 0.3$  nm (PEI/siRNA/PEI-AuNPs). Additionally, a reversal of the  $\xi$ -potential after completion of each layer signified the deposition of each polyelectrolyte (Figure 2B). After purification, the  $\xi$ -potential slightly decreased due to removal of unbound polyelectrolyte. The red shift of the surface plasmon band of gold nanoparticles was used to distinguish between polymer adsorption onto the AuNP surface and interparticulate bridging and aggregation [25-27, 36]. The UV-vis spectra in Figure 2C revealed that the AuNPs predominantly remained disaggregated after coating and that only low interparticulate bridging could have occurred, as the maximum of the plasmon peak shifted between 1 and 2 nm with consecutive layer deposition (Figure 2D). This was confirmed by statistical evaluation of electron micrographs (Figure 2E) that were made after each layer during LbL assembly (500 AuNPs were measured for each type of AuNPs, for micrographs see Figure 3). The majority of AuNPs remained as single particles

during the LbL assembly. Although an increasing amount of AuNP doublets (2 Au cores per aggregate) appeared with consecutive layer build-up, it never surpassed a fraction larger than 7%.

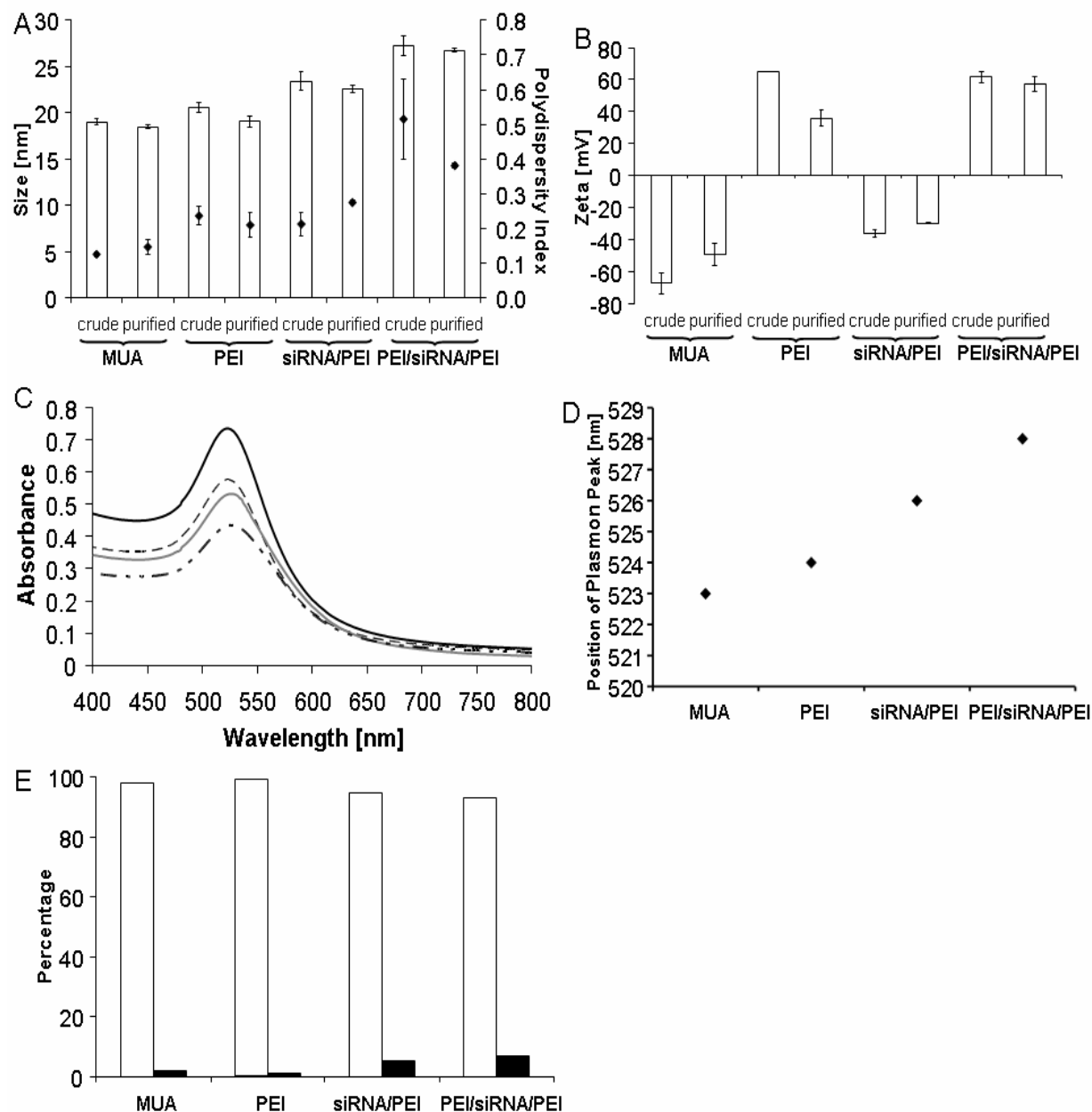


**Figure 2:** Characterization of AuNPs during LbL build-up by different methods. (A) The effect of the subsequent coating steps on the hydrodynamic diameter (white columns) and the polydispersity index (rhombs) of AuNPs before (crude) and after purification (purified) are shown as well as (B) the corresponding zeta potential. The values represent the mean  $\pm$  standard deviation of three sub-runs of sample. One representative experiment of five independent ones is shown. (C) UV-vis spectra of AuNPs from top to bottom: MUA-AuNPs, PEI-AuNPs, siRNA/PEI-AuNPs, PEI/siRNA/PEI-AuNPs and (D) the corresponding maximum position of the plasmon resonance peak. (E) Quantitative evaluation of TEM images (see Figure 4). 500 AuNPs were counted and the fraction of  $n$  Au-cores per aggregate was determined. The number of Au cores was  $n=1$  (white columns) or  $n=2$  (black columns).

Also worth noting is the number of siRNA molecules per AuNP, which was calculated to be around 780 siRNA molecules per siRNA/PEI-AuNP and PEI/siRNA/PEI-AuNP. This number is in a similar range as the one for AuNPs that were functionalized with 15-mer oligonucleotides via a thiol linker [38]. Overall, these results demonstrated that by selecting the experimental parameters accordingly during LbL assembly, most AuNPs remained single and maintained their small and uniform size.

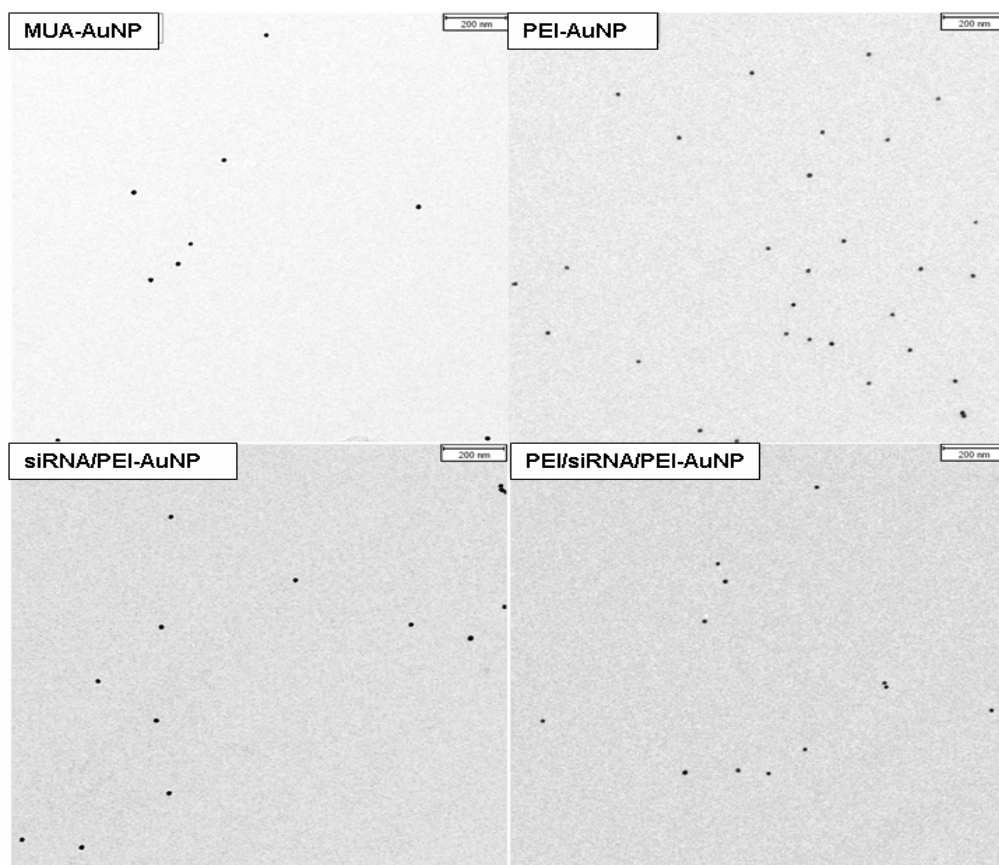


**Figure 3:** Transmission electron micrographs of colloidal AuNPs after the coating steps. Only the cores of AuNPs are visible, as the coating has inherently low contrast under the preparation and imaging conditions chosen. The bar indicates 200 nm.

Random, self-assembled aggregates of PEI and nucleic acids may suffer from severe aggregation when subjected to the high ionic strength of biological fluids [8, 39]. As a result of aggregation, the initial size of these complexes may increase to several micrometers [39]. This feature would make the fabrication of LbL coated nanoparticles tedious and would render their application in cell culture pointless. Hence, AuNPs were exposed to cell culture medium containing fetal bovine serum, and the hydrodynamic diameter and the  $\xi$ -potential were monitored (Figure 4A and B). Irrespective of the type of the outer layer (PEI or siRNA), the hydrodynamic

diameter of AuNPs increased only by a factor of 2.1 to 2.5. This increase in diameter is also reflected in the corresponding UV-vis spectra shown in Figure 4C (maximum of the plasmon peak was as follows: PEI-AuNPs: 530 nm, siRNA/PEI-AuNPs: 532 nm, PEI/siRNA/PEI-AuNPs: 536 nm).

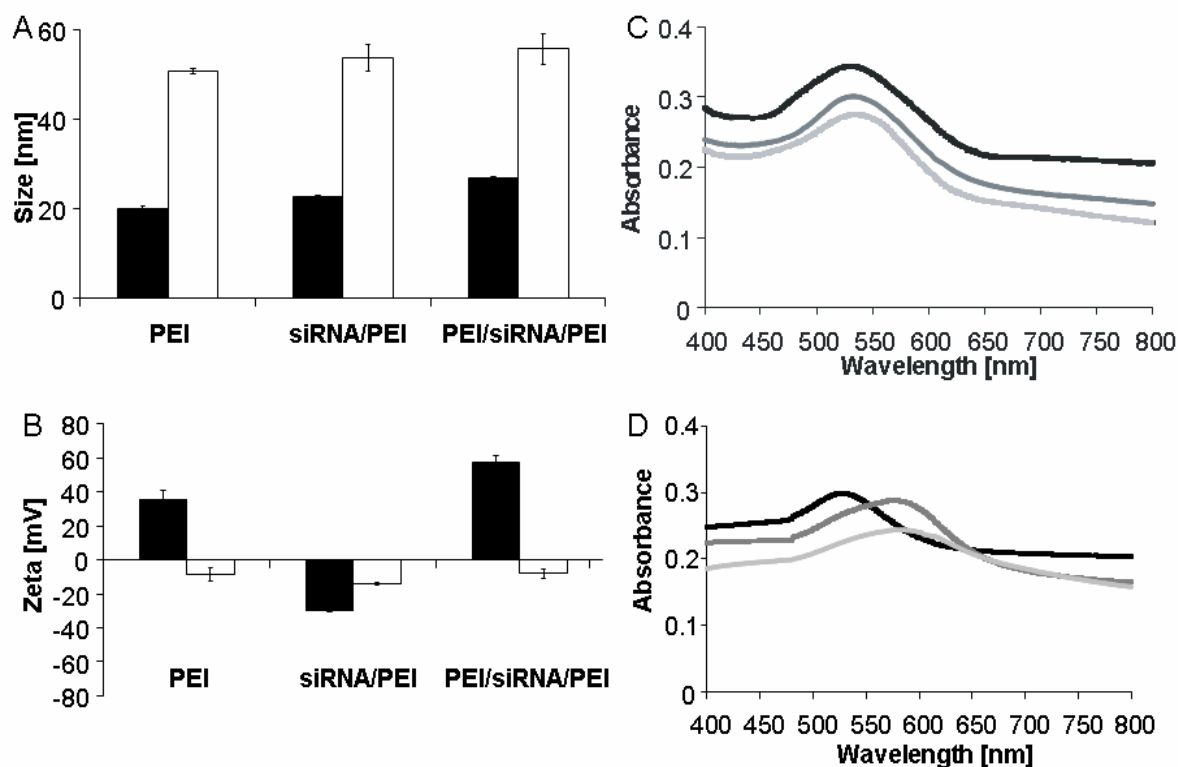


**Figure 4:** Characterization of AuNPs in different media. AuNPs were diluted in Millipore water (■) or serum-containing culture medium (□) and (A) the particle size as well as (B) the zeta potential were measured. The values represent the mean  $\pm$  standard deviation of three sub-runs of one sample. One representative experiment of three independent ones is shown. The UV-vis spectra of AuNPs after dilution in serum-containing (C) or serum-free culture medium (D). The spectra from top to bottom are as follows: PEI-AuNPs, siRNA/PEI-AuNPs, PEI/siRNA/PEI-AuNPs.

The extent of growth in diameter can most likely be attributed to the adsorption of proteins on the surface, as has already shown for unmodified and other oligonucleotide modified AuNPs [16, 40]. Interestingly, the  $\xi$ -potential of all particle types was negative after incubation with serum containing culture medium (Figure 4B). More specifically, the negative  $\xi$ -potential of siRNA/PEI-AuNPs became more positive, while PEI- and PEI/siRNA/PEI-AuNPs showed a charge reversal. After incubation in serum-free culture medium, the particle size increased by 7 to 10 fold (data not shown), and the UV-vis spectra in Figure 4D show that the individuality of AuNPs was lost (maximum of the plasmon peak was as follows: PEI-AuNPs: 575 nm,

siRNA/PEI-AuNPs: 580 nm, PEI/siRNA/PEI-AuNPs: 582 nm), which corroborates the hypothesis that serum proteins are necessary for stabilization of the nanoparticles.

The positive surface charge of self-assembled complexes of PEI and nucleic acids guarantees the cellular entry of negatively charged nucleic acids that are usually not incorporated by cells [39]. Therefore, it was not evident that LbL-assembled nanoparticles with an overall negative surface charge, even with PEI as a surface layer, were taken up by cells. To obtain quantitative data for the number of AuNPs per cell, CHO-K1 cells were incubated for 6 hours with siRNA/PEI- or PEI/siRNA/PEI-AuNPs in serum-containing culture medium and, subsequently, the  $\text{Au}^{3+}$  content of the cell digest was determined by inductively coupled plasma spectroscopy (ICP-OES).

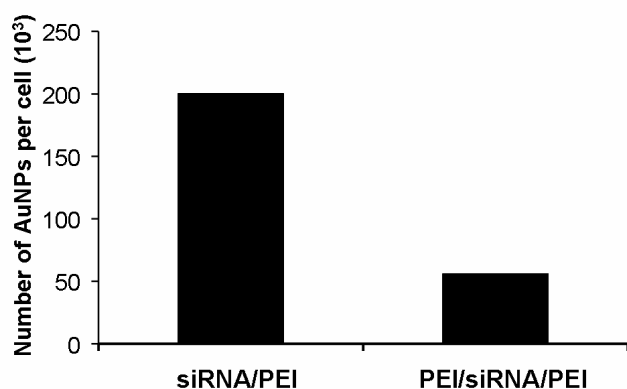


**Figure 5:** The cellular uptake of AuNPs. The number of AuNPs per cell as determined by ICP-OES and cell counting after 6 hours of incubation in serum containing culture medium as a function of surface modification. The initial concentration of AuNPs in the culture medium was 0.32 and 0.30 nM for siRNA/PEI- and PEI/siRNA/PEI-AuNPs, respectively. For each measurement cells from 3 culture flasks (75 cm<sup>2</sup> each) were pooled to obtain values within the calibration range, bars are averages of two measurements of one representative experiment of two independent ones.

Both types of particles were successfully taken up by CHO-K1 cells and the average amount of AuNPs per cell strongly depended on the type of the top layer. CHO-K1 cells internalized more siRNA/PEI-AuNPs (estimated number:  $2.0 \times 10^5$  per cell) in relation to PEI/siRNA/PEI-AuNPs (estimated number:  $5.6 \times 10^4$  per cell) (Figure 5). This difference correlated well with the electron micrographs of sections of CHO-K1 cells (Figures 6 and 7).

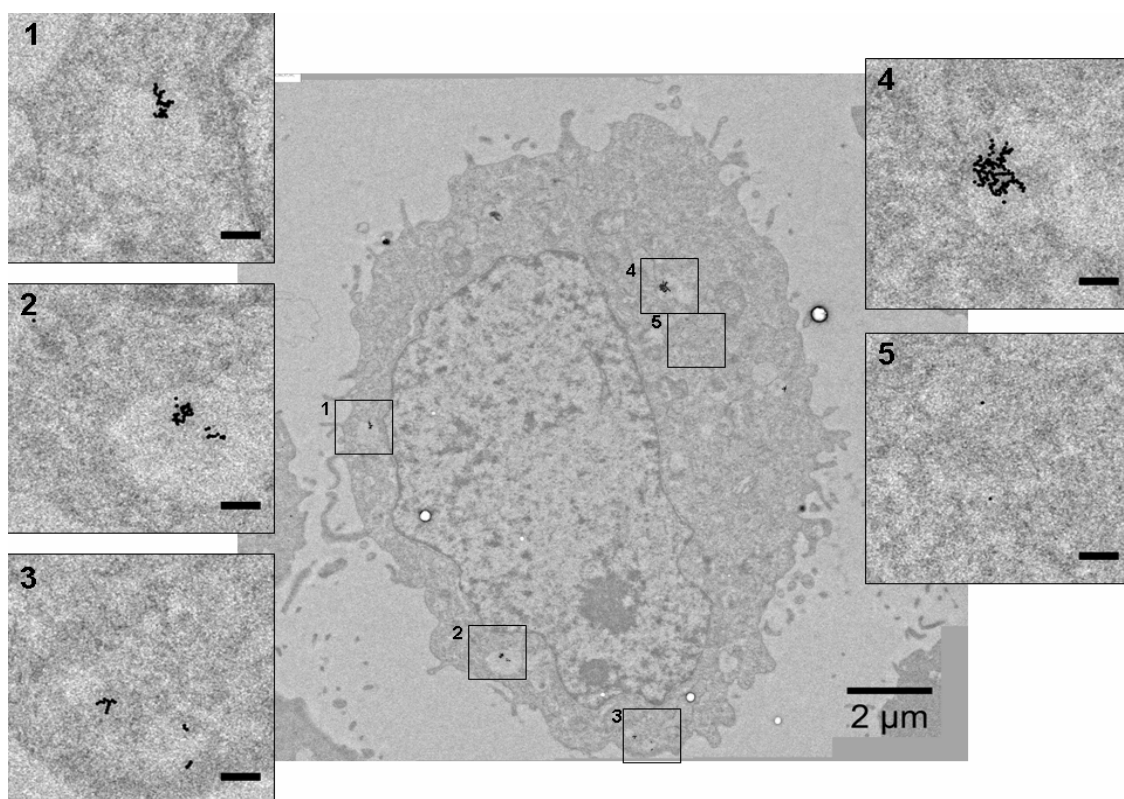


**Figure 6:** Transmission electron micrograph of a 70 nm ultrathin section of a CHO-K1 cell that was incubated with siRNA/PEI-AuNPs for 6 hours in serum-containing culture medium.

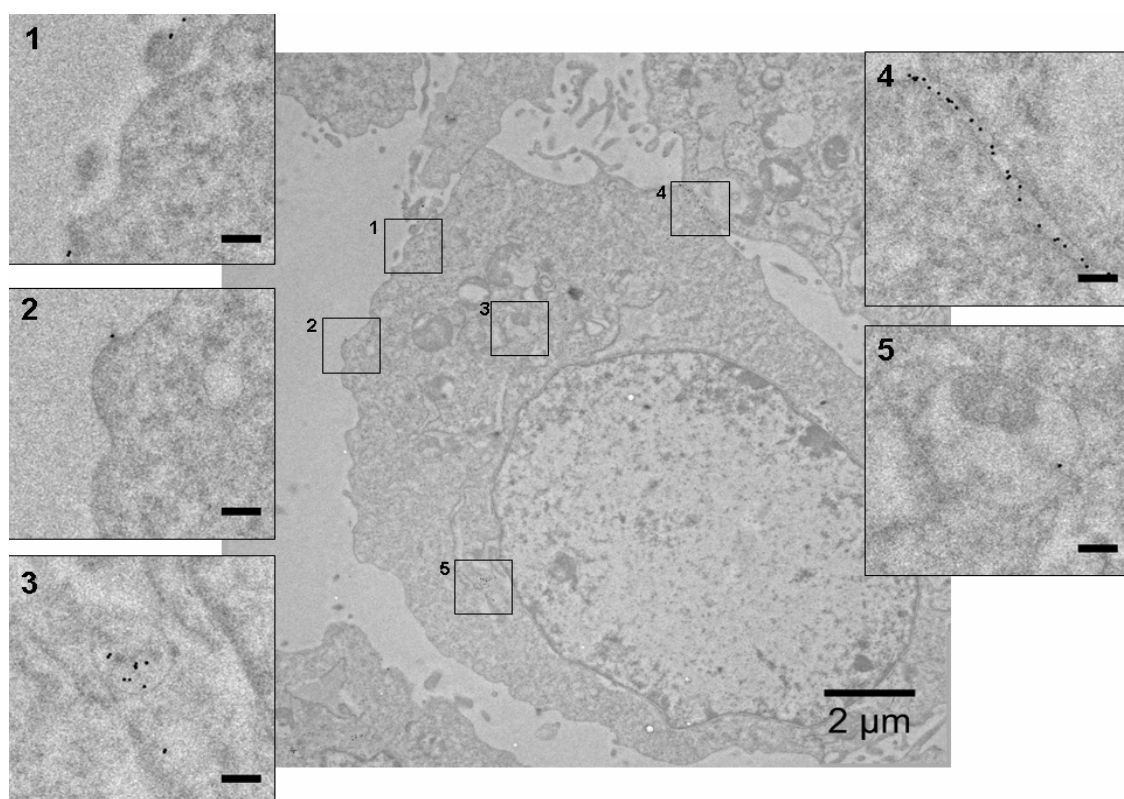


**Figure 7:** Transmission electron micrograph of a 70 nm ultrathin section of a CHO-K1 cell that was incubated with PEI/siRNA/PEI-AuNPs for 6 hours in serum-containing culture medium. Some PEI/siRNA/PEI-AuNPs are not taken up by CHO-K1 cells and stick to the cell surface.

However, it must be noted that no distinction between AuNPs that entered the cells and those stuck on the outside on the cell membrane was made in this method. Transmission electron micrographs of CHO-K1 cells (Figures 6 and 7) illustrate that this consideration must be taken into account for PEI/siRNA/PEI-AuNPs, but not for siRNA/PEI-AuNPs. Therefore, the ICP-OES and the transmission electron micrographs together allow for the conclusion that the number of siRNA/PEI-AuNPs per cell is significantly higher as compared to PEI/siRNA/PEI-AuNPs. In comparison to citrate stabilized AuNPs, the amount of siRNA/PEI- and PEI/siRNA/PEI-AuNPs per cell was much higher [16], while the number of siRNA/PEI-AuNPs per cell was similar to other DNA-modified AuNPs [40].

The significant difference in cellular uptake of AuNPs that are of nearly similar size, but possess different outer layers suggests that surface properties may strongly affect interactions with cells. Their homogeneous size distribution renders the AuNPs highly favorable for this investigation, because it has been shown that the size of AuNPs strongly influences the number of AuNPs that are taken up per cell [16]. Hence, we can conclude the differences in the cellular of siRNA/PEI- and PEI/siRNA/PEI-AuNPs are due to differences in surface properties and not size (due to a broad size distribution). Additionally, we show electron micrographs of sectioned CHO-K1 cells that help to elucidate the intracellular fate of the AuNPs. The micrographs in Figure 8 illustrate that the AuNPs were predominantly trapped within endocytotic vesicles after 6 hours of incubation, and no particles were detected in the nucleus. Figure 8A-C shows a typical image after incubation with siRNA/PEI-AuNPs. Each endocytotic vesicle contained several nanoparticles. Within one vesicle, some particles were still single or have formed a doublet or a triplet (3 Au cores per aggregate), but most have aggregated to larger clusters. In contrast, after incubation with PEI/siRNA/PEI-AuNPs (Figure 8D-F), less vesicles per cell containing AuNPs were counted, and the number of AuNPs per vesicle was also lower as compared to siRNA/PEI-coated particles. It was remarkable that, inside of the endocytotic vesicles, the particles remained either single or formed at most doublets. Some PEI/siRNA/PEI-AuNPs, but not siRNA/PEI-AuNPs, were also detected in caveolae-like structures (Figure 8D). It will be of great interest to investigate the intracellular fate of PEI/siRNA/PEI-AuNPs and siRNA/PEI-AuNPs that are produced in different size ranges in future experiments.



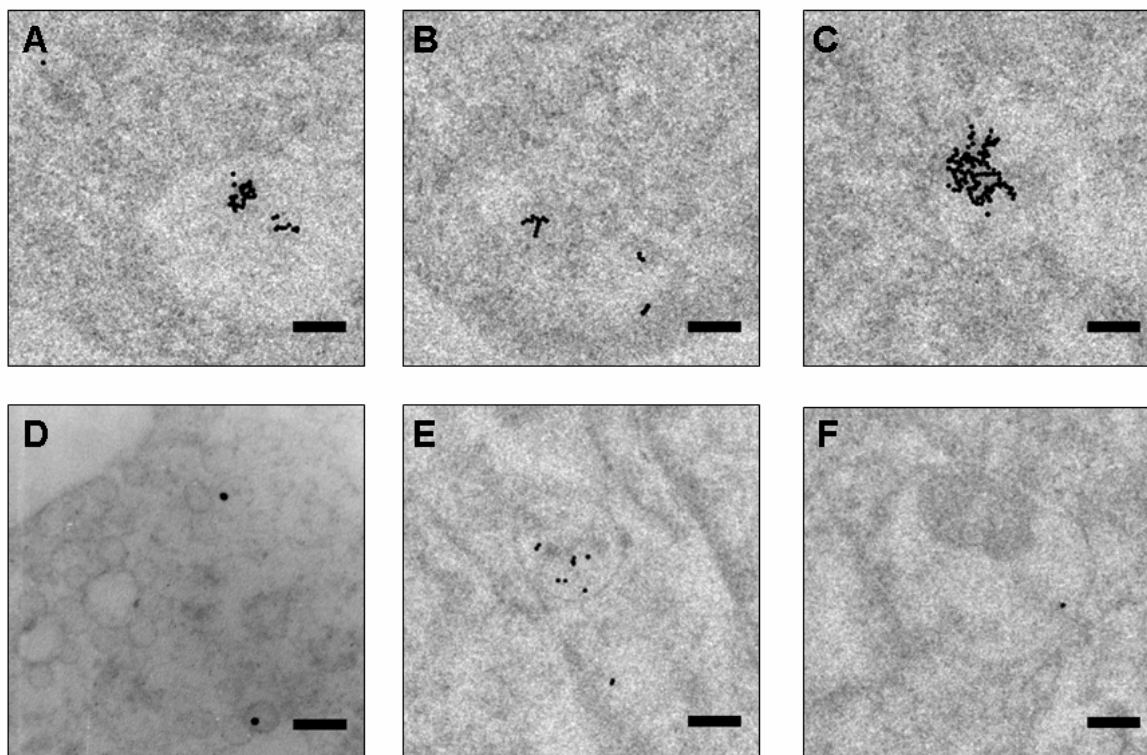


**Figure 8:** The cellular uptake of (A-C) siRNA/PEI-AuNPs and (D-F)PEI/siRNA/PEI-AuNPs into CHO-K1 cells as evaluated by TEM. The bar indicates 0.13  $\mu\text{m}$  in D, and 0.20  $\mu\text{m}$  in all other images.

Having demonstrated that the AuNPs are uniform in size and surface charge and homogeneous in distribution, we wanted to determine their intracellular fate as siRNA carriers. In particular, it was of great importance to provide evidence of activity of the siRNA inside the cells. This capability was tested in CHO-K1 cells stably expressing enhanced green fluorescent protein (CHO-K1/EGFP). To test the specificity of the knock-down, two different types of siRNA were applied for LbL-nanoparticle formation: siRNA against EGFP and a non-targeted siRNA sequence as control. A dose-dependent knock-down was measured for PEI/siRNA/PEI-AuNPs, and the cellular EGFP production was reduced to about 28% (Figure 9A). Control formulations with non-targeted siRNA revealed that gene silencing was highly specific. The cell viability of CHO-K1/EGFP cells was not seriously influenced by the addition of AuNPs (Figure 9B), as it only slightly decreased to  $93.4 \pm 1.1\%$  and  $95.0 \pm 0.8\%$ , respectively, at the highest AuNP concentration.

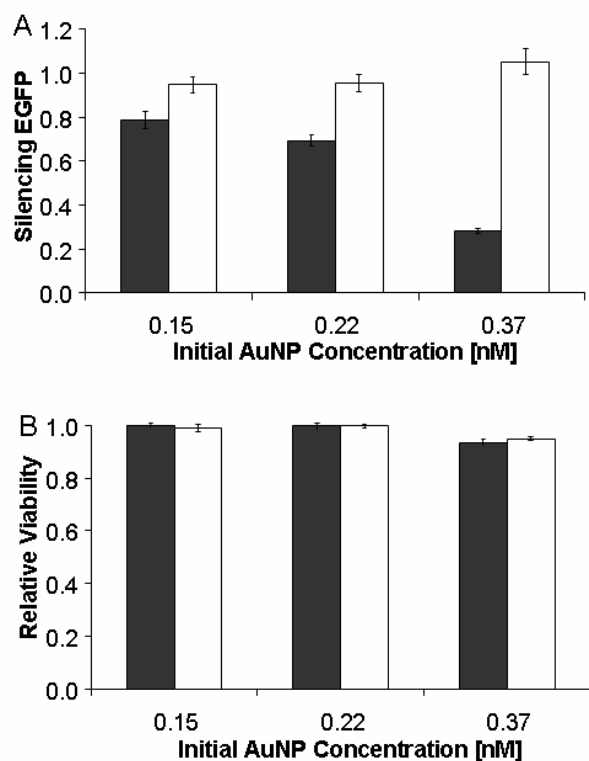


**Figure 9:** (A) Gene silencing of EGFP in CHO-K1 cells stably expressing EGFP and (B) relative cell viability after addition of PEI/siRNA/PEI-AuNPs at various initial concentrations. For LbL assembly of nanoparticles either siRNA against EGFP (■) was used or a non-targeted siRNA control (□). The values represent the mean  $\pm$  standard deviation ( $n=3$ ). One representative experiment of three independent ones is shown.

When siRNA was used as the top layer, no silencing efficacy was detected (Figure 10). Possible reasons may include degradation of unprotected siRNA on the surface of the nanoparticles, inadequate endosomal escape of nanoparticles due to a lower amount of the transfection reagent per particle or even the agglomeration of the AuNPs during cellular uptake.

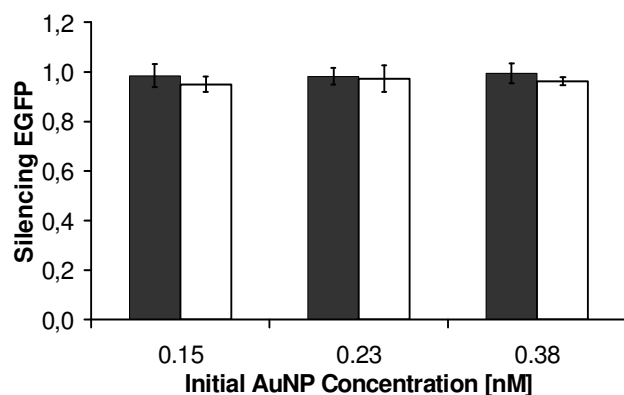


**Figure 10:** Gene silencing of EGFP in CHO-K1 cells stably expressing EGFP after addition of siRNA/PEI-AuNPs at various initial concentrations. For LbL assembly of nanoparticles, either siRNA against EGFP (■) was used or a non-targeted siRNA control (□). The values represent the mean  $\pm$  standard deviation ( $n=3$ ). One representative experiment of two independent ones is shown.

We also compared the parameters of siRNA delivery using PEI/siRNA/PEI-AuNPs with the ones using random-assembled siRNA/PEI-agglomerates. For the same amount of cells, the latter process usually requires 100 nM siRNA in combination with 3.8 to 5.1  $\mu$ g PEI to achieve a similar knock-down in gene expression [34]. In this study, both the siRNA and PEI concentration were higher (siRNA: 1.2 to 2.9 fold; PEI: 12 to 16 fold). The higher siRNA concentration may most likely be necessary because LbL-coated AuNPs are very stable and, hence, the release of siRNA inside cells may occur only to a low extent. Therefore, in future experiments, the fabrication of LbL nanoparticles with polymers that are biodegradable inside cells will most likely allow for improved release of siRNA and, subsequently, a lower AuNP concentration will be sufficient to achieve the same effect. It was remarkable that PEI/siRNA/PEI-AuNPs showed no serious toxicity in cell culture despite a PEI concentration that typically induces devastating cellular toxicity. One possible reason may be the removal of free polymer, as this is usually associated with the high toxicity of PEI [41-43].

## **Conclusion**

In summary, we were the first to successfully show the LbL assembly of the oppositely charged polyelectrolytes siRNA and PEI on AuNPs. This technique offers a unique opportunity to fabricate well-defined and homogeneously distributed nanocarriers for siRNA delivery. In future experiments, these LbL-coated nanoparticles will provide an excellent tool to study how the size and the surface properties influence the portal of entry into cells and direct distinct particles to the correct site of activity. The obtained information will help to detect existing limitations and to design new materials for siRNA delivery.

## **Acknowledgment**

The authors thank Cornelia Rose and Angelika Berié and Dr. Harald Huber for ICP analysis, Angelika Kühn for support with EM preparation, and Siddharth Pathi from Cornell University for proofreading the manuscript.

## References

- [1] Aagaard, L.; Rossi, J. J. *AdV. Drug Deliv. Rev.* **2007**, *59*, 75–86.
- [2] Dykxhoorn, D. M.; Palliser, D.; Lieberman, J. *Gene Ther.* **2006**, *13*, 541–552.
- [3] Conner, S. D.; Schmid, S. L. *Nature (London)* **2003**, *422*, 37–44.
- [4] Whitehead, K. A.; Langer, R.; Anderson, D. G. *Nat. Rev. Drug Discov.* **2009**, *8*, 129–138.
- [5] Juliano, R.; Alam, M.; Dixit, V.; Kang, H. *Nucleic Acids Res.* **2008**, *36*, 4158–4171.
- [6] Zhang, S.; Zhao, B.; Jiang, H.; Wang, B.; Ma, B. *J. Controlled Release* **2007**, *123*, 1–10.
- [7] de Fougères, A.; Vornlocher, H. P.; Maraganore, J.; Lieberman, J. *Nat. Rev. Drug Discovery* **2007**, *6*, 443–453.
- [8] Neu, M.; Fischer, D.; Kissel, T. *J. Gene Med.* **2005**, *7*, 992–1009.
- [9] Pozharski, E. V.; MacDonald, R. C. *Mol. Pharm.* **2007**, *4*, 962–974.
- [10] Chesnoy, S.; Huang, L. *Annu. Rev. Biophys. Biomol. Struct.* **2000**, *29*, 27–47.
- [11] Elouahabi, A.; Ruyschaert, J. M. *Mol. Ther.* **2005**, *11*, 336–347.
- [12] Clamme, J. P.; Azoulay, J.; Mely, Y. *Biophys. J.* **2003**, *84*, 1960–1968.
- [13] Hild, W. A.; Breunig, M.; Goepferich, A. *Eur. J. Pharm. Biopharm.* **2008**, *68*, 153–168.
- [14] Cambi, A.; Lidke, D. S.; Arndt-Jovin, D. J.; Figdor, C. G.; Jovin, T. M. *Nano Lett.* **2007**, *7*, 970–977.
- [15] Javier, D. J.; Nitin, N.; Levy, M.; Ellington, A.; Richards-Kortum, R. *Bioconjug. Chem.* **2008**, *19*, 1309–1312.
- [16] Chithrani, B. D.; Ghazani, A. A.; Chan, W. C. *Nano Lett.* **2006**, *6*, 662–668.
- [17] Bagalkot, V.; Zhang, L.; Levy-Nissenbaum, E.; Jon, S.; Kantoff, P. W.; Langer, R.; Farokhzad, O. C. *Nano Lett.* **2007**, *7*, 3065–3070.
- [18] Thomas, M.; Klibanov, A. M. *Proc. Natl. Acad. Sci. U.S.A.* **2003**, *100*, 9138–9143.
- [19] Liu, Y.; Franzen, S. *Bioconjug. Chem.* **2008**, *19*, 1009–1016.
- [20] Rosi, N. L.; Giljohann, D. A.; Thaxton, C. S.; Lytton-Jean, A. K. R.; Han, M. S.; Mirkin, C. A. *Science* **2006**, *312*, 1027–1030.

- [21] Lee, S. H.; Bae, K. H.; Kim, S. H.; Lee, K. R.; Park, T. G. *Int. J. Pharm.* **2008**, *364*, 94–101.
- [22] Giljohann, D. A.; Seferos, D. S.; Prigodich, A. E.; Patel, P. C.; Mirkin, C. A. *J. Am. Chem. Soc.* **2009**, *131*, 2072–2073.
- [23] Decher, G.; Schlenoff, J. *Multilayer thin films*; Wiley-VCH: Weinheim, 2002.
- [24] Tang, Z.; Wang, Y.; Podsiadlo, P.; Kotov, N. A. *AdV. Mater.* **2006**, *18*, 3203–3224.
- [25] Gittins, D. I.; Caruso, F. *J. Phys. Chem. B* **2001**, *105*, 6846–6852.
- [26] Mayya, K. S.; Schoeler, B.; Caruso, F. *AdV. Funct. Mater.* **2003**, *13*, 183–188.
- [27] Schneider, G.; Decher, G. *Langmuir* **2008**, *24*, 1778–1789.
- [28] Daniel, M. C.; Astruc, D. *Chem. Rev.* **2004**, *104*, 293–346.
- [29] Shukla, R.; Bansal, V.; Chaudhary, M.; Basu, A.; Bhonde, R. R.; Sastry, M. *Langmuir* **2005**, *21*, 10644–10654.
- [30] Ghosh, P.; Han, G.; De, M.; Kim, C. K.; Rotello, V. M. *AdV. Drug Delivery Rev.* **2008**, *60*, 1307–1315.
- [31] Turkevich, J.; Stevenson, P.; Hiller, J. *Discuss. Faraday Soc.* **1951**, *11*, 55–75.
- [32] Frens, G. *Nat. Phys. Sci.* **1973**, *241*, 20–22.
- [33] Snyder, S. L.; Sobocinski, P. Z. *Anal. Biochem.* **1975**, *64*, 284–288.
- [34] Breunig, M.; Hozsa, C.; Lungwitz, U.; Watanabe, K.; Umeda, I.; Kato, H.; Goepferich, A. *J. Control. Release* **2008**, *130*, 57–63.
- [35] Gary, D. J.; Puri, N.; Won, Y. Y. *J. Controlled Release* **2007**, *121*, 64–73.
- [36] Schneider, G.; Decher, G. *Nano Lett.* **2004**, *4*, 1833–1839.
- [37] Hayat, M. A. *Colloidal gold: principles, methods and applications*; Academic Press: San Diego, 1989.
- [38] Hurst, S. J.; Lytton-Jean, A. K. R.; Mirkin, C. A. *Anal. Chem.* **2006**, *78*, 8313–8318.
- [39] Lungwitz, U.; Breunig, M.; Blunk, T.; Goepferich, A. *Eur. J. Pharm. Biopharm.* **2005**, *60*, 247–266.
- [40] Giljohann, D. A.; Seferos, D. S.; Patel, P. C.; Millstone, J. E.; Rosi, N. L.; Mirkin, C. A. *Nano Lett.* **2007**, *7*, 3818–3821.
- [41] Boeckle, S.; von Gersdorff, K.; van der, P. S.; Culmsee, C.; Wagner, E.; Ogris, M. *J. Gene Med.* **2004**, *6*, 1102–1111.

- [42] Moghimi, S. M.; Symonds, P.; Murray, J. C.; Hunter, A. C.; Debska, G.; Szewczyk, A. *Mol. Ther.* **2005**, *11*, 990–995.
- [43] Chollet, P.; Favrot, M. C.; Hurbin, A.; Coll, J. L. *J. Gene Med.* **2002**, *4*, 84–91.

# **Chapter 5**

## **Size Dependent Uptake of Layer-by-Layer Coated Gold Nanoparticles into Mammalian Cells**

Asmaa Elbakry<sup>1</sup>, Alaa Zaky<sup>1</sup>, Renate Liebl<sup>1</sup>, Edith Schindler<sup>1</sup>, Petra Bauer-Kreisel<sup>2</sup>,  
Torsten Blunk<sup>2</sup>, Reinhard Rachel<sup>3</sup>, Achim Goepperich<sup>1</sup>, Miriam Breunig<sup>1</sup>

<sup>1</sup>Department of Pharmaceutical Technology, university of Regensburg,  
Regensburg, Universitätsstraße 31, 93040 Regensburg, Germany

<sup>2</sup>Department of Trauma, Hand, Plastic & Reconstructive Surgery, University  
of Würzburg, Oberdürrbacherstraße 6, D-97080 Würzburg, Germany

<sup>3</sup>Centre for Electron Microscopy at the Institute for Anatomy, University of  
Regensburg, Universitätsstraße 31, 93040 Regensburg, Germany

**Abstract**

Nanoparticles have emerged as promising candidates for nucleic acid delivery. However, most nanoparticle preparations suffer from poor characterization of the size distribution and a huge polydispersity in the particle collective. Unfortunately, the uptake of molecules into cells is complex and highly regulated, and the physicochemical properties of the nanoparticles strongly affect their cellular uptake. Here, we investigated how size influences the cellular uptake of LbL-coated gold nanoparticles (LbL-coated AuNPs) for nucleic acid delivery, and the amount of cargo molecules per cell. We also investigated the relationship between the amount of active substance taken up by the cells and the size of the AuNPs. Our study showed that the smaller AuNPs were more successfully taken up by the cells than larger particles. Interestingly, the amount of active substance was higher for the larger particles. In other words, fewer large particles are required to deliver a similar amount of active molecules per cell. In summary, this study will assist in the future design of nano-structures for nucleic acid delivery for biomedical applications.



## 1. Introduction

Recent years have seen tremendous progress in the design and study of nano-materials geared towards biomedical applications. Many of these advances have had the intention of manipulating or probing structures and processes in a biological context. Due to their small size and the possibility of easily modifying their surface, nanoparticles offer unique advantages in imaging [1, 2], bio-sensing [3, 4], and drug and gene delivery [5-7]. The “nano-bio” interface comprises many physicochemical interactions between nanoparticles and biological systems, but we have just begun to understand the forces and components that shape these interactions, and are still far from having a complete picture. However, the safe and effective design of nano-materials for biomedical applications requires a clear understanding of these interactions.

A major bottleneck for nanoparticles delivering any kind of cargo molecules into cells is their cellular uptake. It is known that the size, shape, chemical composition, and surface properties of nanoparticles strongly affect the nature and extent of the interaction with mammalian cells, thereby determining their access into cells [8-10]. In addition, other properties, such as the effective surface charge, particle aggregation, and the state of dispersion (which are characterized by the surrounding media and include ionic strength, pH, and even the presence of large organic molecules such as proteins) also play an important role in this process [11, 12]. For example, for every particle species that is capable of cellular entry, an optimal radius exists, which accelerates membrane wrapping at the cell surface and promotes particle uptake. Any deviation from this optimal value strongly reduces cellular uptake. For receptor-mediated endocytosis, various models have determined the optimal nanoparticle radius to be in the range of 15 – 30 nm [14-16]. However, most nanoparticle preparations suffer from a poor characterization of the size distribution and a huge polydispersity of the particle collective [17, 18]. This fact leads to inconsistent experimental results concerning the optimal particle diameter for cellular uptake and illustrates the considerable gap in the current understanding of such “nano-bio” interactions.

Gold nanoparticles (AuNPs) have the potential to overcome these limitations because they can be prepared with a high degree of monodispersity and on a relatively large scale using the methodology established by Frens [19]. The resulting AuNPs have unique optical properties dependent on their size and shape, can be

easily modified with functional groups to anchor additional moieties such as ligands, nucleic acids, or proteins, and show a very good biocompatibility [20-23]. Chan and coworkers investigated how the size of citrate-stabilized AuNPs (14, 30, 50, 74 and 100 nm) affects the uptake into HeLa cells [24]. The maximum uptake occurred at a particle size of 50 nm and decreased with smaller and larger particle sizes, which is in good agreement with the theoretical models. The same group also investigated the cellular uptake of AuNPs coated with the ligand transferrin, with the intention of entering the cells via receptor-mediated endocytosis [25]. 50 nm particles were taken up at a higher rate than 14 nm particles because for the smaller particles at least 6 had to cluster together before uptake, while for the membrane wrapping of the 50 nm particles a single AuNP was sufficient. In another study, not only the uptake of AuNPs (ranging from 2 – 100 nm) coated with the antibody Herceptin was highly dependent on the size with the most efficient uptake occurring between 25 and 50 nm, but also the cellular response [26].

Recently, we demonstrated the manufacture of well-defined and homogeneously distributed nano-carriers for nucleic acid delivery by depositing two oppositely charged polyelectrolytes on the surface of AuNPs [27]. We coated AuNPs in a Layer-by-Layer (LbL) approach, starting with positively charged poly(ethylene imine) (PEI) with a Mw of 25 kDa, then deposited a negatively charged nucleic acid (21 bp), and completed the coating with PEI as a last layer. The nanoparticles were small (~25 nm) and delivered nucleic acid into cells that showed a strong biological effect. The main question that arises from the context above is “What is the optimal size for the cellular uptake of LbL-coated AuNPs?” Additionally, it would be of great importance to know which biological significance such a size-dependent cellular uptake would recover because for most preparations delivering nucleic acids into cells not the number of particles internalized is the most important factor, but the amount of active substance taken up. And this latter factor also strongly correlates with the size of the AuNPs, meaning that larger LbL-coated AuNPs have a higher loading capacity for nucleic acid. The results from this study will provide a better understanding in elucidating the relationship how the size of LbL-coated AuNPs affects the cellular uptake.

## 2. Experimental

### 2.1. Materials

Commercially available gold nanoparticles of different sizes (20, 30, 50, and 80 nm) were purchased from BBInternational (Cardiff, England). Poly(ethylene imine) (PEI)  $M_w = 25,000 \text{ g/mol}^{-1}$ , 11- Mercaptoundecanoic acid (11-MUA), D-MEM medium, and Nutrient Mixture F-12 [HAM] (HAM F-12) were purchased from Sigma-Aldrich Chemical Company (Steinheim, Germany). 21 base pair DNA was synthesized by Eurofins MWG Operon (sense strand: 5'-ATGAACTTCAGGGTCAGCTTGC-3' and antisense strand: 5'-GCAAGCTGACCCTGAAGTTCAT-3'). Picryl sulfonic acid solution was purchased from Fluka (Steinheim, Germany). Sodium chloride, sodium hydroxide, nitric acid, hydrochloric acid, and absolute ethanol were purchased from Merck (Darmstadt, Germany). DyLight 649 NHS-Ester was purchased from Thermo scientific (Rockford, U.S.A.). Chinese hamster ovarian cell line (CHO-K1 cells) (ATCC No. CCL-61), human cervical carcinoma cell line (HeLa cells) (ATCC No. CCL-2), human breast cancer cell line (MCF-7 cells) (ATCC No. HTB-22) and human colorectal carcinoma cell line (HCT 116 cells) (ATCC No. CCL-247) were grown in 75cm<sup>2</sup> culture flasks to 90% confluency. Dulbecco's Phosphate buffer saline 1x (DPBS), Dulbecco's Medium and Leibovitz's L-15 medium 1x without phenol red were purchased from (GIBCO) Invitrogen (Germany). Fetal bovine serum (FBS) was purchased from Biochrom AG (Germany). The ultrafiltration units had a 3 KDa cut-off membrane (Nanosep 3K Omega) was purchased from (Pall Corporation, Mexico). All glassware was thoroughly washed with freshly prepared aqua regia (HCl: HNO<sub>3</sub> = 3:1) [Caution! Aqua regia is a strong acid], extensively rinsed with Millipore water several times and oven-dried at 150 °C for 2-3 h before use. All used solution was filtered through 0.22 µm membrane filter (Corning Incorporated, Corning NY 14832, Germany) before use.

### 2.2. Stabilization and LbL coating of AuNPs

The pH of different sized AuNPs was adjusted to 11 with 1N NaOH, followed by the addition of 11-MUA at a final concentration of 0.1 mg/ml. The stabilized particles were purified two times at 15,700 xg for 10 minutes, and resuspended in 1 mM NaCl. The coating of stabilized AuNPs with polyelectrolytes was performed as described previously [27]. In brief, each coating step with PEI or DNA was performed for 30 minutes after the addition of different sizes of AuNPs to the stirring polyelectrolyte

solution. PEI was used at a final concentration of 1.0 mg/ml for the assembly of the first and third layers. DNA was added at a final concentration of 1.5  $\mu$ M to purified PEI-AuNPs. Purification of the crude AuNPs was performed at 15,700 xg for 15 minutes, and the purified AuNPs were resuspended in 10 mM NaCl. For cellular uptake studies using fluorescence activated cell sorting (FACS) analysis and confocal laser scanning microscopy (CLSM) experiments, different sized LbL-AuNPs were coated with PEI 25 KDa that was labeled with DyLight 649. PEI 25 KDa was labeled with DyLight 649 according to the manufacturer's protocol. The labeling reaction was carried out with a molar ratio of 1 dye molecule per 10 PEI molecules at room temperature (RT) in the dark. The excess dye was removed by repeating ultrafiltration MWCO 3 KDa.

### **2.3. Determination of excess polyelectrolyte after purification**

The amount of free polyelectrolytes (PEI and DNA) in the supernatant after purification was determined in order to identify the exact amount of polyelectrolyte adsorbed on the surfaces of different sized LbL-coated AuNPs. The amount of PEI in the supernatant was determined according to the method of Snyder et al. [28] that uses 2,4,6 Trinitrobenzenesulfonic acid (TNBS) for the detection of amines. In brief, 25  $\mu$ l of a 0.03 M TNBS solution were added to 1 ml of the supernatant containing PEI. After 30 minutes at room temperature, the absorbance was read at 420 nm using an Uvikon 941 spectrophotometer. The concentration of PEI was calculated using a standard calibration curve. The amount of free DNA in the supernatant was determined by UV measurement at 260 nm using a standard calibration curve.

### **2.4. Characterization of the LbL-coated gold nanoparticles**

#### **2.4.1. UV-visible spectroscopy of AuNPs**

UV-vis absorbance spectra of the AuNPs after each coating step were recorded using an Uvikon 941 spectrophotometer (Kontron Instruments GmbH).

#### **2.4.2. Size and zeta potential measurements by dynamic light scattering (DLS)**

For the determination of size and  $\xi$ -potential, the samples of AuNPs were thermostated to 25  $^{\circ}$ C and laser light scattering analysis was performed with an incident laser beam of 633 nm at a scattering angle of 173 $^{\circ}$  using the Malvern ZetaSizer Nano-ZS (Malvern Instruments GmbH). The  $\xi$ -potential measurements

were performed in disposable folded capillary cells (Malvern Instruments GmbH), measuring the electrophoretic mobility at 25 °C.

#### **2.4.3. TEM image of the gold nanoparticles**

Transmission electron micrographs (TEM) of AuNPs were taken on a Philips CM12 microscope (FEI, Eindhoven, The Netherlands). Samples were prepared by depositing the colloidal gold solution onto a carbon-coated copper grid and air-dried before analysis. Several micrographs were taken per sample.

#### **2.4.4. Determination of gold nanoparticles concentration by ICP-OES**

The concentration, and consequently the number of AuNPs per volume after synthesis, was determined by using inductively coupled plasma-optical emission spectroscopy (ICP-OES). 500 µl of a sample containing AuNPs was mixed with 200 µl freshly prepared aqua regia [Caution! Aqua regia is a strong acid] and diluted to 5 ml with Millipore water. The Au<sup>3+</sup> content of the solution was determined by ICP-OES analysis on a JY-70 PLUS (Jobin Yvon Instruments S.A.). The plasma flow was 16 L/min argon. All standards were made with gold (III) chloride at concentrations of 0.1, 1, 10 and 100 ppm. The measured concentration of Au<sup>3+</sup> was divided by the number of gold atoms per particle to obtain the concentration of AuNPs in solution [24].

#### **2.4.5. Stability of LbL-coated nanoparticles in cell culture medium**

The stability of AuNPs after each coating step was investigated in serum free and serum containing culture medium (leibovitz's). The change in UV-vis spectra, hydrodynamic diameter, and  $\xi$ -potential were monitored.

### **2.5. Determination the protein adsorption using 2D SDS-PAGE**

The proteins adsorbed to the surface of AuNPs were analyzed after desorption from the surface using two-dimensional sodium dodecylsulfate polyacrylamide gel electrophoresis (2D SDS-PAGE) [29, 30]. First, the LbL-coated AuNPs were incubated in culture medium containing 10% fetal calf serum for 5 minutes at 37 °C, then the particles were purified 5 times to remove free, unbound proteins by repeated centrifugation. Afterwards, the proteins were desorped from the nanoparticles surface by incubation with a solution of sodium dodecylsulafte (SDS) and dithiothreitol (DTT) for 5 minutes at 95 °C. The proteins were analyzed by SDS-PAGE using PROTEAN IEF cell (U.S.A). Electrophoresis was run overnight at 500 V. Gels were stained by silver staining as described by Shevchenko et al. [31].

## **2.6. Cell culture and cellular uptake studies**

### **Cell culture**

Cell lines were cultivated in 75 cm<sup>2</sup> culture flasks at 37°C in a 5% CO<sub>2</sub> humidified environment. CHO-K1 cells were grown in culture medium consisting of HAM F-12. HeLa cells were maintained in Dulbecco's Medium. MCF-7 cells were grown in Minimum Essential Medium (MEM). HCT 116 cells were maintained in D-MEM medium. All cell culture medium were supplemented with 10% FBS.

#### **2.6.1. Cellular uptake kinetics using Flow Cytometry**

Different cell lines were seeded in a 24-well plate at an initial density of 80,000 cells per well for HeLa and CHO-K1 cells and 120,000 cells per well for MCF-7 and HCT 116 cells one day before the experiments. The culture medium was then removed, the cells were washed with PBS, and different volumes of purified LbL-coated AuNPs were added to the cells in Leibovitz's containing 5% serum. Five hours after incubation, the medium (which contained AuNPs that were not taken up by cells) was removed and the cells were prepared for flow cytometry analysis as described previously [32]. In brief, cells were washed with PBS and detached using trypsin for 5 min. Thereafter, the reaction was stopped with serum-containing medium and the cells were isolated by centrifugation for 5 min at 200 xg. Finally, the cells were washed with PBS (4 °C) twice, and resuspended in cold PBS for the measurements. Untreated cells were used to determine the autofluorescence of cells. Measurements were taken on a FACS Calibur (Becton Dickinson, Germany) using CellQuest Pro software (Becton Dickinson, Germany) and evaluated by WinMDI 2.8 software (©1993–2000 Joseph Trotter). DyLight fluorescence was excited at 646 nm and detected in the channel FL4 (661/16) band-pass filter. The percentage of cells that had internalized AuNPs was determined by the number of DyLight positive cells, and mean fluorescence intensity (MFI) of those cells that had taken up AuNPs served as an indirect measure for the number of internalized nanoparticles. All values were normalized to cells that received culture medium only, without particles.

#### **2.6.2. Cellular uptake of LbL-coated AuNPs using ICP-OES**

CHO-K1 Cells were incubated with Leibovitz's with 5% serum containing LbL-coated AuNPs for 6 hours. Thereafter, the cells in three flasks were washed two times with PBS, detached from the flask via trypsinization, pelleted, and washed again with PBS. For the determination of the Au<sup>3+</sup> content by ICP-OES the cell pellet was air

dried, dissolved in 500  $\mu$ l of freshly prepared aqua regia [Caution! Aqua regia is a strong acid] and diluted to 5 ml with Millipore water. ICP-OES analysis of the samples was performed on a JY-70 PLUS (Jobin Yvon Instruments S.A.) with a plasma flow of 16 L/min argon. All standards were made with gold (III) chloride at a concentration of 0.1, 1, 10 and 100 ppm. The measured number of  $\text{Au}^{3+}$  was used to calculate the number of AuNPs as described by Cumberland et al. [33] and related to the total number of cells. The number of total cells was determined by counting the cells of one 75cm<sup>2</sup> culture flasks in a Neubauer Chamber. The samples for cell counting were incubated with AuNPs in the same way as samples for ICP-OES measurements. Cell samples treated as described above but without addition of AuNPs, were used as controls for background subtraction.

### **2.6.3. Intracellular trafficking of LbL-coated AuNPs- confocal laser scanning microscopy (CLSM)**

A Zeiss Axiovert 200 M microscope coupled to a Zeiss LSM 510 scanning device (Carl Zeiss Co. Ltd., Germany) was used for CLSM experiments. The inverted microscope was equipped with a Plan-Apochromat 63 $\times$  objective. CHO-K1 cells were plated in an 8-well Lab-Tek<sup>TM</sup> Chambered Coverglass (Nunc GmbH & Co. KG, Wiesbaden, Germany) at an initial density of 20,000 cells per chamber. After 24 h, the culture medium was removed and the cells were washed with PBS. Afterwards, AuNPs that were fabricated with DyLight 649 labeled PEI were added to the cells, and imaging commenced after 5 h in each well at 37  $^{\circ}$ C. DyLight-labeled PEI was excited at 646 nm and the fluorescence was recorded with a 670 longpass filter. The pinhole was set to one Airy Unit. Approximately 20 images were evaluated for each condition.

### **2.6.4. Cytotoxicity assay**

Cytotoxicity of LbL-coated AuNPs was determined by an MTT (3-(4,5-dimethylthiazol-2-yl)-2, 5-diphenyltetrazolium bromide) assay in CHO-K1 cells. This assay is based on the ability of living cells to reduce a water soluble yellow dye, MTT, to a purple colored water-insoluble formazan product using a mitochondrial enzyme called succinate dehydrogenase. Cells were grown in 96-well plates at an initial density of 14,000 cells per well for 24 h to approximately 100% confluence. For the experiments, the medium was removed and the cells were washed with PBS. AuNPs at different concentrations in 100  $\mu$ l media were added to the wells. After 5 h of incubation, a solution of MTT (0.626 mg/ml in PBS) was added to cells followed by

further incubation for 4 h at 37 °C. Thereafter, the medium was carefully removed and the cells were rinsed with PBS. The formazan crystals formed were dissolved using a 10 % solution of sodium dodecyl sulfate (SDS) in PBS (100 µl/ well). After 16 h of incubation in the dark at RT, the samples were measured by a plate reader (Shimadzu, Duisburg, Germany) at 550 nm.

### 3. Results and discussion

In this study, we used commercially available AuNPs with sizes of 20, 30, 50 and 80 nm. All particles were coated as described, starting with a first layer of PEI, followed by a layer of DNA and a final layer of PEI [27]. PEI was used because it is known to be highly efficient in transfecting cells, and the DNA with a random sequence of 21 bp was used as model for different types of nucleic acids. After each coating step, it was necessary to purify the coated particles from free, unbound polyelectrolytes to avoid the formation of inter-polyelectrolyte complexes between DNA and PEI. The successful polyelectrolyte deposition was monitored by dynamic light scattering (DLS), zeta potential measurements, UV-vis absorbance spectroscopy and transmission electron microscopy (TEM). Figure 1 A shows the hydrodynamic diameter of the AuNPs of different sizes after the last coating step, including the polydispersity index as determined by DLS. The size of AuNPs ranged from  $32.0 \pm 0.2$  nm to  $84.8 \pm 0.1$  nm, and all LbL-coated particles showed a positive zeta potential (Figure 1 B). The surface plasmon resonance (SPR) peak of the UV-vis spectra of the AuNPs shifted about 4 - 6 nm during the coating process, which is in good agreement with the literature (Figure 1 C) [34-36]. Additionally, TEM micrographs revealed that the majority of LbL-coated AuNPs remained single particles during the LbL assembly without any sign of aggregation, and the nanoparticles were spherical (Figure 1 D).



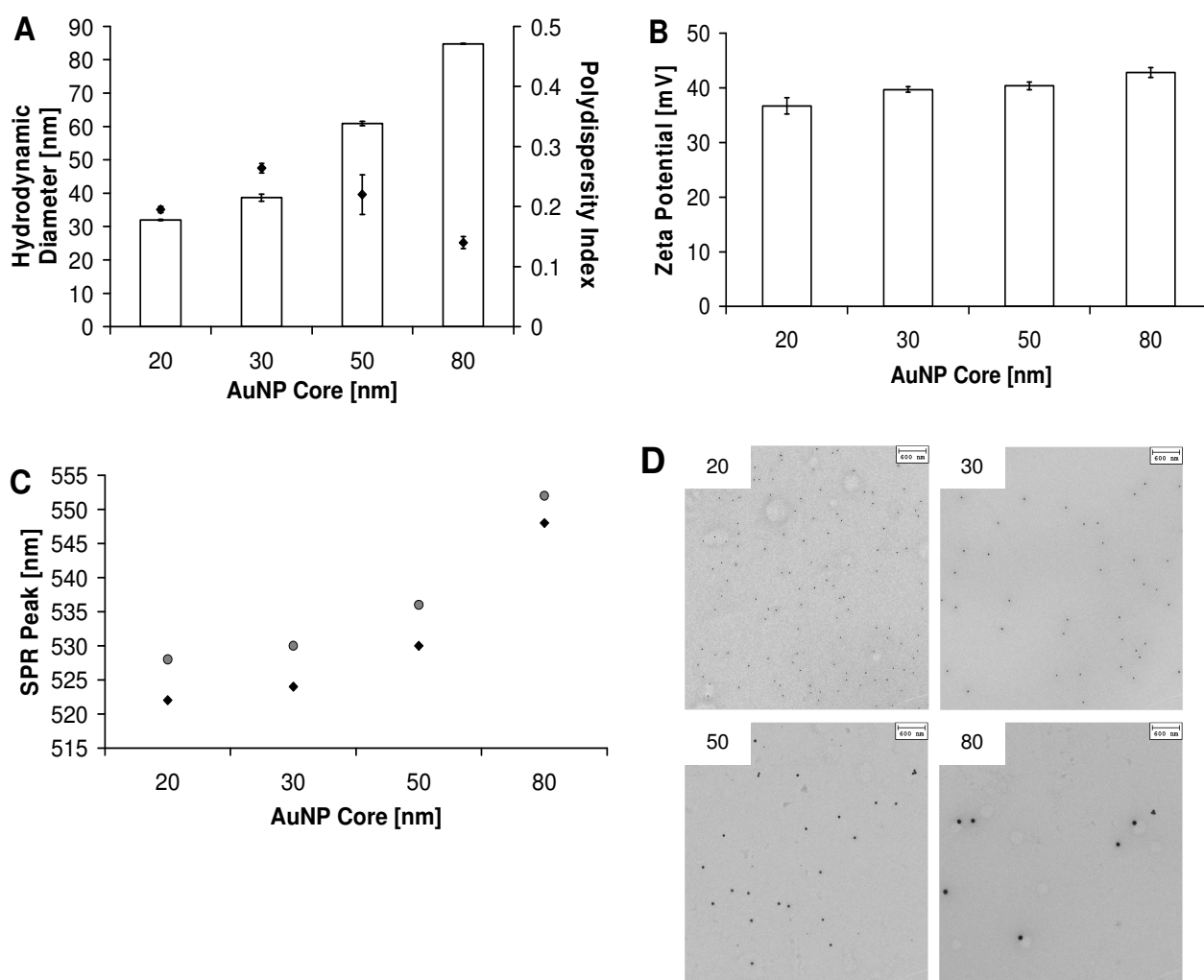
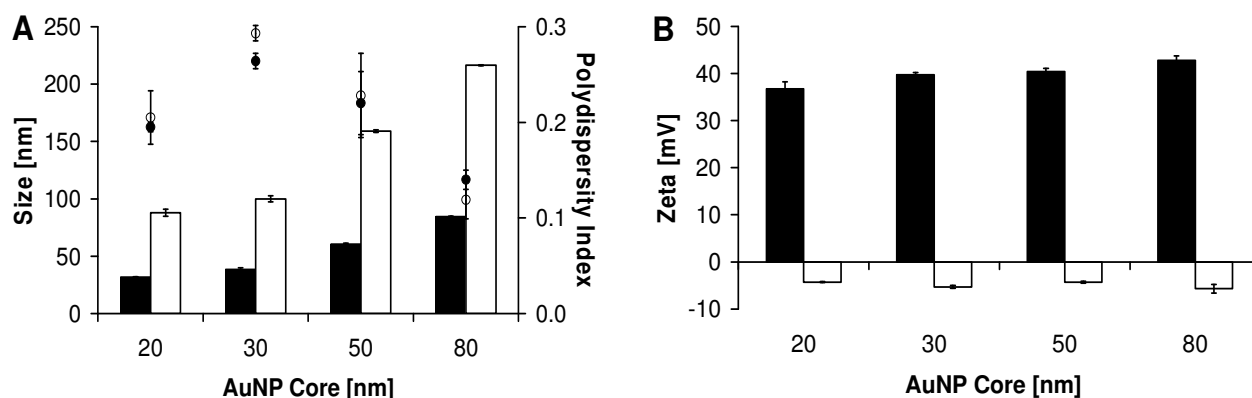


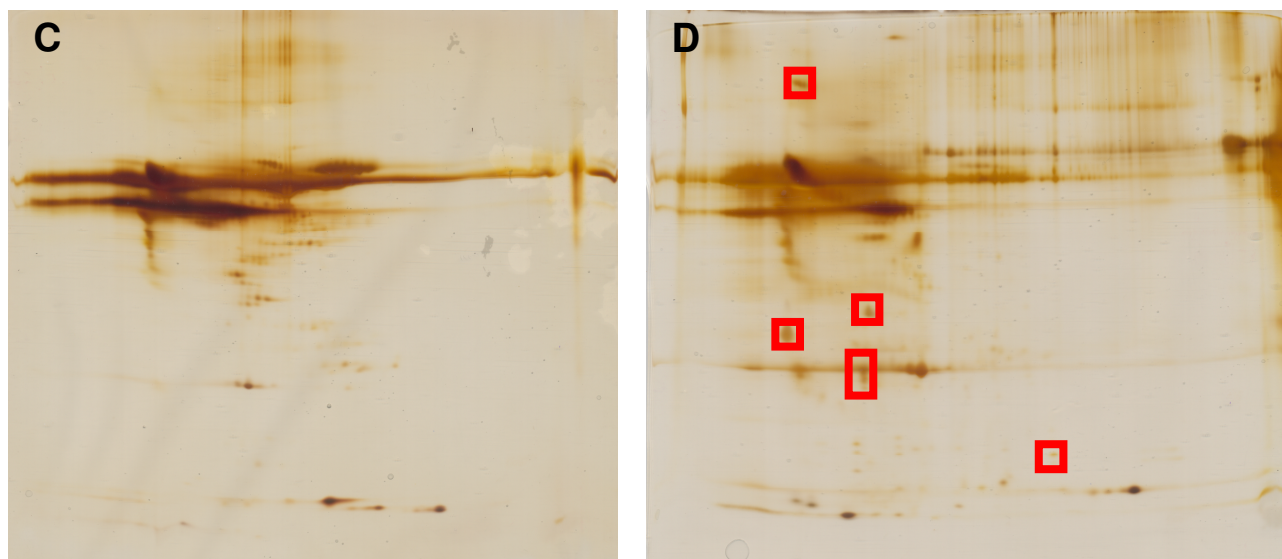
**Figure 1:** Characterization of the AuNPs of different sizes after coating with PEI, DNA, and PEI by different methods. (A) The hydrodynamic diameter (white columns) and the polydispersity index (rhombs) of LbL-coated AuNPs are shown with (B) the corresponding zeta potential. The values represent the mean  $\pm$  standard deviation of three sub-runs of one sample. One representative experiment of three independent ones is shown. (C) The maximum position of the SPR peak of UV-vis spectra of AuNPs is shown before (black rhombs) and after (grey circles) the coating process. (D) Transmission electron micrographs of colloidal AuNPs after the coating steps. Only the cores of AuNPs are visible, as the coating has inherently low contrast with the preparation and imaging conditions chosen. The bar indicates 600 nm.

Another important consideration for the evaluation of the cellular uptake of LbL-coated AuNPs is their stability in cell culture medium. If the particles are susceptible to environmentally induced aggregation, the tedious manufacture and the investigation of different sizes of AuNPs would be useless. It was for this reason that AuNPs were exposed to cell culture medium containing 10% fetal calf serum, and the hydrodynamic diameter and the zeta potential were monitored (Figure 2 A and B). The diameter of the LbL-coated AuNPs increased by approximately 2.6 fold for each particle size, and all particles showed a reversal of the zeta potential. This extent of

the growth in diameter can most likely be attributed to the adsorption of proteins on the surface, as already shown for unmodified and other oligonucleotide-modified AuNPs [24, 37]. At the same time, the polydispersity index did not significantly change, which indicates that the AuNPs only grew due to protein adsorption but not due to particle aggregation. In contrast, after incubation in culture medium without serum, the size of the particles increased by about 5 to 8 fold which is most likely due to the formation of larger aggregates (data not shown). So far, the adsorption of proteins to the surface of AuNPs has only been indirectly confirmed by such data as size or FTIR measurements [24, 38, 39]. In contrast, our intention was to provide direct evidence by analyzing the proteins after desorption from the surface. To this end, particles were incubated in culture medium containing 10% fetal calf serum and then were purified 5 times to remove the free, unbound proteins. After desorption of the proteins from the particle surface, they were analyzed by 2D SDS-PAGE. The proteins were first separated by their isoelectric point, and in the second dimension by their molecular weight [29, 30, 40]. Figure 2 C shows the analysis of pure fetal calf serum and Figure 2 D illustrates the proteins that were desorbed from LbL-coated AuNPs with a core of 20 nm (only qualitative analysis). The gels show that a significant amount of different serum proteins adsorbed to the surface of LbL-coated particles. Additionally, the red boxes in Figure 2 D display some low abundance proteins that are not visible in the gel of pure fetal calf serum (Figure 2 C), but seem to be enriched on the particle surface. This interaction between the nanoparticles and the proteins seems to be of great importance, since it alters not only the surface properties and charge, but also the resistance to particle aggregation.



Continued on next page

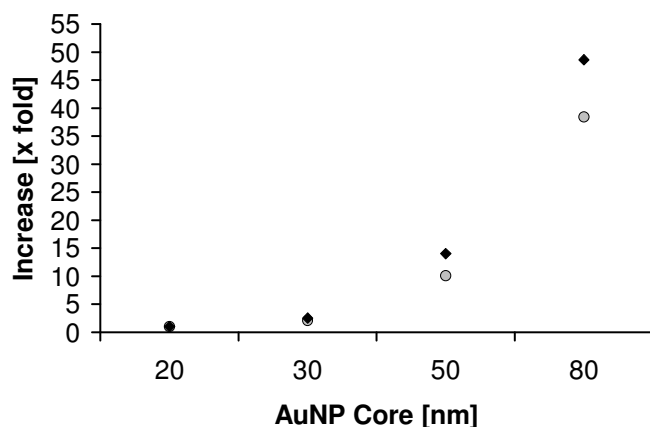


**Figure 2:** Investigation of the stability of LbL-coated AuNPs in culture medium containing fetal calf serum. AuNPs were diluted in Millipore water or serum-containing culture medium and (A) the particle size (black and white bars, respectively), the polydispersity index (black and white circles, respectively), and (B) the zeta potential were measured. The values represent the mean  $\pm$  standard deviation of three sub-runs of one sample. Additionally, 2D SDS-PAGE was performed with (C) pure fetal calf serum as a control and (D) the proteins that were desorbed from LbL-coated AuNPs. The gels can only be compared qualitatively.

Since AuNPs did not aggregate after incubation in serum containing culture medium, the cellular uptake was investigated by two different methods. The extent of particle uptake was quantified either by fluorescence-activated cell sorting (FACS) using LbL-coated AuNPs that were fabricated with fluorescently-labeled (DyLight 649) PEI as a last layer or by inductively coupled plasma spectroscopy (ICP-OES) using unlabeled, LbL-coated AuNPs. Because the FACS method allows for the determination of the amount of fluorescently-labeled PEI inside cells, but not for the amount of AuNPs per cell, it was first necessary to measure the amount of labeled PEI that was adsorbed on the AuNP surface on the different sizes of AuNPs. As expected, the PEI amount, as well as the number of DNA molecules, increased with the size of the AuNPs (Table 1). Figure 3 shows that this increase in the adsorption of polyelectrolytes depending on the size runs exponentially, with the amount of PEI per AuNP increasing up to about 38 fold, and amount of DNA per AuNP up to about 49 fold, using the AuNPs with a core ranging from 20 – 80 nm.

**Table 1:** Number of DNA and PEI (in the last layer) molecules per AuNP

AuNP Core [nm]	DNA molecules / AuNP	PEI last layer [fg] / AuNP
20	2.2E+02	1.0
30	5.6E+02	2.1
50	3.1E+03	10.0
80	1.1E+04	38.2

**Figure 3:** Exponential increase of the amount of PEI (grey circles) and DNA (black rhombs) depending on the size of the AuNP core.

The importance of this information becomes even more evident after reviewing the results from the cellular uptake measured by FACS analysis. First of all, over 99% of all CHO-K1 cells had taken up fluorescently-labeled particles independently of the particle size or concentration. The histogram in Figure 4 gives an example of the FACS analysis and shows that the cells treated with LbL-coated AuNPs shifted to much higher fluorescence values compared to control cells.

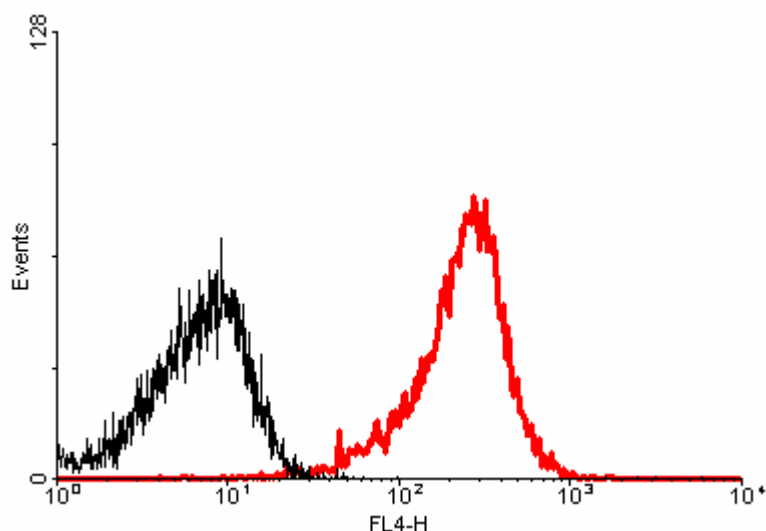


**Figure 4:** Example of a histogram from the FACS analysis. The black curve is from the control cells, and the red curve is from the CHO-K1 cells that were incubated with 30 nm LbL-coated AuNPs at a concentration of  $68 \mu\text{M Au}^{3+}$ .

The mean fluorescence intensity (MFI) of cells positive for particles was then used for the further evaluation of the data (the MFI is an indirect measure for the amount of PEI associated with the cells). In Figure 5 A, the MFI of CHO-K1 cells after incubation with the different sizes of LbL-coated AuNPs is plotted against the  $\text{Au}^{3+}$  concentration in the culture medium. The graph reveals that the larger the LbL-coated AuNPs, the more PEI molecules are taken up by the cells. In addition, Figure 5 B in which the MFI is referred to the amount of PEI per AuNP makes evident that more smaller than larger LbL-coated AuNPs are taken up by the cells. Therefore, one can conclude that fewer larger particles are necessary to deliver a similar amount of PEI or DNA molecules per cell. Most studies plot the cellular uptake versus the hypothetical  $\text{Au}^{3+}$  concentration in the culture medium that would be generated if the AuNPs were completely dissolved. In contrast to this, Figure 5 C shows that the MFI is dependent on the AuNPs in the culture medium. Here, it becomes immediately evident that less LbL-coated AuNPs of 80 nm (compared to 20 nm) are required to obtain a significantly higher fluorescent signal per cell. The same trend and similar results were also measured in HeLa cells (Figure 6) and in MCF-7 cells (data not shown).

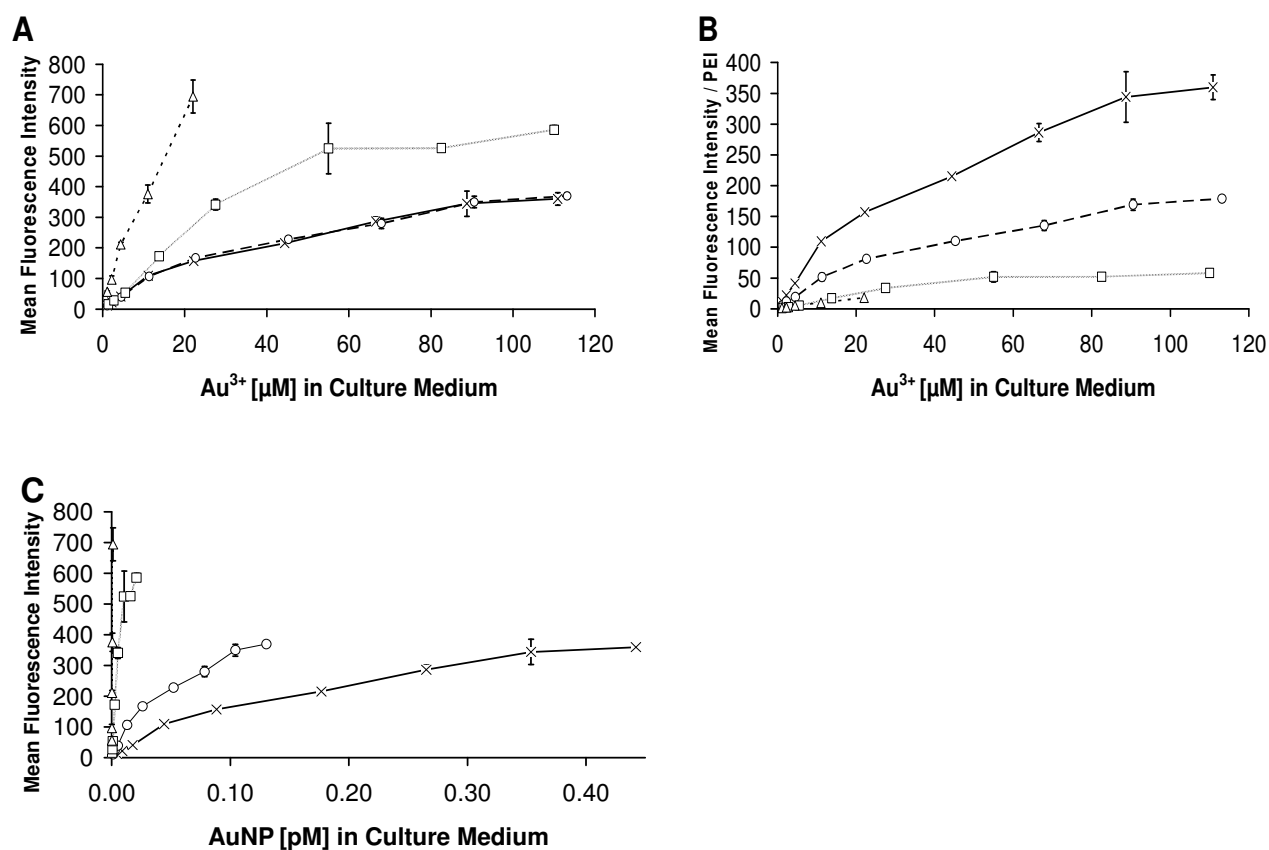


**Figure 5:** The uptake of fluorescently labeled LbL-coated AuNPs with an AuNP core of (x) 20, (o) 30, (□) 50 and (Δ) 80 nm into CHO-K1 cells as determined by FACS analysis. The values represent the mean  $\pm$  standard deviation of three independent samples. One representative experiment of four independent ones is shown.

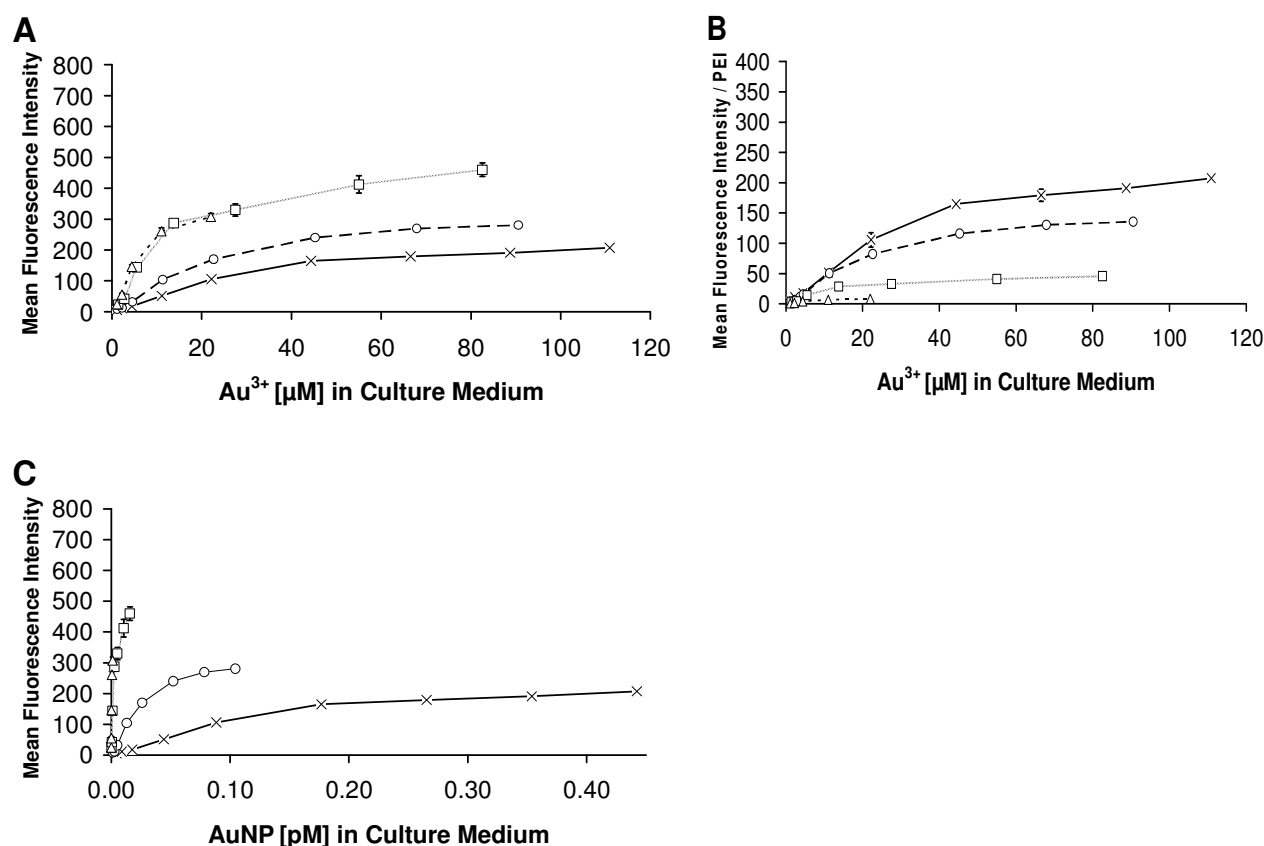


**Figure 6:** The uptake of fluorescently labeled LbL-coated AuNPs with an AuNP core of (x) 20, (o) 30, (□) 50 and (Δ) 80 nm into HeLa cells as determined by FACS analysis. The values represent the mean  $\pm$  standard deviation of three independent samples. One representative experiment of two independent ones is shown.

Additionally, fluorescently labeled, LbL-coated AuNPs were observed with confocal laser scanning microscopy (CLSM) after incubation with CHO-K1 cells (Figure 7). The images also proved that the nanoparticles did not form any larger aggregates after incubation with cells in serum-containing culture medium. In general, there were no large differences visible between the AuNPs of different sizes. One could speculate that CHO-K1 cells endocytosed more particles of 20 nm than of the larger sizes, but one has to keep in mind that for a quantitative conclusion the confocal images have to be statistically evaluated which was not done.



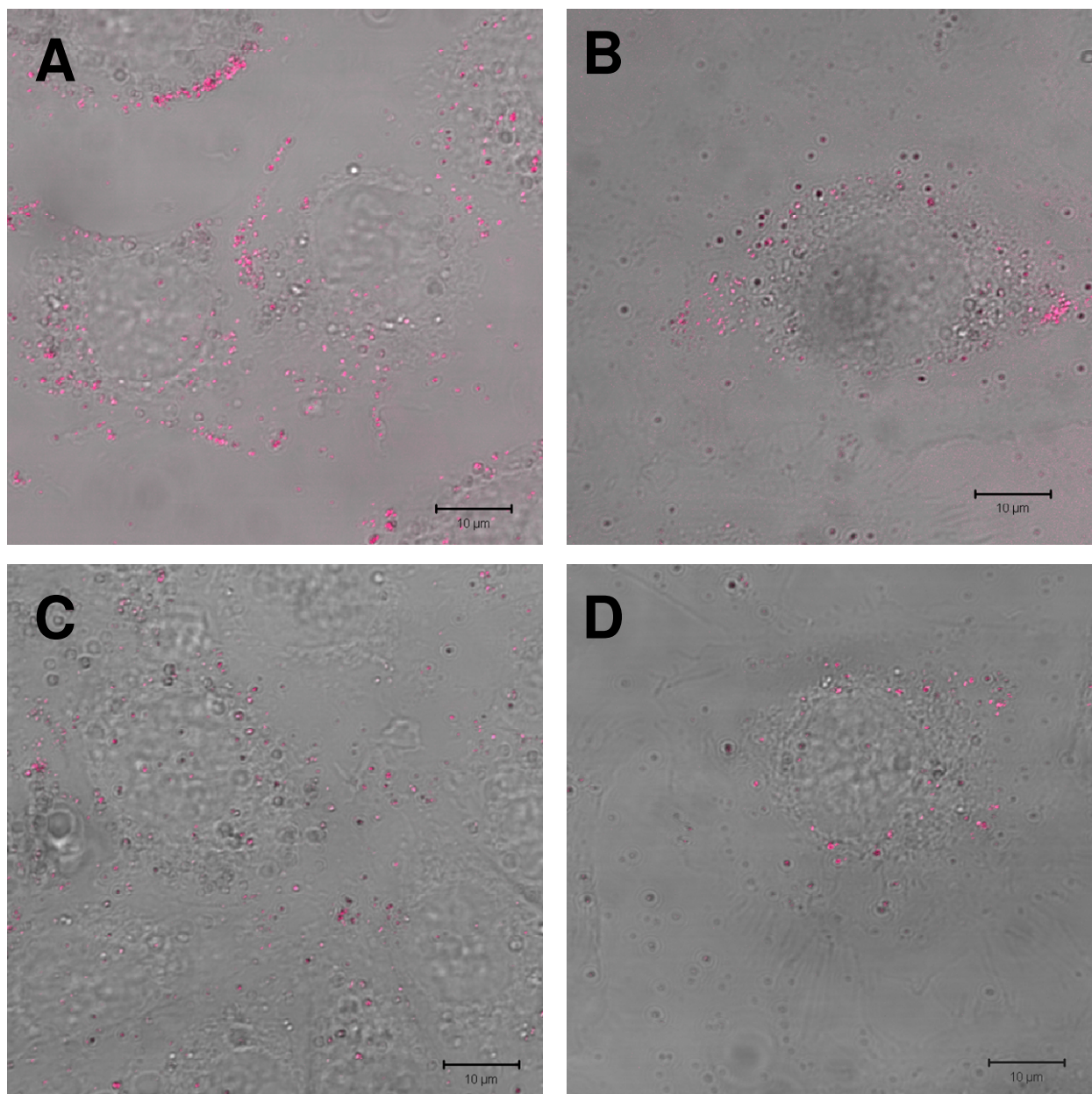


**Figure 7:** Confocal images of CHO-K1 cells after 5 hours of incubation with fluorescently labeled, LbL-coated AuNPs with a core of (A) 20, (B) 30, (C) 50 and (D) 80 nm. Images are an overlay of the transmitted light and fluorescence emission. Each bar indicates 10 μm.

To obtain quantitative data for the number of AuNPs per cell, CHO-K1 cells were incubated for 6 hours with LbL-coated AuNPs in serum-containing culture medium and subsequently the  $\text{Au}^{3+}$  content of the cell digest was determined by ICP-OES. The particles were applied at the concentration that yielded the highest fluorescent signal in the FACS experiment for each particle species. Figure 8 shows the amount of AuNPs per cell depending on the size of the AuNP core. The ICP-OES confirmed the FACS experiments that many more small particles are taken up by the cells in comparison to larger particles. Looking at the absolute amount of particles, this



difference becomes even more impressive. About 13500 AuNPs with a core of 20 nm, which corresponds to 32.0 nm after the coating with all 3 polyelectrolyte layers, were taken up per cell. This number significantly decreased with the size of the AuNP core to about 400 at an AuNP core size of 80 nm, which corresponds to 84.8 nm after the coating with all 3 polyelectrolyte layers. A comparison with data from literature indicated that the optimal particle diameter for the cellular uptake with an AuNP core of 25 – 50 nm can only be performed very roughly, because these studies do not take into account that the size of the AuNPs significantly increases after incubation in serum containing culture medium [24, 26]. With respect to the size of LbL-coated AuNPs directly after the coating process, our results are in good agreement with literature values. However, if considering that the protein corona adds a significant size to the AuNPs, it is not possible to make a comparison because one has to deal then with particles ranging from about 87.8 to 216.9 nm.

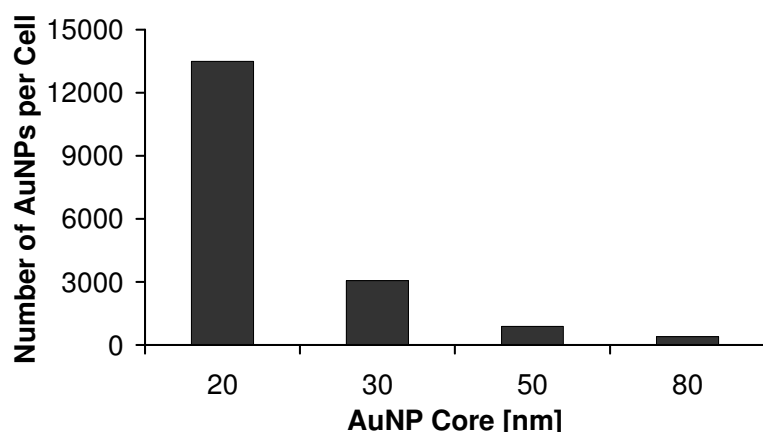


**Figure 8:** The number of AuNPs per cell as determined by ICP-OES and cell counting after 6 hours of incubation in serum containing culture medium as a function of the size of the AuNP core. For each measurement, cells from 3 culture flasks (75 cm<sup>2</sup> each) were pooled to obtain values within the calibration range. Bars are averages of two measurements of one representative experiment of three independent ones performed.

With these data it was now possible to calculate the amount of DNA and PEI molecules that were hypothetically delivered into one CHO-K1 cell depending on the size of LbL-coated AuNPs. It was remarkable that the overall amount of nucleic acid molecules that were estimated for the delivery into one cell was in the same order of magnitude (Table 2).

**Table 2:** Amount of DNA and PEI molecules delivered per cell as a function of the size of the AuNP core.

AuNP Core [nm]	DNA molecules / cell	PEI [fg] / cell
20	3.0E+06	1.3E+04
30	1.7E+06	6.3E+03
50	2.7E+06	8.9E+03
80	4.3E+06	1.5E+04

In the view of a potential future *in vivo* application, the safety of LbL-coated AuNPs is of great significance. Hence, last but not least, the toxicity of the AuNPs was tested using an MTT assay [41]. Figure 9 impressively shows that all particles were not toxic to the cells at the concentrations applied during the cellular uptake experiments.

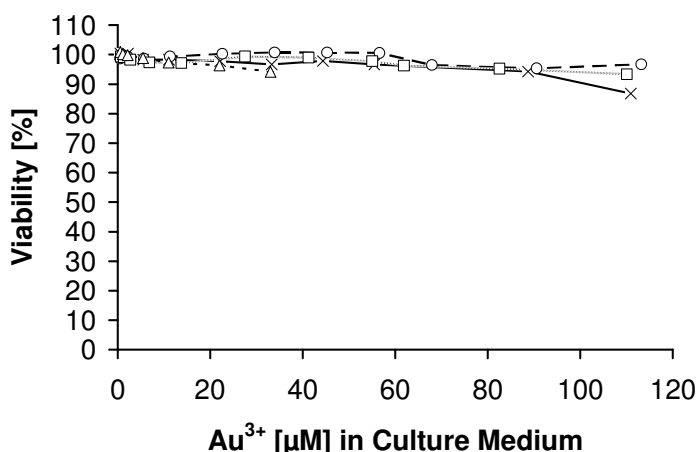


**Figure 9:** Evaluation of the toxicity of LbL-coated AuNPs with a core of (x) 20, (o) 30, (□) 50 and (Δ) 80 nm in CHO-K1 cells using a MTT assay. The values represent the mean  $\pm$  standard deviation of eight independent samples. One representative experiment of two independent ones is shown

#### **4. Conclusion**

In summary, in this study we investigated the effect of different sizes of LbL-coated AuNPs on their cellular uptake. We found that the smaller AuNPs were taken up by the cells to a higher extent than larger ones. Moreover, there was a positive correlation between the amount of active substances taken up by the cells and the size of LbL-coated AuNPs. The number of PEI, as well as DNA molecules, increased with the size of the AuNPs. Therefore, much fewer larger particles are necessary to deliver a similar amount of active molecules per cell. Here, we successfully addressed some important parameters to close the gap of how the physicochemical properties influence the cellular uptake of nanoparticles. In conclusion, this finding will assist in the future design of nano-structures delivering nucleic acids for biomedical applications.

## 5. References

- [1] Gindy, M. E.; Prud'homme, R. K. Multifunctional nanoparticles for imaging, delivery and targeting in cancer therapy. *Expert Opinion on Drug Delivery* 2009; **6**: 865-878.
- [2] Nune, S. K.; Gunda, P.; Thallapally, P. K.; Lin, Y-Y.; Forrest, M. L.; Berkland, C. J. Nanoparticles for biomedical imaging. *Expert Opinion on Drug Delivery* 2009; **6**: 1175-1194.
- [3] Chumbimuni-Torres, K Y.; Wang, J. Nanoparticle-induced potentiometric biosensing of NADH at copper ion-selective electrodes. *Analyst* 2009; **134**: 1614-1617.
- [4] Zhu, S.; Yongqi Fu, C e. Fabrication and characterization of rhombic silver nanoparticles for biosensing. *Opt. Mater.* 2009; **31**: 769-774.
- [5] Mishra, B.; Patel, B. B.; Tiwari, S. Colloidal nanocarriers: a review on formulation technology, types and applications toward targeted drug delivery. *Nanomedicine: Nanotechnology, Biology, and Medicine* 2010; **6**: 9-24.
- [6] Kasuya, T.; Kuroda, S. Nanoparticles for human liver-specific drug and gene delivery systems: *in vitro* and *in vivo* advances. *Expert Opinion on Drug Delivery* 2009; **6**: 39-52.
- [7] Tetsuya, O.; Yuuki, T. Drug and gene delivery system using nano-sized particles. *Pharm Tech Japan* 2008; **24**: 445-449.
- [8] Win, K. Y.; Feng, S-S. Effect of particle size and surface coating on cellular uptake of polymeric nanoparticles for oral delivery of anticancer drugs. *Biomaterials* 2005; **26**: 2713-2722.
- [9] Mahesh D. C.; Ayman, K.; Jayanth, P. Nanoparticles for cellular drug delivery: mechanism and factors influencing delivery. *J. Nanoscience and Nanotechnology* 2006; **6**: 2651-2663.
- [10] Gratton, S. E. A.; Ropp, P. A.; Pohlhaus, P. D.; Luft, J. C.; Madden, V. J.; Napier, M. E.; DeSimone, J. M. The effect of particle design on cellular internalization pathways. *Proc. Natl. Acad. Sci. U.S.A* 2008; **105**:11613-11618.
- [11] Lundqvist, M.; Stigler, J.; Elia, G.; Lynch, I.; Cedervall, T.; Dawson, K. A. Nanoparticle size and surface properties determine the protein corona with possible implications for biological impacts. *Proc. Natl. Acad. Sci. U.S.A* 2008; **105**:14265-14270.
- [12] Mailänder, V.; Landfester, K. Interaction of nanoparticles with cells. *Biomacromolecules* 2009; **10**: 2379-2400.
- [13] Alberola, A. P.; Radler, J. O. The defined presentation of nanoparticles to cells and their surface controlled uptake. *Biomaterials* 2009; **30**: 3766-3770.

- [14] Gao, H., Shi, W.; Freund, L. B. Mechanics of receptor-mediated endocytosis. *Proc Natl Acad Sci U. S. A.* 2005; **102**: 9469-9474.
- [15] Zhang, S., Li, J., Lykotrafitis, G., Bao, G.; Suresh, S. Size-dependent endocytosis of nanoparticles. *Adv.Mater.* 2009; **21**: 419-424.
- [16] Decuzzi, P.; Ferrari, M. The role of specific and non-specific interactions in receptor-mediated endocytosis of nanoparticles. *Biomaterials* 2007; **28**: 2915-2922.
- [17] Munier, S.; Messai, I.; Delair, T.; Verrier, B.; Ataman-Onal, Y. Cationic PLA nanoparticles for DNA delivery: comparison of three surface polycations for DNA binding, protection and transfection properties. *Colloids Surf. B Biointerface* 2005; **43**: 163-173.
- [18] Gaumet, M.; Vargas, A.; Gurny, R.; Delie, F. Nanoparticles for drug delivery: the need for precision in reporting particle size diameters. *Eur. J. Pharm. Biopharm.* 2008; **69**: 1-9.
- [19] Frens, G. Controlled nucleation for the regulation of the particle size in monodisperse gold suspensions. *Nature Phys. Sci.* 1973; **241**: 20-22.
- [20] Giljohann, D. A.; Seferos, D. S.; Daniel, W. L.; Massich, M. D.; Patel, P. C.; Mirkin, C. A. Gold nanoparticles for biology and medicine. *Angew. Chem. Int. Ed.* 2010; **49**: 3280-3294.
- [21] Boisselier, E.; Astruc, D. Gold nanoparticles in nanomedicine: preparations, imaging, diagnostics, therapies and toxicity. *Chem. Soc. Rev.* 2009; **38**: 1759-1782.
- [22] Long, N. N.; Vu, LV.; Kiem, D.C.; Doanh, C. S.; Nguyet, T. C.; Hang, T. P.; Thien, D. N.; Quynh, M. L. Synthesis and optical properties of colloidal gold nanoparticles. *Journal of Physics: Conference Series* 2009; **187**: 012026.
- [23] Zhou, J.; Ralston, j.; Sedev, R.; Beattie, D.A. Functionalized gold nanoparticles: synthesis, structure and colloid stability. *Journal of Colloid and Interface Science* 2009; **331**: 251-262.
- [24] Chithrani, B. D., Ghazani, A. A.; Chan, W. C. Determining the size and shape dependence of gold nanoparticle uptake into mammalian cells. *Nano Lett.* 2006; **6**: 662-668.
- [25] Chithrani, B. D.; Chan, W. C. W. Elucidating the mechanism of cellular uptake and removal of protein-coated gold nanoparticles of different sizes and shapes. *Nano Lett.* 2007; **7**: 1542-1550.
- [26] Jiang, W., KimBetty, Y. S., Rutka, J. T.; ChanWarren, C. W. Nanoparticle-mediated cellular response is size-dependent. *Nat Nano* 2008; **3**: 145-150.
- [27] Elbakry, A., Zaky, A., Liebl, R., Rachel, R., Goepferich, A., Breunig, M. Layer-by-Layer assembled gold nanoparticles for siRNA Delivery. *Nano Lett.* 2009; **9**: 2059-2064.

- [28] Snyder, S. L.; Sobocinski, P. Z. An improved 2,4,6-trinitrobenzenesulfonic acid method for the determination of amines. *Anal. Biochem.* 1975; **64**: 284-288.
- [29] Blunk, T.; Hochstrasser, D. F.; Sanchez, J. C.; Mueller, B. W.; Mueller, R. H. Colloidal carriers for intravenous drug targeting: plasma protein adsorption patterns on surface-modified latex particles evaluated by two-dimensional polyacrylamide gel electrophoresis. *Electrophoresis* 1993; **14**: 1382-1387.
- [30] Blunk, T.; Lueck, M.; Calvo, A.; Hochstrasser, D. F.; Sanchez, J. C.; Mueller, B. W.; Mueller, R. H. Kinetics of plasma protein adsorption on model particles for controlled drug delivery and drug targeting. *Eur. J. Pharm. Biopharm.* 1996; **42**: 262-268.
- [31] Shevchenko, A.; Wilm, M.; Vorm, O.; Mann, M. Mass spectrometric sequencing of proteins from silver-stained polyacrylamide gels. *Anal. Chem.* 1996; **68**: 850-858.
- [32] Breunig, M.; Hozsa, C.; Lungwitz, U.; Watanabe, K.; Umeda, I.; Kato, H.; Goepferich, A. Mechanistic investigation of poly(ethylene imine)-based siRNA delivery: Disulfide bonds boost intracellular release of the cargo. *J. Control. Release* 2008; **130**: 57-63.
- [33] Cumberland, S. L.; Strouse, G. F. Analysis of the nature of oxyanion adsorption on gold nanomaterial surfaces. *Langmuir* 2002; **18**: 269-276.
- [34] Schneider, G.; Decher, G. Functional core/shell nanoparticles via Layer-by-Layer assembly. Investigation of the experimental parameters for controlling particle aggregation and for enhancing dispersion stability. *Langmuir* 2008; **24**: 1778-1789.
- [35] Schneider, G.; Decher, G. From functional core/shell nanoparticles prepared via layer-by-layer deposition to empty nanospheres. *Nano Lett.* 2004; **4**: 1833-1839.
- [36] Mayya, K.S.; Schoeler, B.; Caruso, F. Preparation and organization of nanoscale polyelectrolyte-coated gold nanoparticles. *Adv. Funct. Mater.* 2003; **13**: 183-188.
- [37] Giljohann, D. A.; Seferos, D.S.; Patel, P.C.; Millstone, J. E.; Rosi, N. L.; Mirkin, C. A. Oligonucleotide loading determines cellular uptake of DNA-modified gold nanoparticles. *Nano Lett.* 2007; **7**: 3818-3821.
- [38] Jiang, X.; Jiang, J.; Jin, Y.; Wang, E.; Dong, S. Effect of colloidal gold size on the conformational changes of adsorbed cytochrome c: probing by circular dichroism, UV-visible, and infrared spectroscopy. *Biomacromolecules* 2005; **6**: 46-53.
- [39] Chithrani, B. D.; Stewart, J.; Allen, C.; Jaffray, D. A. Intracellular uptake, transport, and processing of nanostructures in cancer cells. *Nanomedicine: Nanotechnology, Biology, and Medicine* 2009; **5**: 118-127.

- [40] Celis, J E.; Gromov, P. 2D protein electrophoresis: can it be perfected? *Current Opinion in Biotechnology* 1999; **10**: 16-21.
- [41] Mosmann, T. Rapid colorimetric assay for cellular growth and survival: application to proliferation and cytotoxicity assays. *J. Immunol. Methods* 1983; **65**: 55-63.





# **Chapter 6**

## **Summary and Conclusion**

## Summary

The delivery of nucleic acids to cells has gained significant attention and shown tremendous promise for the treatment of genetic and acquired diseases. The basic goal of nucleic acid delivery is to transfer therapeutic genetic material (i.e. nucleic acids) into the cells of an individual with the intention of expressing certain proteins via DNA or knocking down unwanted proteins with complementary short interfering RNA (siRNA). RNA interference is a fundamental mechanism for sequence specific gene knockdown and can be exploited by introducing siRNA into cells [1-3]. The delivery of siRNA into cells requires a carrier, since the siRNA is prone to enzymatic degradation, very large (~ 13 KDa), and too negatively charged to cross cellular membranes [4, 5]. Although viral vectors are highly efficient and remain the most popular tool for siRNA delivery, their broad use is limited by severe safety risks [6, 7]. Therefore, non-viral carriers have emerged as a promising alternative for siRNA delivery both *in vitro* and *in vivo* [8, 9].

Common approaches for siRNA delivery include the creation of nanoparticles using a surplus of either cationic polymers or lipids to compensate for the negative charge of the nucleic acid [10-12]. However, most of these carriers form random self-assembled aggregates with siRNA. These aggregates are generally heterogeneous and poorly defined particle collectives. In addition, these nanoparticles are of various compositions and sizes, which are in equilibrium with free carrier molecules and free siRNA, as shown in Figure 1. This system makes it difficult to determine which species is responsible for the overall biological effects observed, and the optimization of existing formulations is therefore difficult to achieve. Thus, new and optimized strategies are required for the highly efficient delivery of siRNA to cells.

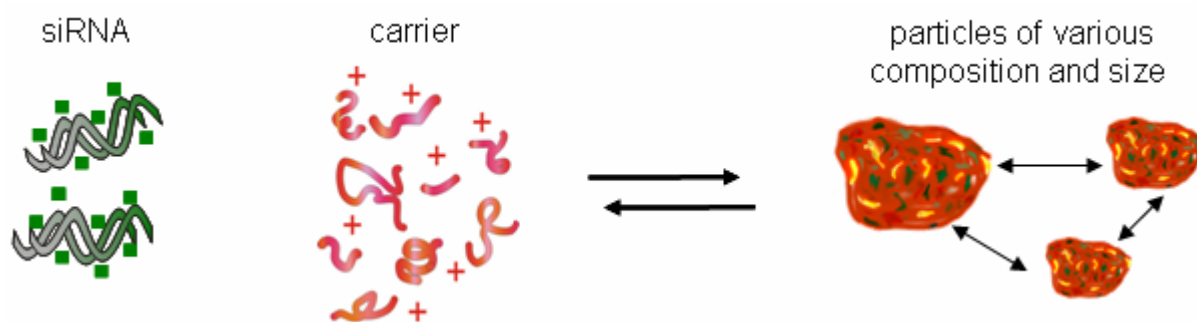


**Figure 1:** The various sub-species existing in random siRNA formulation: nanoparticles of various composition and size, free siRNA and free carrier.

Therefore, the main goal of this thesis was the fabrication of homogeneously distributed nano-carriers with well defined size and surface properties to deliver siRNA into the cells. In order to achieve this goal, we utilized the Layer-by-Layer (LbL) technique using gold nanoparticles (AuNPs) as a template. This allowed us to manufacture a carrier for siRNA delivery that remained monodisperse during the assembly process and delivered active siRNA into cells. In order to fabricate these uniform nanoparticles, our strategy was to deposit siRNA as negatively charged polyanion and a positively charged polycation in alternative order on AuNPs via the LbL technique.

In order to obtain monodisperse and uniform AuNPs suitable for coating with polyelectrolytes by the LbL strategy, the AuNPs were first dispersed in aqueous medium, and were prepared by citrate reduction of auric chloride solutions. Thereafter, the AuNPs were stabilized with 0.1 mg/ml 11-mercaptoundecanoic acid (11-MUA), yielding stabilized AuNPs suitable for the subsequent coating steps. The produced nanoparticles had a narrow particle size distribution and a low polydispersity index. Afterwards, the MUA stabilized AuNPs (MUA-AuNPs) were investigated at different pH values and ionic strength to identify the optimum conditions to produce stable monodisperse nanoparticles. These optimum conditions should be suitable for the complete wrapping of the polyelectrolytes around the nanoparticle surface, yet still allow for the sufficient stability of the nanoparticles. MUA-AuNPs showed a good stability over the time and in a wide range of pH values, which allowed for further coating at physiological pH. Moreover, MUA-AuNPs had a good stability in low ionic strength (1-10 mM NaCl), which is important for the flexibility of the polymer chain. This reduces the chain stiffness and allows the complete wrapping of the polymer around AuNPs. In summary, these MUA-AuNPs provide a good foundation for further coating by polyelectrolytes via LbL technology (chapter 2).

For the successful coating of MUA-AuNPs with polyelectrolytes via the LbL technique for nucleic acid delivery, appropriate parameters had to be identified, including the polyelectrolyte type, concentration, the ionic strength of the adsorption solution and the particle surface properties. First, the suitability of the polycations protamine and poly(ethylene imine) (PEI) 25 KDa using 21 base pair DNA as a model was investigated. Although, the MUA-AuNPs coated well with protamine and the zeta potential of nanoparticles inverted to positive (reflecting successful deposition), the

protamine-AuNPs aggregated during the purification process. It was also difficult to remove free unbound protamine after coating-an important prerequisite for the subsequent coating step. The aggregation during purification could be attributed to the low molecular weight of protamine (only about 5 KDa). It was therefore determined that protamine is not large enough to maintain the stabilization of nanoparticles during purification. In contrast to protamine, PEI showed good stability during coating and after repeated purification steps. 1 mg/ml PEI at 1 mM NaCl and 1.5  $\mu$ M 21 bp DNA at 10 mM NaCl were successfully wrapped around AuNPs in alternative order via the LbL approach. The resulting PEI/DNA/PEI-AuNPs were small ( $\sim$  26 nm), monodisperse with narrow particle size distribution, and had a low polydispersity index. Interestingly, these nanoparticles did not show any sign of toxicity after incubation with CHO-K1 cells, which is attributed to the successful purification and removal of free unbound PEI from the particles. Moreover, the produced nanoparticles showed good stability in culture medium containing serum, which is most likely due to the adsorption of serum protein on the nanoparticles surfaces. These results corroborate the hypothesis that serum proteins are necessary for the nanoparticles stabilization. In addition, this finding is considered a prerequisite for successful cellular uptake of monodisperse nanoparticles. Both types of particles (DNA/PEI- and PEI/DNA/PEI-AuNPs) were taken up by the CHO-K1 cells and the amount of particles per cell depended on the type of the top layer. CHO-K1 cells internalized more DNA/PEI-AuNPs ( $66.1 \times 10^3$  per cell) in relation to PEI/DNA/PEI-AuNPs ( $37.7 \times 10^3$  per cell). This signified that surface properties may strongly influence internalizations of nanoparticles with cells. Overall, the delivery of nucleic acid can be achieved via LbL technology using AuNPs as a template by selecting the experimental parameters accordingly during LbL assembly ([chapter 3](#)). After the appropriate parameters had successfully been investigated, the next step was to fabricate LbL-coated AuNPs for siRNA delivery using PEI 25 KDa as a polycation ([chapter 4](#)). The physicochemical characteristics of the LbL-coated nanoparticles allowed for the successful coating of the nanoparticles. Most AuNPs remained single and maintained their small and uniform size after coating. Since dispersity should strongly influence the cellular uptake of nanoparticles, the stability of nanoparticles in cell culture medium was investigated after each coating step. The nanoparticles showed good stability in culture medium containing serum and the zeta potential inverted to negative due to the adsorption of serum protein. Moreover, both

PEI/siRNA- and PEI/siRNA/PEI-AuNPs were taken up by the CHO-K1 cells and the number of siRNA/PEI-AuNPs per cell ( $2.0 \times 10^5$ ) was significantly higher as compared to PEI/siRNA/PEI-AuNPs ( $5.6 \times 10^4$ ), as determined by inductively coupled plasma spectroscopy (ICP-OES) and transmission electron micrographs of CHO-K1 cells. Additionally, the electron micrographs of sectioned CHO-K1 cells demonstrated the intracellular fate of the AuNPs. AuNPs were predominantly trapped within endocytotic vesicles after 6 hours of incubation, and no particles were detected in the nucleus. It was of great importance to provide evidence of the activity of the siRNA inside the cells. Therefore, the functionality of the successfully coated AuNPs was determined by measuring the gene knockdown of nanoparticles in CHO-K1 cells stably expressing enhanced green fluorescent protein (CHO-K1/EGFP). A dose dependent knockdown was measured for PEI/siRNA/PEI-AuNPs and the cellular EGFP production was reduced to about 28 %. The technique showed highly specific gene silencing and the cell viability of CHO-K1/EGFP cells was about 95 %. In contrast, no silencing efficacy was detected when siRNA was used as the top layer, which could be attributed to the degradation of unprotected siRNA on the surface of the nanoparticles.

Lastly, we showed how size influences the cellular uptake of nanoparticles and the amount of cargo molecules per cell. Different sizes of AuNPs (20, 30, 50 and 80 nm) were coated with PEI and 21 bp DNA via the LbL technique, and the physicochemical characteristics, as well as the stability of nanoparticles, were investigated. All the AuNPs of different sizes were successfully coated via the LbL approach and investigated for their physicochemical properties. The sizes of LbL-coated AuNPs were 32, 38.7, 60.9, and 84.8 nm after the last coating step, and all LbL-coated nanoparticles showed a positive zeta potential. Additionally, all the LbL-coated AuNPs showed good stability in culture medium containing serum. Afterwards, the proteins bound to the nanoparticle surface were investigated qualitatively, and the results showed a significant amount of different serum proteins adsorbed to the surface of LbL-coated AuNPs. This finding opens the way for further study to identify these protein types in future experiments. Additionally, the cellular uptake of different sized LbL-coated AuNPs was investigated. The investigation showed that the smaller AuNPs were taken up by the cells to a higher extent than larger ones. Moreover, there was a positive correlation between the amount of active substances taken up by the cells and the size of LbL-coated AuNPs. The number of

PEI as well as DNA molecules increased with the size of the AuNPs. Therefore, much smaller particles are necessary to deliver a similar amount of active molecules per cell. Furthermore, these LbL-coated AuNPs did not show any sign of toxicity to the cells at the concentrations applied during cellular uptake experiments, which is considered a prerequisite for future *in vivo* application. In summary, these results provide a better understanding of how the size of LbL-coated AuNP affects the cellular uptake, thereby determining the amount of cargo molecules per cell. ([chapter 5](#)).

### **Conclusion and outlook**

In conclusion, this thesis successfully demonstrated strategies for the highly efficient nucleic acid delivery via the LbL technique. This technique offers a unique opportunity to fabricate well-defined and homogeneously distributed nano-carriers for siRNA delivery. The result showed how the surface properties and the size of LbL-coated AuNPs had a great impact on their internalization. Therefore, this finding will assist in the future design of nano-structures delivering nucleic acids for biomedical applications. Moreover, this technique could be a good candidate for further investigation of cellular uptake and the specific pathways into cells, in order to deliver nucleic acid to specific intracellular destinations and determine the intracellular fate of nanoparticles. In future studies, the determination of the types of proteins adsorbed onto the surface of AuNPs is of great importance because the types of adsorbed protein differ with regard to the outer layer and affect the cellular uptake of nanoparticles. Here, protein identification could assist in making cellular uptake more specific. In addition, the surface of the LbL-coated AuNPs can be modified in order to prevent nonspecific uptake into cells via PEG modification. Afterwards, targeted delivery of nanoparticles into specific cells can be achieved via the attachment of targeting ligands onto the surface of these PEG modified nanoparticles. Overall, the LbL strategy presented here could be an excellent basis for future studies directed at specific cell targets. Last but not least, the success of this study opens the way towards the delivery of not only nucleic acid, but also other charged drug molecules into cells via LbL technology using AuNPs as a template.

## References

- [1] Elbashir, S. M.; Harborth, J.; Lendeckel, W.; Yalcin, A.; Weber, K.; Tuschl, T. Duplexes of 21-nucleotide RNAs mediate RNA interference in cultured mammalian cells. *Nature* 2001; **411**: 494-498.
- [2] Whitehead KA, Langer R, Anderson DG. Knocking down barriers: advances in siRNA delivery. *Nat. Rev. Drug Discov.* 2009; **8**: 129–138.
- [3] Castanotto, D.; Rossi, JJ. The promises and pitfalls of RNA-interference-based therapeutics. *Nature* 2009; **457**: 426-433.
- [4] Aagaard, L.; Rossi, J.J.; RNAi therapeutics: principles, prospects and challenges, *Adv. Drug Deliv. Rev.* 2007; **59**: 75 –86.
- [5] Reischl, D.; Zimmer, A. Drug delivery of siRNA therapeutics: potentials and limits of nanosystems, *Nanomedicine: Nanotechnology, Biology and Medicine* 2009; **5**: 8-20.
- [6] Lehrman, S. Virus treatment questioned after gene therapy death. *Nature* 1999; **401**:517–518.
- [7] Sun, J Y.; Anand-Jawa, V.; Chatterjee, S.; Wong KK, Jr. Immune responses to a deno-associated virus and its recombinant vectors. *Gene Therapy*. 2003; **10**:964–976.
- [8] Akhtar, S. Benter, I. F. Non viral delivery of synthetic siRNAs in vivo, *J. Clin. Invest.* 2007; **117**: 3623 – 3632.
- [9] Li, S. D.; Huang, L. Non-viral is superior to viral gene delivery. *J. Controlled Release* 2007; **123**:181-183.
- [10] Schroeder, A.; Levins, C. G.; Cortez, C.; Langer, R. Anderson, D. G. Lipid-based nanotherapeutics for siRNA. *J. Intern. Med.* 2010; **267**: 9-21.
- [11] Kim, W.J.; Kim, S. W. Efficient siRNA delivery with non-viral polymeric vehicles. *Pharm. Res.* 2009; **26**: 657-666.
- [12] de Martimprey, H.; Vauthier, C.; Malvy, C.; Couvreur, P. Polymer nanocarriers for the delivery of small fragments of nucleic acids: oligonucleotides and siRNA. *Eur. J. Pharm. Biopharm.* 2009; **71**: 490-504.





# **Appendix**



**Abbreviations**

$\lambda_{\max}$	Peak of maximum absorption
$\xi$ -potential	zeta potential
AuNP	gold nanoparticle
AuNPs	gold nanoparticles
Ago2	argonaute 2
AIDS	acquired immune deficiency syndrome
AMD	age-related macular degeneration
bp	base pair
<i>C. elegans</i>	<i>Caenorhabditis elegans</i>
CHO-K1	chinese hamster ovarian cell line
CHS	chalcone synthetase
CLSM	confocal laser scanning microscopy
CO <sub>2</sub>	carbon dioxide
DLS	dynamic light scattering
DMEM	Dulbecco's modified eagle's medium
DNA	deoxyribonucleic acid
dsRNAs	double-stranded RNAs
DTT	dithiothreitol
EGFP	enhanced green fluorescent protein
FACS	fluorescence activated cell sorting
FBS	fetal bovine serum
GFP	green fluorescent protein
Ham's F-12	Nutrient Mixture F-12
HCT 116	human colorectal carcinoma cell line
HeLa	human cervical carcinoma cell line
HCl	hydrochloric acid
HNO <sub>3</sub>	nitric acid
ICP-OES	inductively coupled plasma-optical emission spectroscopy
kDa	kilo Dalton
LbL	Layer-by-Layer
MEM	minimum essential medium
mRNA	messenger RNA
MCF-7	human breast cancer cell line

---

MFI	mean fluorescence intensity
MTT	[3-(4,5-dimethylthiazol-2-yl)-2,5-diphenyltetrazolium bromide]
MUA	mercaptoundecanoic acid
MUA-AuNPs	mercaptoundecanoic acid stabilized gold nanoparticles
Mw	molecular weight
MWCO	molecular weight cut off
NaOH	sodium hydroxide
NP	the ratio of nitrogens in polymer to phosphates in DNA
PAH	poly(allylamine hydrochloride)
PBS	phosphate-buffered saline
PEG	polyethylene glycol
PEI	poly(ethylene imine)
PI	polydispersity index
PSS	poly(styrene sulfonate)
PLL	poly(L-lysine)
RISC	RNA-induced silencing complex
RNAi	RNA interference
RNA	ribonucleic acid
rpm	rotations per minute
RT	room temperature
siRNA	short interfering RNA
siRNAs	short interfering RNAs
SDS	sodium dodecyl sulfate
SDS-PAGE	sodium dodecyl sulfate polyacrylamide gel electrophoresis
SPR	surface plasmon resonance
SF	serum free
TEM	transmission electron microscopy
TNBS	trinitrobenzenesulfonic acid
UV	ultraviolet light or irradiation
V	volt
VEGF	vascular endothelial growth factor
VEGFR	vascular endothelial growth factor receptor

**Curriculum vitae**

Name: Asmaa Mohamed Elbakry  
Date of birth: March 25, 1976  
Place of birth: Cairo, Egypt  
Nationality: Egyptian  
Marital status: Married

***Education and Professional Training***

07.1993	School graduation certificate (Abitur)
09.1993 - 06.1998	Studies of Pharmacy, Al-Azhar University, Cairo, Egypt
06.1998 - 05.1999	Practical education at Makah Pharmacy in Cairo, Egypt
03.1999 - 06.2004	Administrator in the Faculty of Pharmacy, Al-Azhar University, Cairo, Egypt
03.1999 - 06.2004	Master program in Pharmaceutical Science, Al-Azhar University, Cairo, Egypt
06.2004	Master Degree in Pharmaceutical Science, Al-Azhar University, Cairo, Egypt
06.2004 - 09.2006	Assistant Lecturer in the Faculty of Pharmacy, Al-Azhar University, Cairo, Egypt
10.2006 - today	PhD program at the Department of Pharmaceutical Technology, University of Regensburg, Germany

**List of publications****Publications**

Kassem, A.A., El-Bagory, I.M. and Elbakry, A.M. Preparation of casein-chitosan sustained release microspheres containing indomethacin. *Sci. J. Az. Med. Fac. (Girls)*, (23), 1427-1444 (2002).

El-Bagory, I.M., Kassem, A.A. and Elbakry, A.M. Preparation and evaluation of indomethacin sustained release cross-linked chitosan microspheres. *Sci. J. Az. Med. Fac. (Girls)*, (24), 1329-1350 (2003).

Elbakry, A., Zaky, A., Liebl, R., Rachel, R., Goepferich, A., and Breunig, M. Layer-by-Layer assembled gold nanoparticles for siRNA delivery. *Nano Letters* (9), 2059-2064 (2009) (chapter 4).

Zaky, A., Elbakry, A., Ehmer, A., Breunig, M., Goepferich, A. Protein release mechanism from triglycerides microspheres, *J. Control. Release*, in Press, DOI: 10.1016/j.jconrel.2010.07.110

**Conference abstracts**

Elbakry, A., Zaky, A., Liebl, R., Rachel, R., Breunig, M., Goepferich, A.: Gold Nanoparticles for siRNA Delivery Fabricated via Layer-by-Layer Technology. DPhG Jahrestagung, Jena (2009).

Zaky, A., Elbakry, A., Ehmer, A., Breunig, M., Goepferich, A.: Protein Release Mechanism from Triglycerides Microspheres. DPhG Jahrestagung, Jena (2009).

Elbakry, A., Zaky, A., Liebl, R., Rachel, R., Langer, R., Goepferich, A., Breunig, M.: Layer-by-Layer fabrication and cellular delivery of different-sized, small interfering RNA-gold nanoparticles. 7th PBP Worldmeeting 2010, Malta (2010).

## Acknowledgements

I want to express my sincere gratitude to all those who contributed to the success of this work over the past four years.

First and foremost, I would like to express my greatest gratitude and respectful appreciation to Prof. Dr. Achim Göpferich for giving me the opportunity to join his research team and for offering such an interesting project to me. I greatly appreciate his trust, encouragement, and valuable scientific guidance throughout this research. Moreover, I appreciate his readiness to support my scholarship and to prepare me for anything, with many emails and correspondences to Egypt.

This thesis would not have been possible without the help, support and patience of Dr. Miriam Breuing. I thank her for her continuous guidance, valuable discussion, comments, and encouragement. I appreciate the great effort she spent, during both the practical work and preparation of my manuscripts and this thesis.

I am very grateful to Prof. Dr. Torsten Blunk for his interest in my work and the valuable discussions and comments during our meetings.

I would like to thank Dr. Jörg Teßmar for his productive discussions during meetings.

My deep thanks go to Dr. Alaa Zaky, my husband and lab mate, for standing beside me and providing continuous encouragement, love, support, and motivation. I also appreciate his participation in this work.

My sincere thanks to Renate Liebl for her work in cell culture experiments. I truly appreciate her friendship and effort throughout this work.

I'm also grateful to Dr. Reinhard Rachel for the TEM measurement, Dr. Harald Huber, Angelika Berié and Cornelia Rose for ICP analysis, Angelika Kühn for support with TEM preparation, Edith Schindler for her work in protein determination, and Dr. Petra Bauer-Kreisel for support in protein determination.

Moreover, I am very thankful for our friendly secretaries Lydia Frommer, Liane Öttl, and Dominika Mögele, who were always helpful, and somehow managed the organization of our daily routine.

My thanks also go to Stefan Kolb and Andrea Blaimer, the technical assistants for their help in organizational and technical matters.

I express my deep gratitude to all my former and present German and Egyptian colleagues in the workgroup of the Department of Pharmaceutical Technology. They created an atmosphere of companionship and unity, making the time spent at the department both valuable and unforgettable for me. Many special thanks go to the following colleagues:

1. Dr. Ferdinand Brandl for his continuous and excellent bits&bytes support. I appreciate his friendly help in finding the person who proofread my thesis
2. Dr. Wolfgang Hild for support he gave to me, especially in the beginning of practical work and the helpful discussions during work

3. Mathias Henke for his assistance in solving internet and computer troubles and the installation of new programs
4. Mathias Ferstl for his help with borrowing books
5. Anne Heller for ordering the literature from Subito
6. Julia Baumer and Sonja Bauhuber for their constant friendship, and for being exemplary in keeping good tempers during bad times.

I would like to say thank you to everybody in the Department of Pharmaceutical Technology for the kind hospitality during my residence in Regensburg.

Special thanks to Siddharth Pathi from Cornell University for proofreading the manuscript, and sincere gratitude to Mark Kalinich from the Massachusetts Institute of Technology for the critical revision of this thesis.

Many thanks go to the Egyptian Government and Egyptian Ministry of Higher Education for the financing of my scholarship to study my PhD in Germany. My thanks also go to all the workers in the Egyptian Cultural Council in Berlin for their continuous support and help during the time of my scholarship in Germany.

Finally, I want to express my deep thanks to my family for their endless love and continuous support. I owe much to my parents for their unconditional love, support, and unwavering belief in me. I want to also thank my lovely kids Ahmed and Arwa for giving me happiness and joy.

Without all of you, I would not be the person who I am today. For that, I would like to thank everyone for being here for me.